

**MOLD DEFLECTION AND MOLD PARTING PLANE SEPARATION DURING
THE INJECTION MOLDING PROCESS**

A Thesis

Presented in Partial Fulfillment of the Requirements for
the Degree of Master of Science in the
Graduate School of The Ohio State University

By

Christopher S. Marks, B.S.

* * * * *

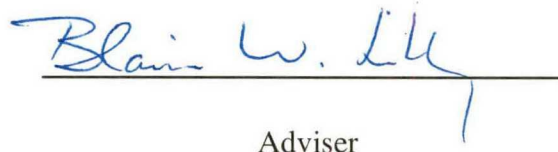
The Ohio State University
2005

Master's Examination Committee:

Professor Blaine Lilly, Adviser

Professor Jose Castro

Approved by


Adviser

Department of Mechanical Engineering

ABSTRACT

Mold deformation and mold separation at the parting plane can influence the geometric features of size on high precision, injection molded parts. In multi-cavity mold designs it is critical to reduce the amount of variance from cavity to cavity in order to control part quality. To quantify the effects of mold deformation and mold separation at the parting plane, experiments were performed on an eight cavity mold. Three strain gage rosettes were affixed to the movable mold half in order to monitor the mold strain during the injection molding process. Additionally, four linear variable differential transformers were used to measure mold separation during the study. Several process control variables were adjusted in order to study the effects on the mold during this process. The experimental results were compared with a parallel research project in which finite element simulation of mold was conducted. An ANOVA analysis of the experimental results was performed as well. Recommendations for future work, such as mold optimization for insert placement and further cavity pressure studies were made.

Dedicated to Jamie L. Marks

ACKNOWLEDGMENTS

I would like to first and foremost thank my advisor, Dr. Blaine Lilly, for his great support and guidance during this project. His ideals in the field of engineering and values for education have influenced my passion to achieve. I would also like to thank Dr. Jose Castro for his collaborative assistance in this project.

Graduate students, Eric J. Wilson and Brian S. Carpenter, have played a vital role in getting my feet wet in this project. Both have assisted me throughout the project as excellent resources for the tools used in experimentation and computation. I would also like to thank Claudia Gonzalez for her work in the computer simulation and modeling aspects. Her paralleled work in finite element analysis is of great value to this project.

A special thanks goes out to Necip Berme and Cedric Sze, who both helped with the adhesion of the strain gages and wire soldering.

Furthermore, Mary Hartzler and Bob Miller have been exceptional resources in the molding lab and have helped me greatly in my willingness to learn and apply.

Finally, I would like to thank my wife, Jamie, for her support and extreme patience in my pursuit of a master's degree. She has stood by me and motivated me to pursue my dreams. To her, I say thank you.

VITA

March 23rd, 1979.....Born - Youngstown, Ohio

2001.....B.S. Mechanical Engineering, Cum Laude
The Ohio State University, Columbus, OH

2001-2003.....Product Engineer
The Timken Corporation, Canton, OH

2003-2004.....Graduate Teaching Assistant
Department of Mechanical Engineering
The Ohio State University, Columbus, OH

2004-2005.....Graduate Research Assistant
Department of Industrial Systems Engineering
The Ohio State University, Columbus, OH

FIELD OF STUDY

Major Field: Mechanical Engineering

TABLE OF CONTENTS

	Page
Abstract	ii
Acknowledgements	iv
Vita.....	v
List of Tables	viii
List of Figures	x
Chapters:	
1. Introduction.....	1
1.1 The Injection Molding Process	1
1.2 Project Description.....	7
2. Literature Survey	10
3. Experimental Setup.....	13
3.1 Experimental Setup.....	13
3.2 The Multi-Cavity Mold.....	13
3.3 Sumitomo SH50M Injection Molding Machine	23
3.4 Linear Variable Displacement Transformers	25
3.5 Mold Cooling Hardware	27
3.6 Data Acquisition System.....	29
3.7 Strain Gage and LVDT Calibration	31
4. Simulations	43
4.1 Simulations	43
4.2 MoldFlow TM Simulations	44
4.3 ABAQUS TM Simulations	52
5. Results.....	57
5.1 Results.....	57
5.2 Experimental Conditions	57
5.3 Strain Gage Results.....	65
5.4 ABAQUS TM Strain Results.....	79
5.5 LVDT Results	90

5.6 Part Results	102
6. Conclusions.....	116
6.1 Conclusions.....	116
6.2 Future Work.....	118
Appendix A: Specification for Sumitomo SH50M.....	121
References.....	123

LIST OF TABLES

Table	Page
3.1 Summary of LVDT sensitivities (in/V)	32
3.2 Summary of strain gage sensitivities ($\mu\epsilon/mV$).	39
5.1 Summary of maximum pack pressures relative to injection velocity.(All values are %FS of machine capability).....	59
5.2 Process parameters varied during the experiments.....	60
5.3 Summary of gate freeze off times (sec).	65
5.4 Summary of average strain at worst case loading condition for the injection of cavity configuration one. (40% FS injection velocity, 20% FS packing pressure)	67
5.5 Summary of average strain at worst case loading condition for the injection of cavity configuration two. (40% FS injection velocity, 20% FS packing pressure)	68
5.6 Summary of average strain at worst case loading condition for the injection of cavity configuration three. (40% FS injection velocity, 20% FS packing pressure)	68
5.7 Summary of average strain at worst case loading condition for the injection of cavity configuration four. (40% FS injection velocity, 20% FS packing pressure)	69
5.8 Summary of average strain at worst case loading condition for the injection of cavity configuration five. (40% FS injection velocity, 20% FS packing pressure)	69
5.9 Average strain on the mold during clamping (microstrain).....	72
5.10 Summary of the average mold separation at the parting plane at worst case loading condition for the injection of cavity configuration one. (40% FS injection velocity, 20% FS packing pressure).....	91

5.11	Summary of the average mold separation at the parting plane at worst case loading condition for the injection of cavity configuration two. (40% FS injection velocity, 20% FS packing pressure).....	92
5.12	Summary of the average mold separation at the parting plane at worst case loading condition for the injection of cavity configuration three. (40% FS injection velocity, 20% FS packing pressure).....	92
5.13	Summary of the average mold separation at the parting plane at worst case loading condition for the injection of cavity configuration four. (40% FS injection velocity, 20% FS packing pressure).....	93
5.14	Regression model fits for the mass response (configuration one).	109
5.15	Regression model fits for the D1 dimension (configuration one).....	110
5.16	Regression model fits for the D2 dimension (configuration one).....	110
A.1	Specifications for the Sumitomo SH50M injection molding machine.	122

LIST OF FIGURES

Figure		Page
1.1	Schematic of an injection molding machine.....	2
1.2	Generic mold cavity pressure history over an injection cycle.	5
1.3	Illustration of the molded part from the eight-cavity mold. (Dimensions in inches)	9
3.1	Image of the multi-cavity mold halves investigated.	15
3.2	Schematic of the tunnel gate in movable mold insert.	16
3.3	Schematic of a stacked strain gage rosette.....	19
3.4	Photograph of the strain gage rosettes mounted on the movable mold half.	21
3.5	Sumitomo SH50M and experimental setup used for the mold analysis.	24
3.6	Arrangement of LVDTs mounted to extensions fixed to the moving platen.....	26
3.7	Temperature controllers used to control the mold temperature.	28
3.8	Setup used for the data acquisition system for the mold analysis.....	30
3.9	Calibration Curve for LVDT0.	33
3.10	Calibration Curve for LVDT1.	34
3.11	Calibration Curve for LVDT2.	35
3.12	Calibration Curve for LVDT3.	36
3.13	Schematic of a quarter model Wheatstone Bridge.....	38
3.14	Image of the Wheatstone bridge circuitry and data acquisition hardware.	38
3.15	Calibration curves for strain gage rosette one.....	40

3.16	Calibration curves for strain gage rosette two.	41
3.17	Calibration curves for strain gage rosette three.	42
4.1	Midplane cavity mesh and 1-D tunnel gate mesh in MoldFlow™	46
4.2	Meshed cavity and runner system generated in MoldFlow™	47
4.3	Pressure at injection location over an injection cycle.	49
4.4	Cavity-runner pressure distribution in mold at t = 0.813 seconds. (corresponding to peak fill pressure)	50
4.5	Contour plot of melt freeze time for the sprue and runner system.	51
4.6	Solid, partitioned model generated in ABAQUS™	53
4.7	FEM free mesh generated in ABAQUS™	54
5.1	Strain Gage Locations and Orientations	70
5.2	Strain gage rosette 1 curves for configuration 1, 40% injection velocity and 20% packing pressure.....	75
5.3	Strain gage rosette 2 curves for configuration 1, 40% injection velocity and 20% packing pressure.....	76
5.4	Strain gage rosette 3 curves for configuration 1, 40% injection velocity and 20% packing pressure.....	77
5.5	Beam analogy for strain apparent in rosette 3.	79
5.6	Strain results generated in ABAQUS™ for direction 1. (Configuration 1, 40% FS injection velocity, 20% FS pack pressure)	80
5.7	Strain results generated in ABAQUS™ for direction 2. (Configuration 1, 40% FS injection velocity, 20% FS pack pressure)	81
5.8	Strain results generated in ABAQUS™ for direction 3. (Configuration 1, 40% FS injection velocity, 20% FS pack pressure)	82
5.9	Strain gage rosette one results comparison for configuration one (μϵ) for 40% FS injection velocity and 20% FS pack pressure.	83

5.10	Strain gage rosette two results comparison for configuration one ($\mu\epsilon$) for 40% FS injection velocity and 20% FS pack pressure.	84
5.11	Strain gage rosette three results comparison for configuration one ($\mu\epsilon$) for 40% FS injection velocity and 20% FS pack pressure.....	84
5.12	Strain gage rosette one results comparison for configuration four ($\mu\epsilon$) for 40% FS injection velocity and 20% FS pack pressure.	86
5.13	Strain gage rosette two results comparison for configuration four ($\mu\epsilon$) for 40% FS injection velocity and 20% FS pack pressure.	87
5.14	Strain gage rosette three results comparison for configuration four ($\mu\epsilon$) for 40% FS injection velocity and 20% FS pack pressure.....	87
5.15	Mold deformation prediction by ABAQUS TM for secondary and tertiary runner loading. (Configuration 1, 40% FS injection velocity, 20% FS pack pressure).....	89
5.16	LVDT curves for configuration 1, 40% injection velocity and 20% packing pressure.	94
5.17	LVDT curves for configuration 2, 40% injection velocity and 20% packing pressure.	95
5.18	LVDT curves for configuration 3, 40% injection velocity and 20% packing pressure.	96
5.19	LVDT curves for configuration 4, 40% injection velocity and 20% packing pressure.	97
5.20	MoldFlow TM prediction of cavity pressure distribution at the end of fill.	101
5.21	Sheffield Coordinate Measuring Machine.	103
5.22	CMM jig used to fixture parts during measurement.....	104
5.23	Schematic illustrating mold separation at the parting plane.	105
5.24	Main effects plot for mass (g) of cavity one, configuration one. (V =Injection Velocity, P = Packing Pressure)	108
5.25	Interaction effects plot for mass (g) of cavity one, configuration one. (V =Injection Velocity, P = Packing Pressure)	108

5.26	Main effects plot for dimension D1 (in) of cavity one, configuration one. (V =Injection Velocity, P = Packing Pressure)	111
5.27	Interaction plot for dimension D1 (in) of cavity one, configuration one. (V =Injection Velocity, P = Packing Pressure)	111
5.28	Main effects plot for dimension D2 (in) of cavity one, configuration one. (V =Injection Velocity, P = Packing Pressure)	112
5.29	Interaction plot for dimension D2 (in) of cavity one, configuration one. (V =Injection Velocity, P = Packing Pressure)	112

CHAPTER 1

INTRODUCTION

1.1 The Injection Molding Process

“They don’t make them like they used to.” This common phrase can be heard today when people describe things like a vacuum cleaner or automobile. Why? Well many things today are composed mainly of thermoplastics, unlike the ferrous days of the past. Polymer products are an integral part of our everyday lives, from the medical field to the automotive industry. They can vary in geometry from simple to complex. Accuracies of products can vary depending on the fit, form, and function of the product. Some products are produced one at a time, while others are produced in high volume. Many of these parts are produced to net shape, requiring little or no additional processes to finish a part. A common process used in the production of these polymer products is injection molding. Injection molding is a process in which a polymer is melted and injected into a mold cavity in order to produce a negative of the mold itself. Molding machines can range in size and complexity, varying according to the size and complexity of the product itself. Figure 1.1 shows a generic schematic of an injection molding machine.

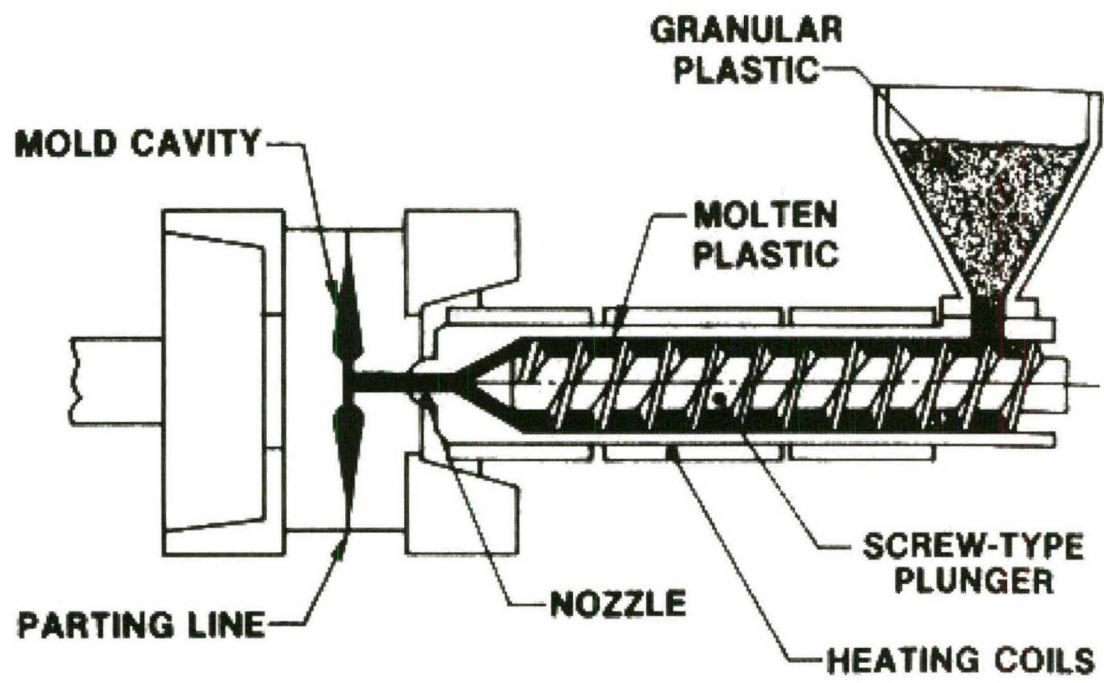


Figure 1.1: Schematic of an injection molding machine.
(Reference: www.cnpkg.com/injectionmolding.asp)

The molding process itself is relatively simple. The three main stages that occur during the molding process can be seen in Figure 1.. The first stage, being the filling or injection phase, is where a polymer melt is injected into the mold cavity by an injector screw. A clamping system is engaged during injection to keep the mold closed. After the polymer has filled the mold cavity, the polymer is placed under a high pressure and held. This stage of the process is the holding or packing phase. Parts are held under pressure to ensure the cavity has completely filled, as well as reduce the chance of part shrinkage and/or other part defects. The final stage of the process is the cooling phase. This stage allows the part(s) to cool in the mold cavity until the polymer has solidified. Once solidification has occurred, the mold can be reopened and part(s) can be ejected from the mold. During this time the injection unit will plasticize more polymer for the next shot into the mold. The process can then repeat itself.

The molding machine is comprised of many thermal, mechanical, and electrical systems that work together in synchronization to produce parts. The polymer is generally melted using multiple heater bands located around the injector screw unit. The injector screw unit is fixed on a moveable platform that is typically hydraulically controlled. The platform moves the injector head to contact the sprue bushing on the mold. The mold itself may contain cooling lines in order to maintain a desired mold temperature, as well as improve the cooling time, reducing the overall cycle time. Typically a machine has two platens. One platen remains stationary while the other platen is moveable. The moveable platen slides along on tie rods and is controlled by the clamping unit. The clamping unit is typically a hydraulic system operated through the machine controller.

This unit will usually contain the ejector system as well, which ejects the parts from the mold at the end of the cooling phase.

Pressure History in an Injection Molded Part

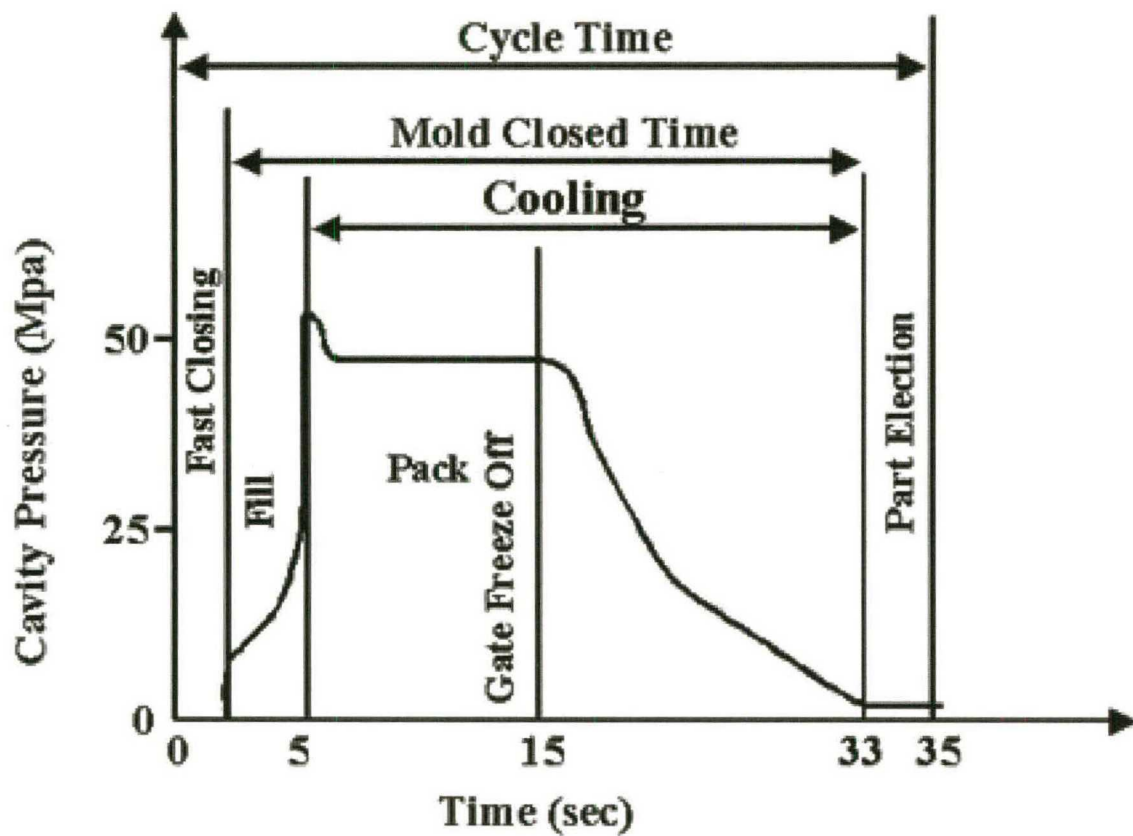


Figure 1.2: Generic mold cavity pressure history over an injection cycle.
(Reference: islnotes.cps.msu.edu/trp/inj/int_bas.html)

This molding process is representative of the classic manufacturing problem of minimizing cycle time and maximizing part quality. In the end, quality constraints will dictate the cycle time. Quality is not just a function of the dimensional characteristics of the mold, but the process parameters as well. In the case of multi-cavity, high precision parts, and aside from mold construction, thermal effects, mold separation at the parting plane, and mold deflection can affect the quality of a part. As previously mentioned, part shrinkage plays a large role in the molding of plastic parts. Typically an engineer will compensate for shrinkage by designing a mold cavity to be larger than the final product. While a good mold operator can minimize shrinkage effects by optimizing process parameters, shrinkage can never be fully eliminated, only minimized. Especially in multi-cavity molds, it is important to reduce shrinkage and minimize any part variance from cavity to cavity.

Even though a mold unit is clamped under high pressure, excessive clamping can cause mold distortion, which can lead to other types of part defects. While clamping loads are adjusted to reduce mold distortion they may in fact not be large enough to resist mold separation at the parting plane. This phenomenon can occur at the end of the filling phase and/or at beginning of the packing phase, also known as the velocity-pressure switchover. Here is where the mold cavity pressure is typically near or at a maximum. Any finite separation of the mold that exists may lead to a growth in overall part width, especially if the gates of the parts have not solidified. If the mold separation is non-uniform across the mold face in a multi-cavity configuration, part variance will not be

minimized. Therefore, it can be seen that understanding this phenomenon could be extremely helpful in a mold optimization problem.

Finally mold deflection itself can be an issue in high dimensional accuracy parts. While machine designers try to reduce machine deflections, the platens and molds are not rigid bodies. In reality, if the machine was extremely rigid it could not comply with the extreme loading conditions it may see in a cycle. This would result in large concentrated stresses in the machine itself, including the mold halves. Likewise, if a mold cavity deforms under load and the deformation is retained during the part solidification, then the mold cavity deformation will be transferred to the molded parts. While some mold deformation is unavoidable it is preferred to minimize this effect in order to achieve good quality control. In fact, there are great advantages in estimating deformation for part compensation optimization.

1.2 Project Description

Multi-cavity, thin-walled molds make up a large portion of the thermoplastic molding industry today. In this project the aforementioned quality issues: mold parting plane separation and mold deformation, will be studied experimentally in an eight-cavity mold. Preliminary investigation showed the eight-cavity mold of interest to have excellent thermal characteristics, so thermal effects will not be studied at this time, only minimized. Mold separation will be evaluated using four linear variable displacement transformers (LVDTs) affixed to the moving platen. The transducers will be used to measure the absolute displacement between the two mold halves. Ideally, the LVDTs

would be affixed to the mold halves themselves, but due to space and size constraints they will be mounted on the moving platen.

Mold deflection will be analyzed using strain gages mounted to the mold itself. Due to accessibility, three strain gage rosettes will be mounted on the back surface of the moveable mold only. In an initial investigation, parts measured on a coordinate measuring machine (CMM) showed the greatest change in dimensions, relative to changes in process parameters, were molded from the moveable mold half. A separate but parallel research project, involving a finite element analysis (FEA) simulation of the mold will be generated using the software package ABAQUS™. Experimental results from the strain gage data will be compared to the finite element model (FEM) in an effort to validate the model's prediction capabilities. With a good correlation of the FEM to the experimentation, the model could then be used as a numerical solution to quantify mold deformation.

Due to the large amount of process parameters available for optimization, the two parameters of greatest interest in this study are injection velocity and packing pressure. It is predicted that these two parameters have a dominating effect on mold deformation and mold separation at the parting plane. Experimentation will be conducted with a small design of experiments (DOE) varying the previously mentioned parameters over three levels each. The eight-cavity mold also has the capability to turn off a gate of any cavity allowing a finite number of mold configurations. Various cavity configurations will also be investigated in this study. The following figure displays an image of the parts to be molded in this study.

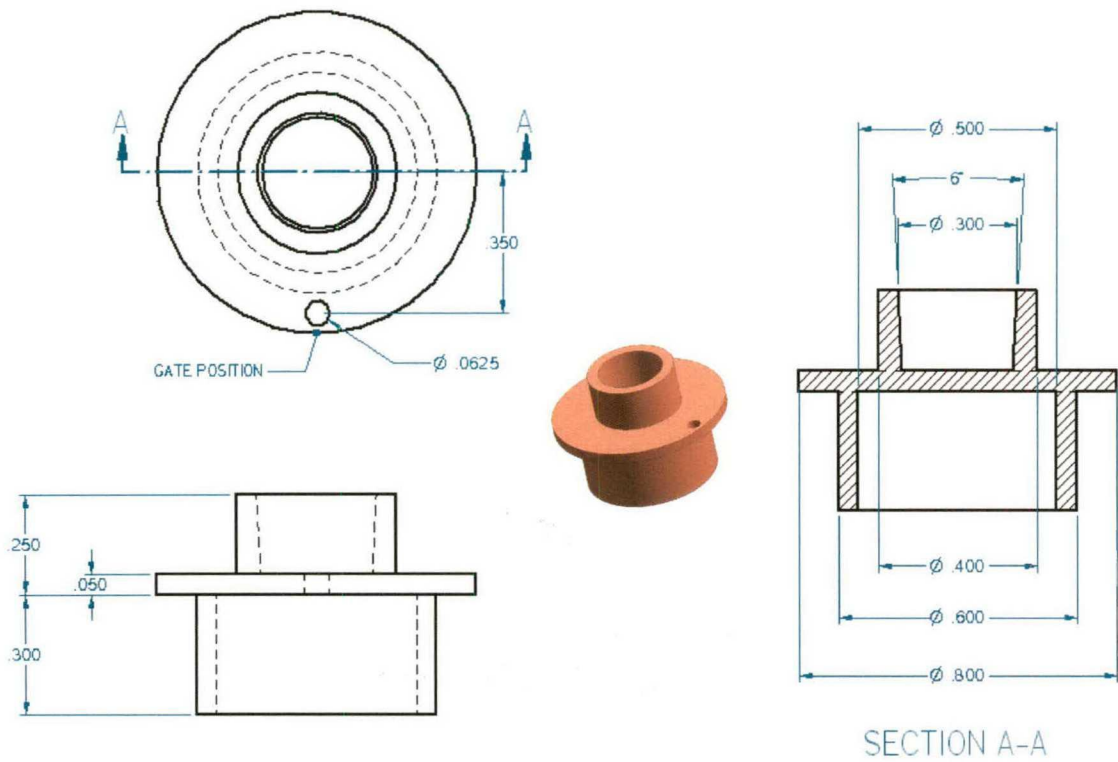


Figure 1.3: Illustration of the molded part from the eight-cavity mold
(Dimensions in inches)

CHAPTER 2

LITERATURE SURVEY

While performing the literature survey, little information was found that dealt with elastic mold deformation analysis and mold separation at the parting plane for the injection molding process using multi-cavity molds, producing thin-walled parts. Prior research has been conducted to quantify similar phenomena for die casting, using both Finite Element Analysis (FEA) and experimental methods. [1,2] While functionally similar to injection molding, die casting typically involves the injection of a molten material, such as zinc, magnesium or aluminum, into a steel die cavity. Die and material temperatures are in general much higher in die casting and the process itself tends to be much more damaging to the dies themselves.

The most recent mold deformation analysis in injection molding was performed as a graduate research study at The Ohio State University. [3] A large one-cavity mold was equipped with strain gages and pressure transducers to measure mold deflection during an injection cycle. Experimental data was combined with a Finite Element Model (FEM) of the mold to predict elastic mold deformation. MoldFlow™, an injection molding software package, was used to predict the cavity pressure distribution, which was in turn used in an ABAQUS™ structural model to predict mold deformation. Strain results from the experiment were used to assess the predictive capabilities of the

simulation. In the end, the FEM was again in the “ball park” in terms of its predictive capabilities. As in most Finite Element Models, the definition of the model, its boundary conditions and model interfaces, were deemed of utmost importance.

Further experimental work has been executed in the investigation of mold separation at the parting plane in thin-walled parts in injection molding. [4] Chen et al. investigated the effects of process parameters on mold separation at the parting plane in a two-cavity mold. Four LVDTs, affixed to the four corners of the mold halves were used to measure the mold separation at the parting plane during an injection cycle. Maximum mold separation was found to occur at the end of the filling regime, where the internal cavity pressure was highest. It was determined that part weight exhibited a “monotonic correspondence with mold separation.” An ANSYSTM FE simulation was performed to validate the use of CAE predictive tools for such a process. Correlation results showed “good coincidence” and had “reasonable consistency with physical experiments.”

Additional work has also been performed in the area of process control in order to compensate for mold separation during the injection molding process. [5] The research was focused on identifying the main effects parameters to use in a closed-loop control system to optimize an injection cycle for minimal mold deflection. Parameters such as packing pressure and injection velocity were found to be important to the control of mold deflection. The concept involved adding a mold-deflection transducer, requiring “little or no tooling work.” The machine control operator would be required to set acceptable mold deflection magnitudes. The loop control would then adjust parameters such as packing pressure during an injection cycle to minimize mold deflection.

A study by Delaunay and Le Pot, on the influence of mold deflection on pressure history and shrinkage was also found. [6] This study focused on two things: mold rigidity and the effect of mold deformation on part dimensional properties for a single plate cavity. It is believed that with the estimation of mold rigidity, molds can be designed to reduce mold deflection. In-plane shrinkage was determined to be “less influenced” by any mold deflection, where as part thickness was more affected.

Finally, Leo and Cuvelliez [7], performed a study on the effects of packing parameters and mold elasticity on the final dimensions of a molded, flat, thin walled plate approximately 40mm by 150mm. Conclusions were made that constant packing pressure and a large gate could in “no way” make a part with uniform shrinkage. Parts with smaller gate geometry showed more correlation to filling parameters, as parts are typically “interrupted by the early freeze-off of the gate.” Furthermore, in an overpacking condition, where the final part dimensions are greater than the internal cavity dimensions, showed a residual cavity pressure at the end of the cycle. Expected overpacking was predicted to occur between 100-150 MPa, where experimentally it was seen as low as 60 MPa. The observed overpacking effects played a role in the elastic mold deformation and packing efficiency. As a mold deformed and packing efficiency increased, the stored energy in the mold walls was used to further pack the polymer. Hence, resulting in an oversized part.

CHAPTER 3

EXPERIMENTAL SETUP

3.1 Experimental Setup

In order to investigate the molding process and phenomena of interest during molding, experiments were conducted using a Sumitomo SH50M injection molding machine. An experimental eight-cavity mold was used with three strain gage rosettes applied to the back surface of the movable mold half. LVDTs were also utilized in the experiment in order to analyze mold parting plane separation during the filling and packing of the mold. Two Advantage SK-1035 temperature controllers, a coolant manifold, laptop computer, and National Instruments data acquisition hardware were also used. While it is important to discuss each of these in more detail, it is most important to discuss the eight-cavity mold and its features.

3.2 The Multi-Cavity Mold

The eight-cavity mold used in the experiment was designed and built as a master's thesis project by Eric J. Wilson at The Ohio State University. The project, funded by the Kodak Eastman Company, was to design and build a high precision mold with great flexibility and interchangeability. The mold, pictured below in Figure 3.1, was designed to have an interchangeable insert-core system, which allows cavities to be

repositioned in the mold. The inserts themselves are made from P-20 tool steel and the cores are made from Moldmax XL copper-nickel-tin alloy. The Moldmax XL has excellent thermal conductance properties, and is highly efficient in removing heat from the cavity during the injection cycle. The molded part itself is molded from the geometry located on both mold halves' insert-core system. Each mold half is constructed of two plates that are fastened together. The mold halves both have complex assemblies consisting of many components. Therefore, there is some question as to whether the mold's rigidity will play a large role in its response to the application's loading conditions.

The mold runner system is machined completely into the moving mold half. Each cavity is connected to a runner by a single tunnel gate. The tunnel gate is a unique gating system that allows the molded parts to be separated from the runner during part ejection. The gates, as seen in Figure 3.2, were generated using an EDM machine, and "tunnel" under the parting plane of the mold. In this design, the tunnel gate has a conical shape. It is vital that each gate remain smooth, as any minute scratches on the surface could cause the solidified polymer to adhere to the gate surface during part ejection. This could cause lengthy delays in the production of parts. Due to the complex gate geometry and manufacturing process, there are some inconsistencies in size from gate to gate. These differences will be further discussed later in conjunction with the results. The runner system is designed so that the runner length from the sprue is equidistant to each cavity. This helps reduce any unbalance in the runner system.

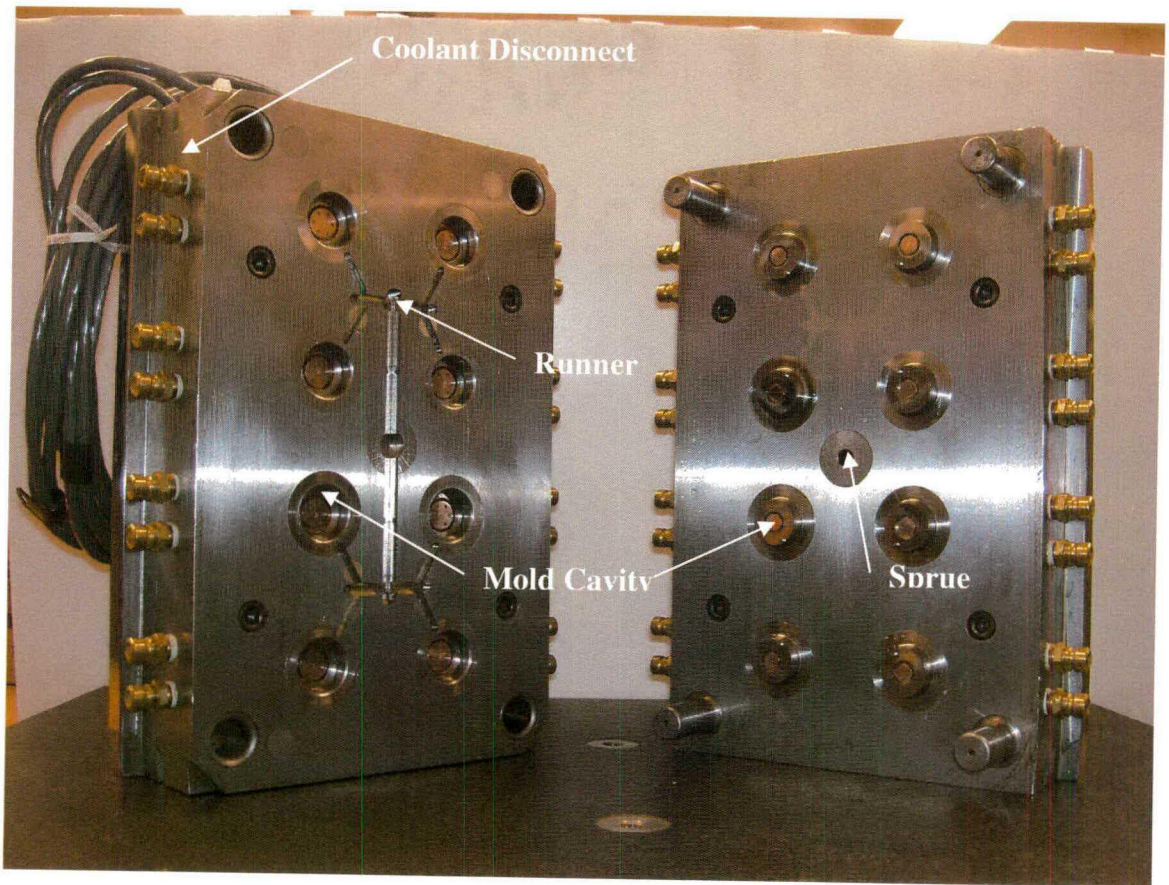


Figure 3.1: Image of the multi-cavity mold halves investigated.

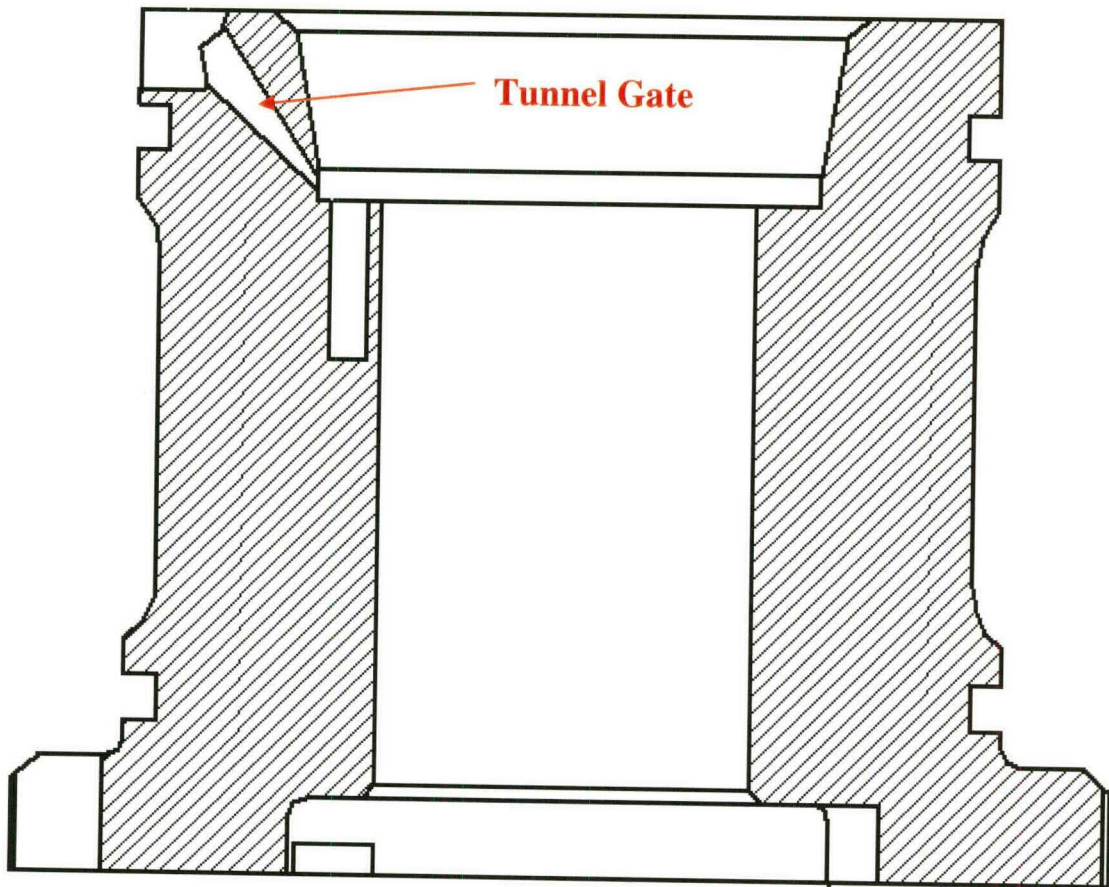


Figure 3.2: Schematic of the tunnel gate in movable mold insert.

Another beneficial feature designed into the mold was a valve at each gate. The gate valve offers the mold a great flexibility in that the number of injectable cavities can range from none to eight. This provides the user a large range of cavity configurations to study and will be utilized in the study of the mold.

Each cavity is designed to have its own cooling channel. Figure 3.1 above shows the cooling channel disconnects for the mold's cavities. This would allow a user to control the coolant to each cavity independently, allowing for a greater optimization of the mold and further opportunity for experimental studies. There are also cooling channels built in each mold half around the runner system and the sprue bushing. All of these design features make the mold a very efficient heat removal system. It is important to note that the fixed mold half has a tapered feature that mates to the movable mold half. Therefore, the mold halves must have similar temperatures maintained in order to prevent the mold halves from expanding at different rates and causing potential problems during clamping.

As previously mentioned, the movable mold half is equipped with three, stacked, rectangular, strain gage rosettes. The rectangular $0^{\circ}/45^{\circ}/90^{\circ}$ rosettes are equipped with three strain gages each. Each strain gage has a resistance of $120\ \Omega$ and a gage factor, S_g , of 2.11. The decision for strain gage placement was determined by the space availability in and around the mold, as well as preliminary investigations in the molded part dimensions. An early study showed the dimensional features with the most variance were molded from the movable mold insert-core. Therefore it was decided to focus on the movable mold half in the analysis of the process. In order to prevent interference

with the complex ejector pin system on the movable mold half, the gages were positioned so as to reduce the risk of contact with the ejector plate on the mold. A schematic of a strain gage rosette can be seen in Figure 3.3 below.

It is also important to note that the strain gages were specified with a thermal compensation feature. This is advantageous when a strain gage is mounted on a surface that may see a large temperature change over time. Fortunately, during the experiments, the temperature does not largely exceed room temperature. Furthermore, the strain gages are far removed from the surfaces in direct contact with the molten polymer. Because of the thermal compensation feature, if the mold were to be run without coolant, the strain gages would compensate for any erroneous thermal effects.

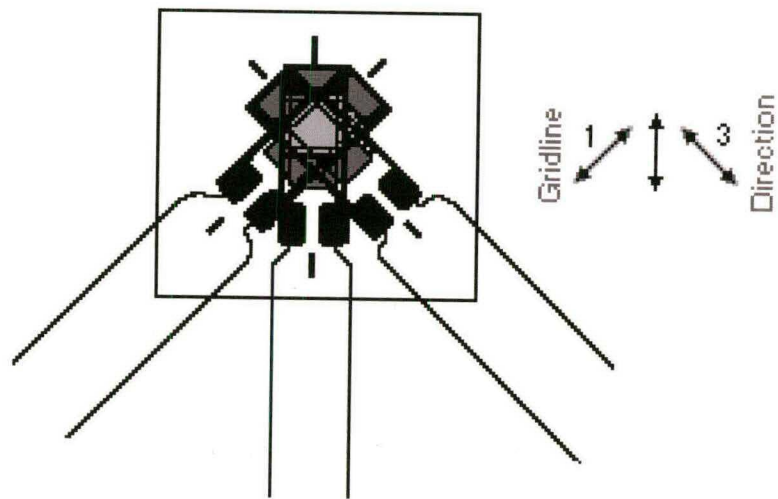


Figure 3.3: Schematic of a stacked strain gage rosette.

The first strain gage was positioned on the mold vertical centerline between the guide-pin holes atop the mold back face. The second strain gage was positioned near the center of the mold. An ejector pin is located in the mold's center so the gage had to be slightly offset. Finally, a third gage was positioned on the mold horizontal centerline near the mold guide wings, which locate the mold in the Master Unit Die (MUD) base. Figure 3.4 shows a photograph of the mounted positions of the strain gages on the actual mold.

The strain gages themselves were mounted with a 100% solids epoxy adhesive, Vishay bond kit AE-10. The adhesive has very good moisture resistant properties and heat resistant properties, well withstanding operating temperatures up to 95° C. These adhesive thermal characteristics are important because the mold may be run with or without coolant. Additionally, when the mold is run with coolant there may be a considerable of moisture in the system, so its moisture resistant properties are important as well. Each strain gage's lead wires were soldered to a terminal, which in turn were soldered to twisted, magnetically shielded wire. Each wire was carefully strain relieved in order to prevent inaccurate strain readings as well as resist any contact with the ejector pin system.

A strain gage rosette is used in order to determine the principal strains and principal strain orientation at a point on the mold that can be later compared to an ABAQUS structural simulation. If the strain is known in any three directions at a point, the principal strains can be calculated. Using the following strain gage theory equations, the correlating experimental strain gage readings can be converted into principal strains.

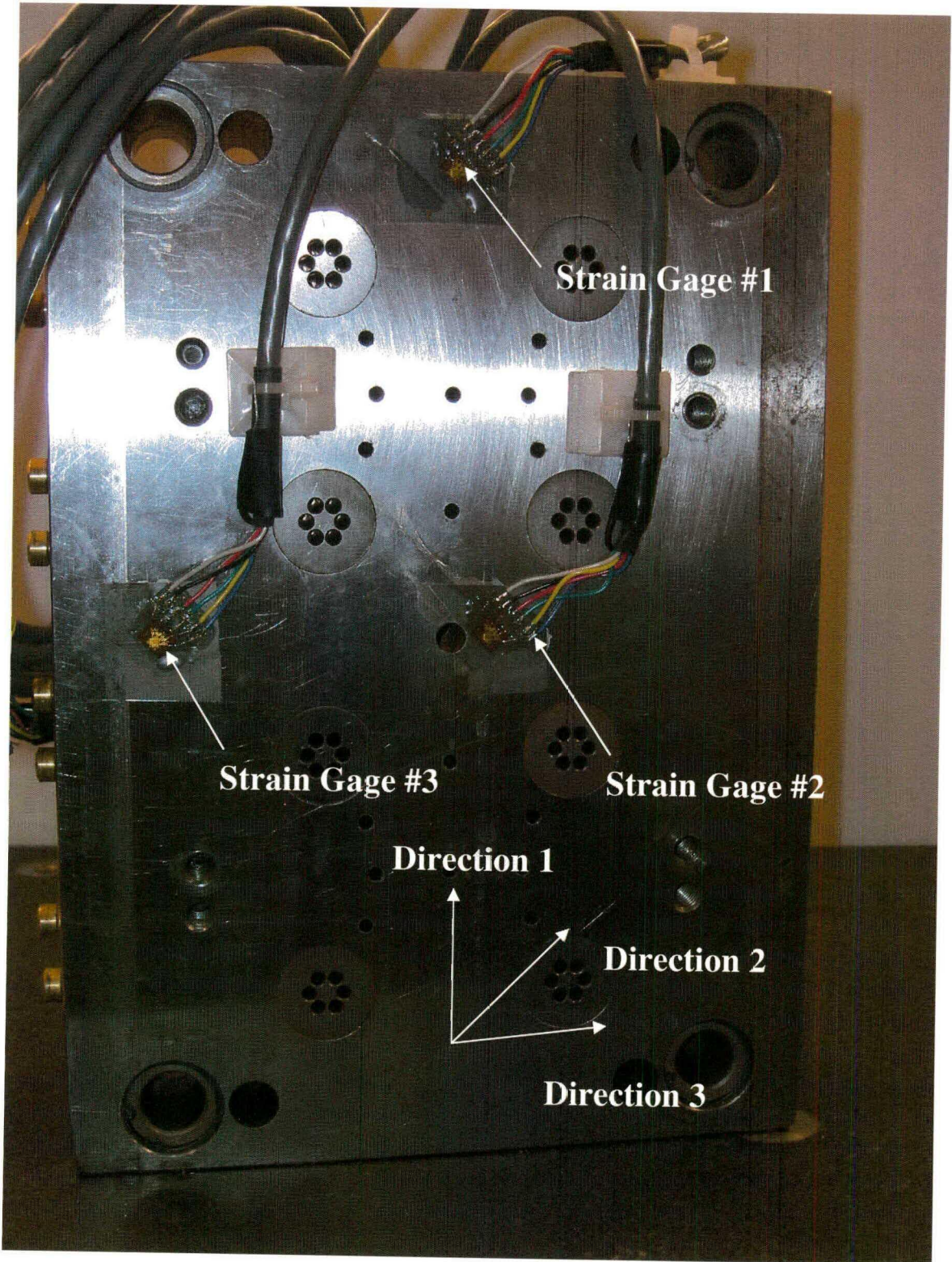
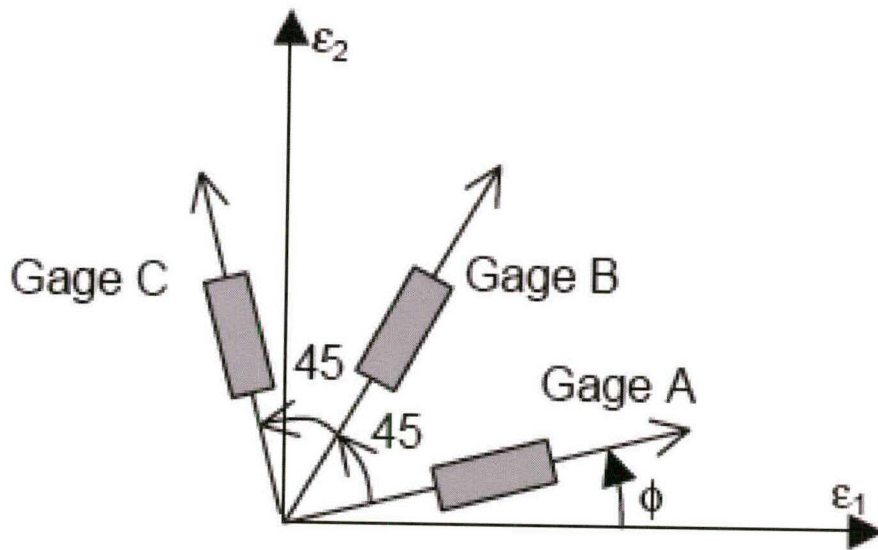


Figure 3.4: Photograph of the strain gage rosettes mounted on the movable mold half.



$$\varepsilon_{1,2} = \frac{\varepsilon_A + \varepsilon_C}{2} \pm \frac{1}{\sqrt{2}} \sqrt{(\varepsilon_A - \varepsilon_B)^2 + (\varepsilon_B - \varepsilon_C)^2}$$

$$\phi = \frac{1}{2} \tan^{-1} \left(\frac{\varepsilon_A - 2\varepsilon_B + \varepsilon_C}{\varepsilon_A - \varepsilon_C} \right)$$

Equation 3.1: Strain gage rosette equations used to calculate the principal strains.

In the eight cavity mold, the C direction in Equation 3.1 is chosen in the vertical direction, the B direction is 45° clockwise to direction one, and the A direction is 90° clockwise to direction one. Each strain gage is connected to a Wheatstone bridge that is used to analyze the small strain changes in the mold. The calibration of these strain gages and details pertaining to the Wheatstone bridge circuitry will be discussed in Section 3.7.

3.3 Sumitomo SH50M Injection Molding Machine

All experiments were conducted on a Sumitomo SH50M injection molding machine. The machine, as seen in Figure 3.5, uses a hydraulic clamping and injection unit. The hydraulic clamping unit has a maximum mold clamping force of 50 metric tons and maximum injection velocity of 160 mm/sec. There are four electric heating elements on the screw barrel that melt the polymer during its operation. Additional machine specifications can be found in detail in the Appendix A.

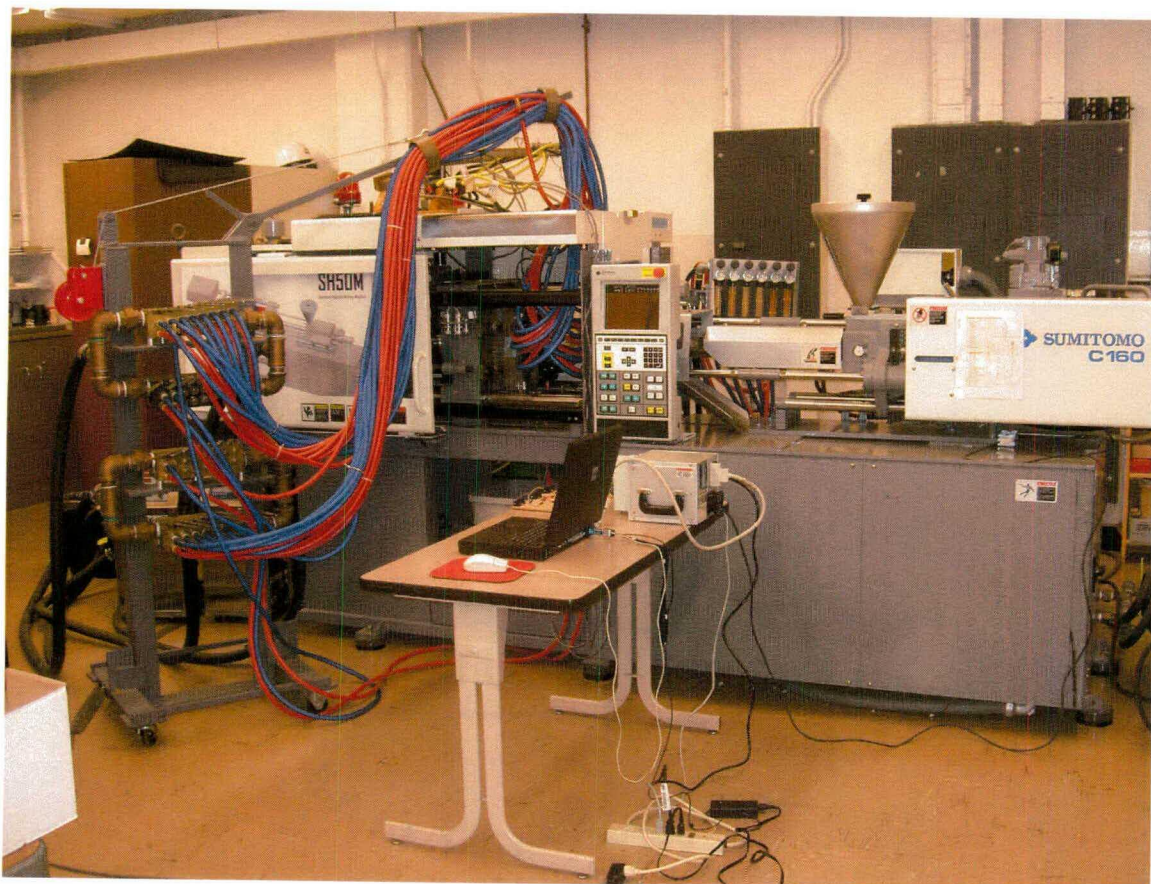


Figure 3.5: Sumitomo SH50M and experimental setup used for the mold analysis.

3.4 Linear Variable Displacement Transformers

While the strain gage rosettes are used to measure the strain in the mold and correlate to mold deformation, four linear variable displacement transformers or LVDTs, are utilized to measure the mold separation at the parting plane during the injection cycle. The LVDTs, manufactured by Schaevitz, have a full linear range of ± 0.125 inches. They were individually mounted to the moving platen with mounting extensions as seen in Figure 3.6. Ideally, the LVDTs would have been mounted rigidly to the mold halves themselves, but due to spatial limitations and unwanted mold modifications, it was decided to mount the gages to the moving platen. Due to the fact that both platens are rigid compared to the mold halves it is believed that any relative platen deformation would be negligible. Furthermore, there are many other transducer options that would better suit this application in accuracy and space limitations. But, due to cost constraints and the availability of existing hardware, it was decided the LVDTs would be suitable for this study.

In addition to the four LVDTs mounted to the moving platen there is a LVDT mounted to the injector screw on the injection unit. This LVDT has a six-inch range and uses a 24 V DC excitation voltage that is provided by a voltage transformer that uses 110VAC at 60 Hz. The LVDT will be used to monitor the injector screw position relative to the strain gage and LVDT data. The signal will provide an understanding of what occurs during an injection cycle.

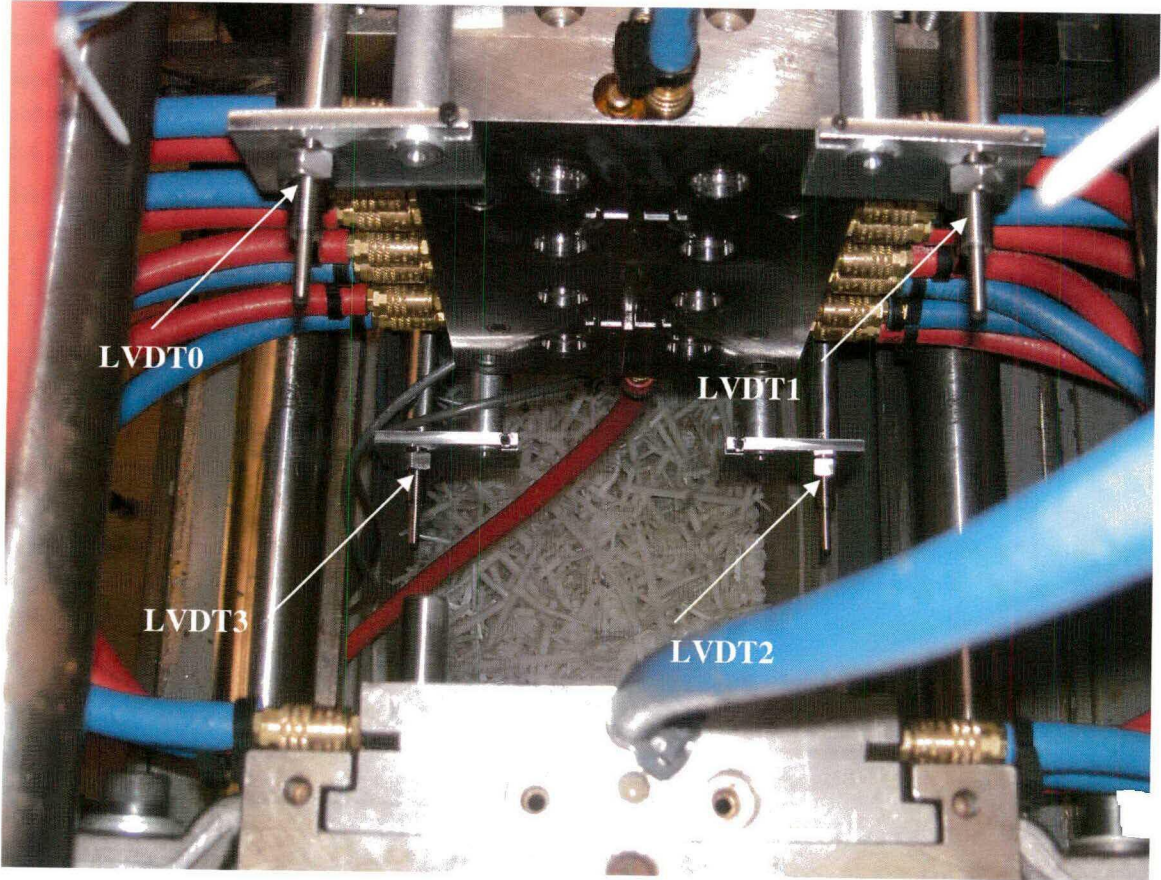


Figure 3.6: Arrangement of LVDTs mounted to extensions fixed to the moving platen.

3.5 Mold Cooling Hardware

During the conducted experiments it was important to minimize thermal effects that may effect the part variance. To do this, the mold coolant temperature was run near room temperature, at 75° F. This was accomplished by using two Advantage SK-1035 temperature controllers as seen in Figure 3.7. Each controller was utilized to individually regulate the flow and temperature of coolant sent and received from a single mold half.

Before the coolant was sent to the mold it was dispensed to each set of coolant lines through a manifold. The manifold divides the flow of coolant to each set of cooling lines equally. It also allows the control of flow to each set of coolant lines through valves located internally to the manifold. For the experiments performed the valves remained open to their full position in order to achieve maximum flow and optimal heat removal. Each cooling line connects to the mold with a valved coupler that allows a quick, leak-proof connection. The cooling manifold is visible in Figure 3.5 above. Each set of lines is color coded for a send or return line. From Figure 3.6 above, the cooling lines can be better seen as they are attached to the mold. Because the lines may cause some resistance to the mold, as it is in its closed position, all experiments were run with these lines intact in order to minimize any underlying effects on the results.



Figure 3.7: Temperature controllers used to control the mold temperature.

3.6 Data Acquisition System

The data acquisition setup used to collect data was comprised of a Dell laptop computer and National Instruments (NI) data acquisition hardware. The data acquisition card had sixteen available channels, of which eight were utilized. A NI terminal block SCXI 1321 was used to collect the strain gage data and LVDT data from the injector screw. The terminal block itself had four usable channels. Channel one was used to capture the injector screw position and channels two through four were used to capture the three directions of a single strain gage rosette. Due to the fact that three rosettes with three strain gages were used, a total of nine channels would have been required to capture all of the strain gage data at once. Because of the terminal block's limitation the experimental conditions were repeated three times in order to obtain all of the strain data during one injection cycle.

The terminal block 1321 provided a 3.33 V excitation voltage for the strain gages as well as their balancing circuitry. An external transformer supplied the excitation voltage for the LVDT on the injector screw. Internal jumpers on the terminal block were set for the signals to be conditioned with a 4 Hz low pass filter. The gain for the LVDT channel was set to 1 while it was set to 1000 for the strain gages. These values helped minimize the noise in the signal while producing the most visible signal.

Furthermore, an additional NI terminal block, SCXI 1315, was used to obtain the LVDT signals used in the separation of the mold parting plane analysis. The terminal block, with 8 usable channels, was set for a 4 wire LVDT to use a 3 V_{RMS} voltage at 10kHz. Similar to the 1321 terminal block, the gain was set to the terminal block

operations manual recommendation. A software program called LabView™ was used to collect the data for all eight channels simultaneously. The strain gages and LVDTs were sampled at a frequency of 1 kHz, and the output was stored in a spreadsheet format for further analysis.

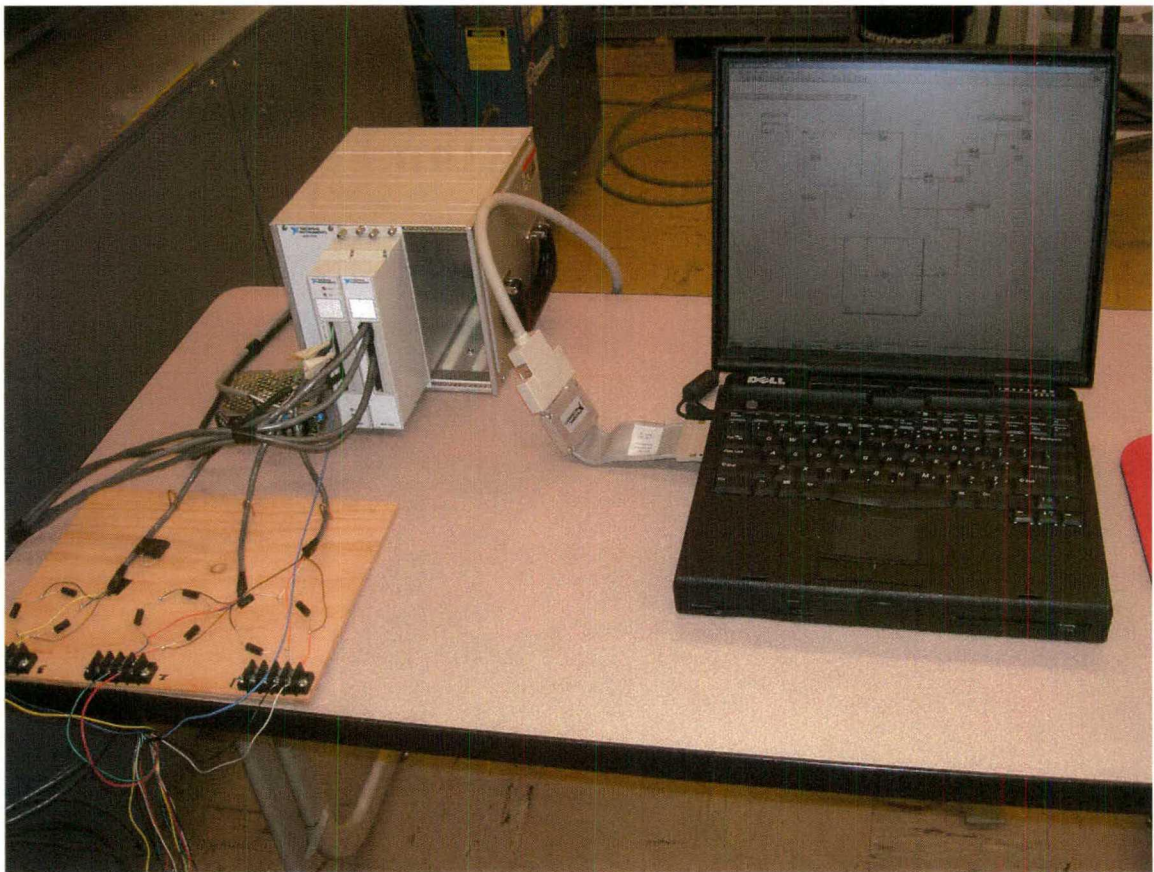


Figure 3.8: Setup used for the data acquisition system for the mold analysis.

3.7 Strain Gage and LVDT Calibration

While the methods of measuring the desired transducer's output have been discussed, it is also important to calibrate each device accurately in order to correlate the recorded voltage data in the data acquisition to the proper units. In total, there were three sets of calibrations performed, each of which was performed with the help of LabView™.

The first calibration performed was for the LVDT on the injector screw. The LVDT is an extremely linear device and a two-point calibration was performed using the Sumitomo machine controller. Since this LVDT is only used to understand the position of the screw relative to the strain gage and LVDT data on the platen, a high precision calibration is not required. The calculated sensitivity of the LVDT injector screw was determined to be 0.499 inch/V.

The next devices calibrated were the LVDTs used to measure the mold parting plane separation. In order to calibrate the LVDTs with extreme precision, a Mitutoyo micrometer with a precision of 0.0001 inches was used. The micrometer was mounted in a jig that would locate the LVDT opposite the micrometer head. The LVDT was compressed to a similar distance it would see when mounted in the injection molding machine. The LVDT was calibrated to eleven points over a 0.25 inch range. The calibration was performed multiple times to ensure repeatability in the calibration curve. The summary of the LVDT calibration sensitivities can be found in Table 3.1. These values will be used to convert the voltage signals from the LVDTs acquired during the experiment.

LVDT	0	1	2	3
Sensitivity	0.1649	0.1578	0.1588	0.1609

Table 3.1: Summary of LVDT sensitivities (in/V)

The repeatability of the LVDTs was experimentally determined to be ± 0.0001 ". The repeatability was investigated from an increasing and decreasing measurement so hysteresis would be taken into account. Figures 3.9-3.12 show the calibration curves for each LVDT. It should be noted that LVDT2 had the worst variance from calibration to calibration.

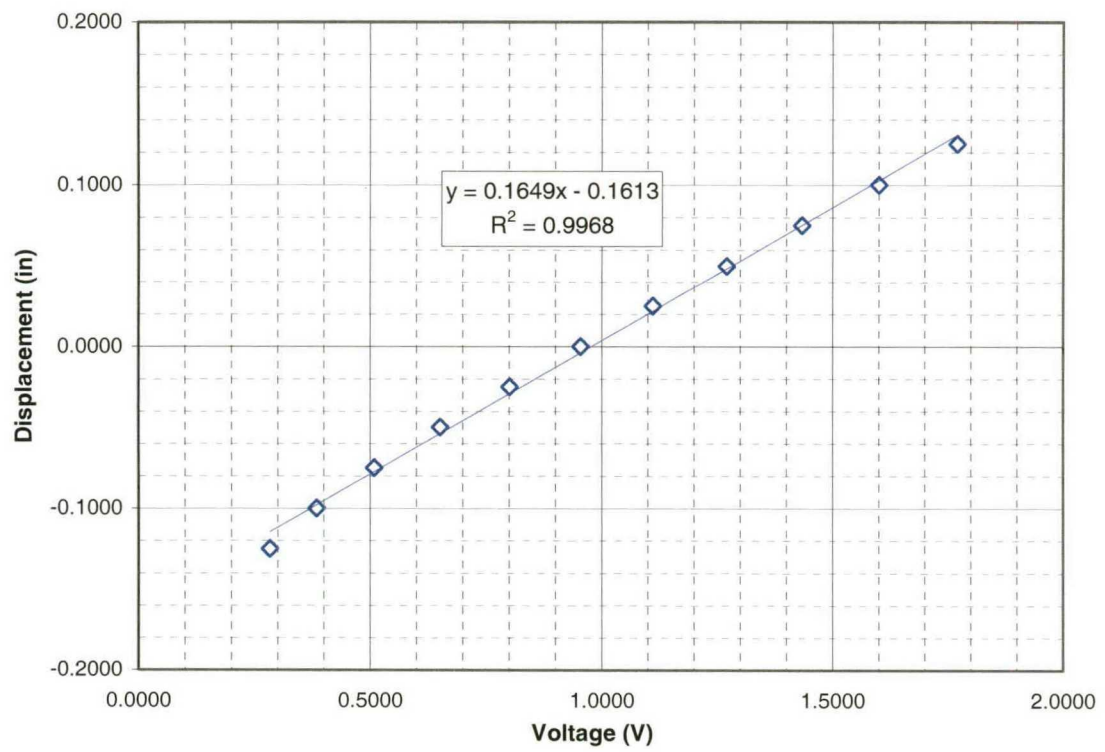


Figure 3.9: Calibration Curve for LVDT0.

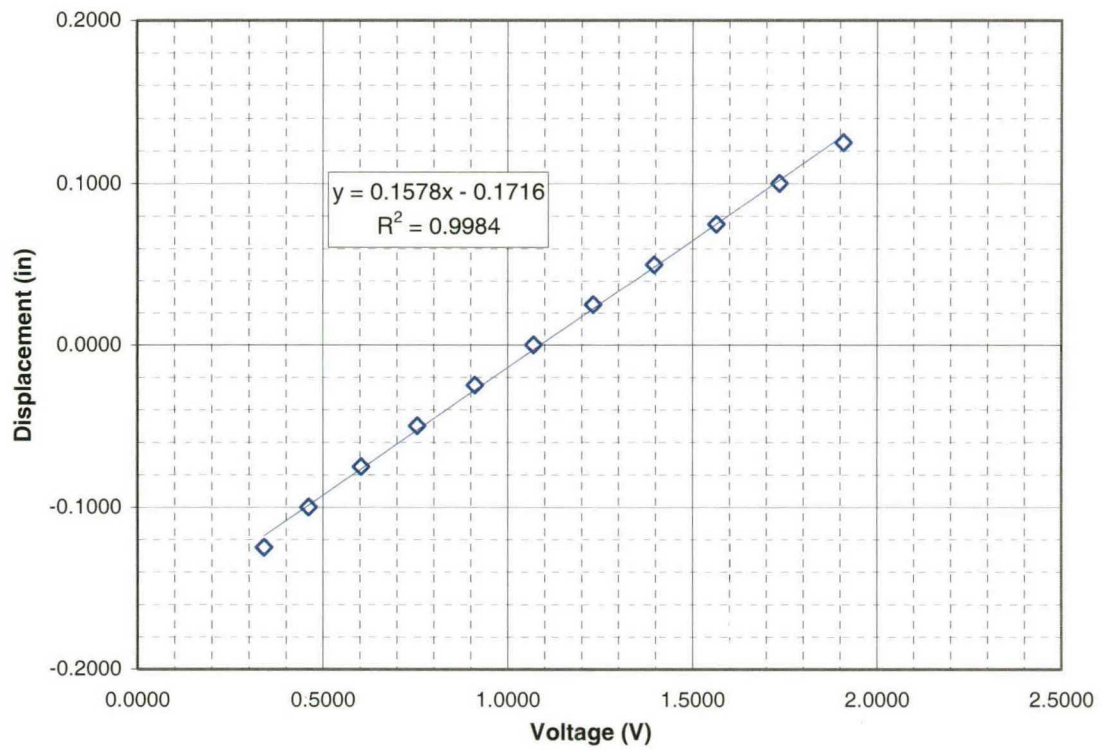


Figure 3.10: Calibration Curve for LVDT1.

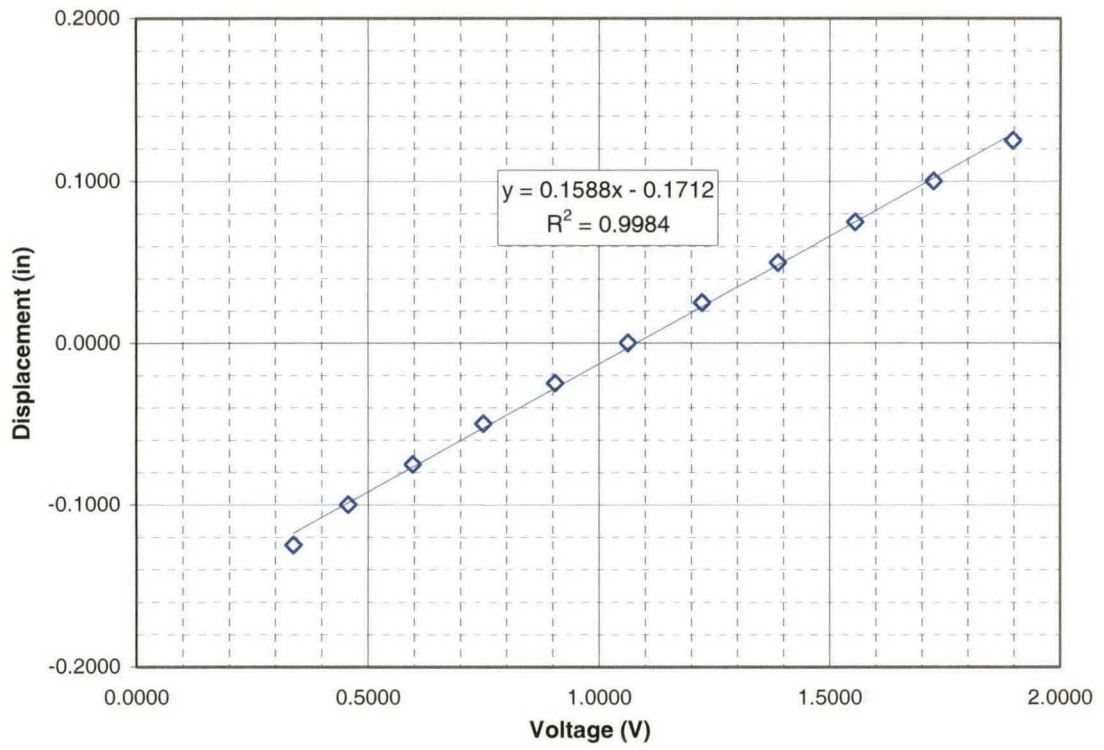


Figure 3.11: Calibration Curve for LVDT2.

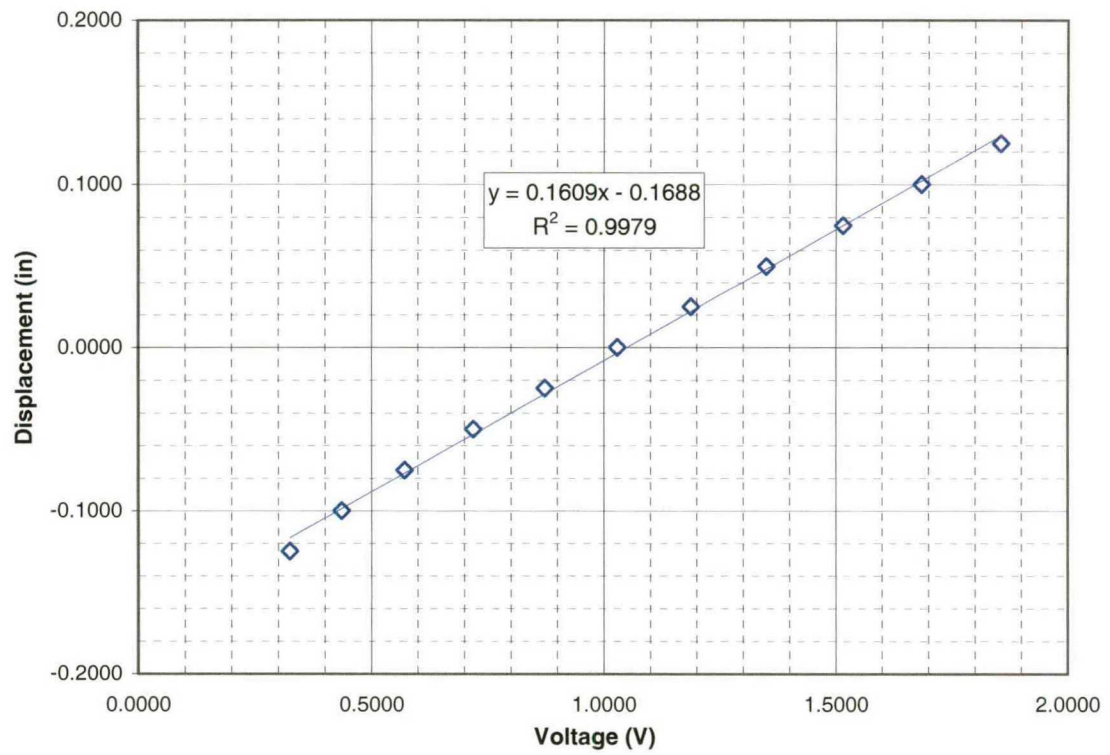


Figure 3.12: Calibration Curve for LVDT3.

The final transducers calibrated were the strain gage rosettes. The strain gages were used in conjunction with a Wheatstone bridge, and represent one leg of the Wheatstone bridge, also known as a one-quarter bridge. Fortunately, from a previous master's thesis project, the Wheatstone bridge circuitry preexisted and was utilized.

All of the bridges used in the experiments have a sensitivity of approximately one. In other words, each leg of the bridge has an equivalent resistance. Therefore, each leg of the bridge has an electrical resistance of 120 Ω . The resistances were carefully verified with a multi-meter. The Wheatstone bridge works as follows: when the resistance of one leg in the bridge changes (i.e. strain gage) a voltage change can be measured across the bridge. This voltage change can be correlated to a resistance change of the corresponding leg in the bridge. For a strain gage, there is a correlation between a resistance change and a change in strain. This correlation was calculated in the calibration experiment.

Since strain gages are extremely linear devices, a two-point calibration was performed. For the calibration, a shunt resistor of known resistance, R_c , is placed in parallel to the strain gage of resistance, R_g , with strain gage factor, S_g , and a simulated strain on the gage, ϵ , can be calculated by the following equation:

$$\epsilon = \frac{R_g}{S_g (R_g + R_c)}$$

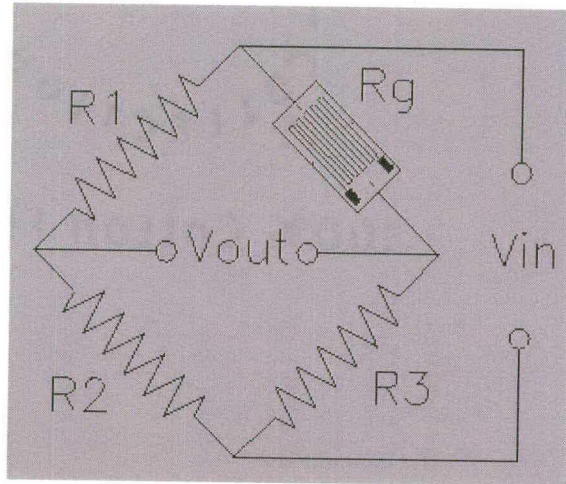


Figure 3.13: Schematic of a quarter model Wheatstone Bridge.

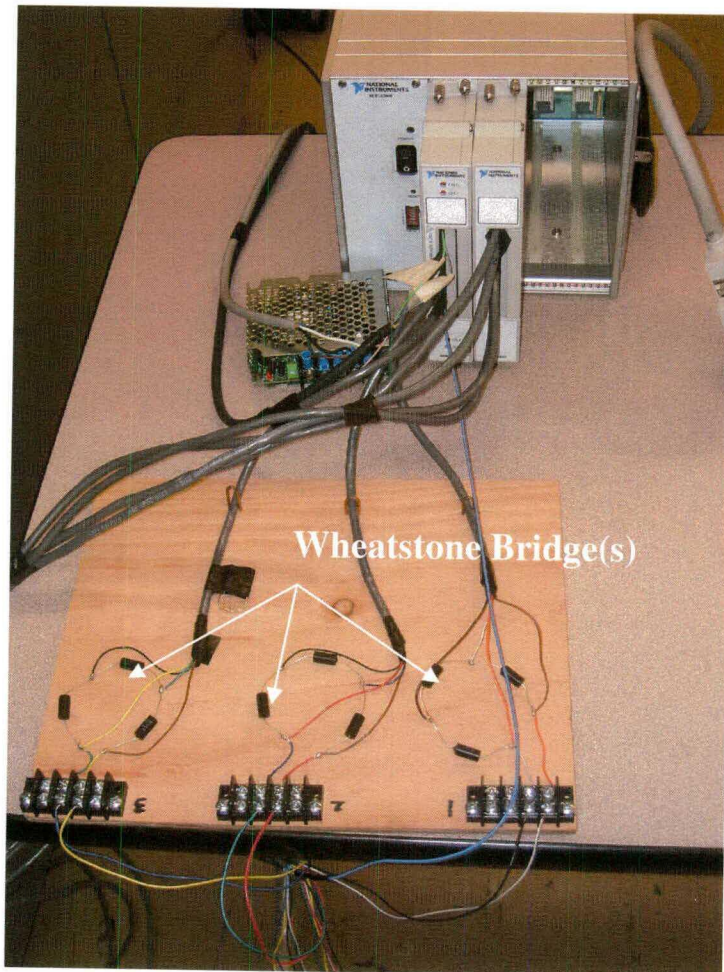


Figure 3.14: Image of the Wheatstone bridge circuitry and data acquisition hardware.

Fixed precision resistors, with a 5% tolerance band, of 10 k Ω and 22 k Ω were used to calibrate each strain gage. The exact values of the resistors were determined using a multi-meter. Each resistor placed in parallel to a strain gage corresponds to a simulated strain on that strain gage. The aforementioned resistor values resulted in an approximate simulated strain of 2600 and 600 microstrain ($\mu\epsilon$) respectively. A summary of the sensitivities of each strain gage is listed below.

	Rosette 1	Rosette 2	Rosette 3
Direction 1	565.4	567.6	564.7
Direction 2	567.4	567.1	564
Direction 3	570.8	564.2	564

Table 3.2: Summary of strain gage sensitivities ($\mu\epsilon/mV$).

The results of Table 3.2 can be viewed in graphical form in Figures 3.15 through 3.17. Each strain gage rosette shows its linearity with respect to the voltage change across the Wheatstone bridge. The R^2 value validates the linearity of each strain gage.

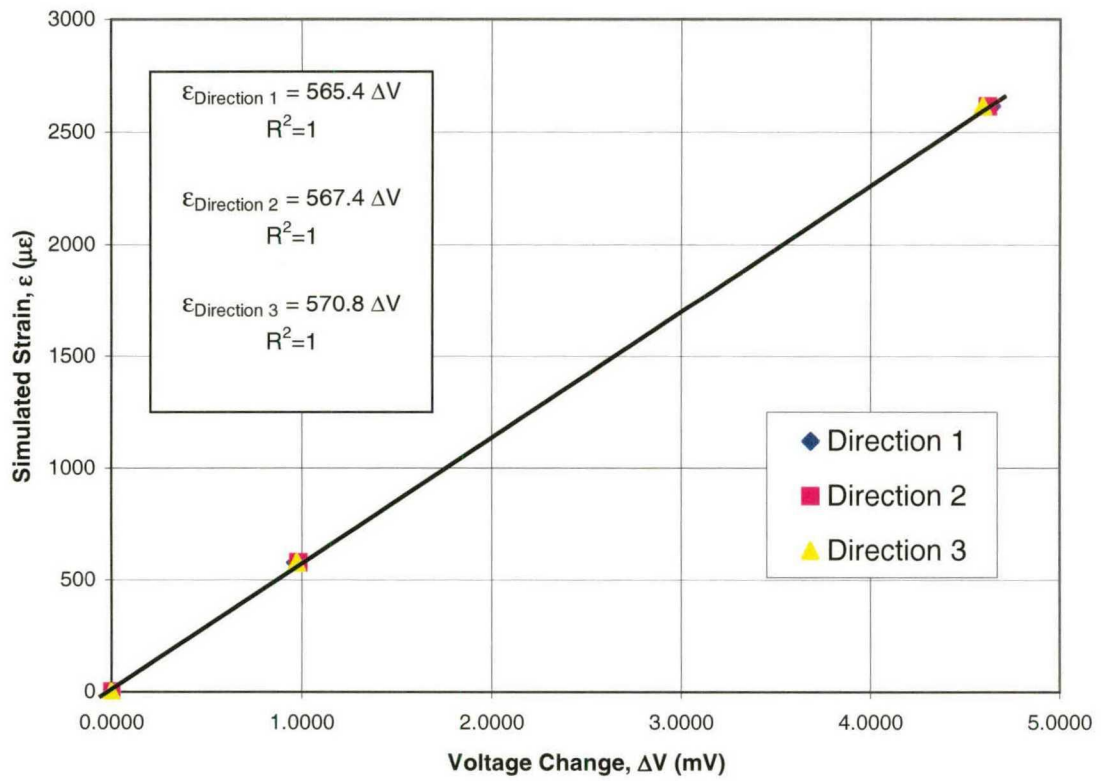


Figure 3.15: Calibration curves for strain gage rosette one.

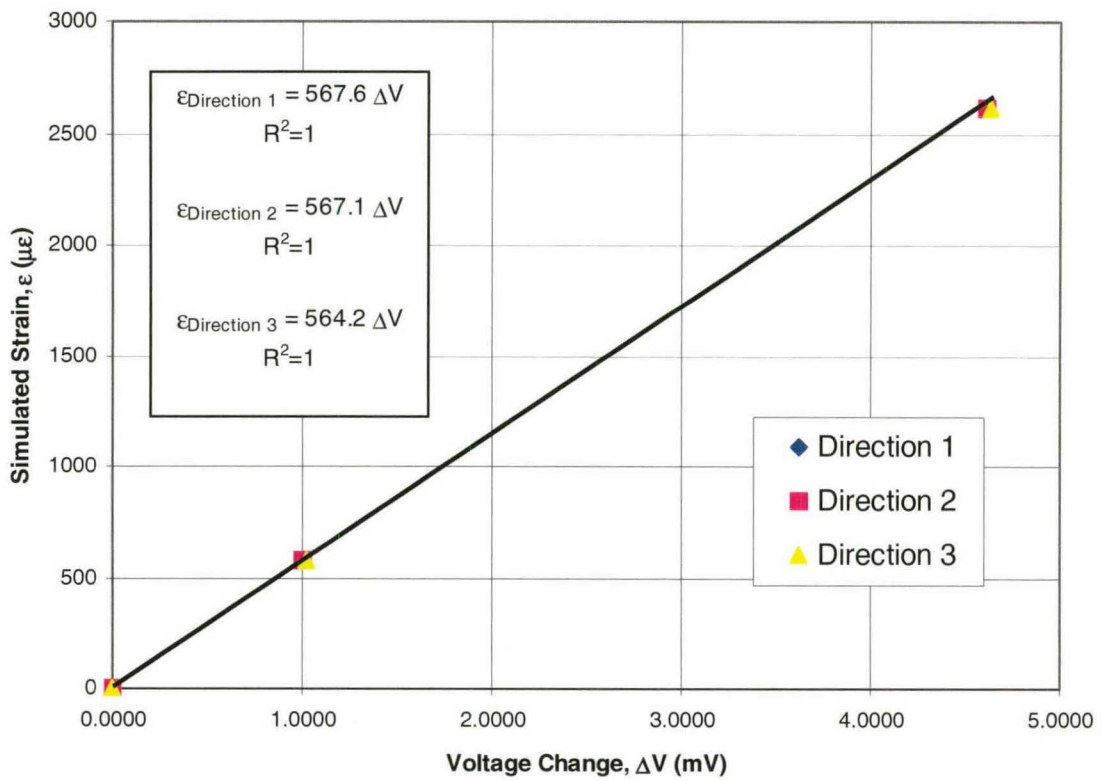


Figure 3.16: Calibration curves for strain gage rosette two.

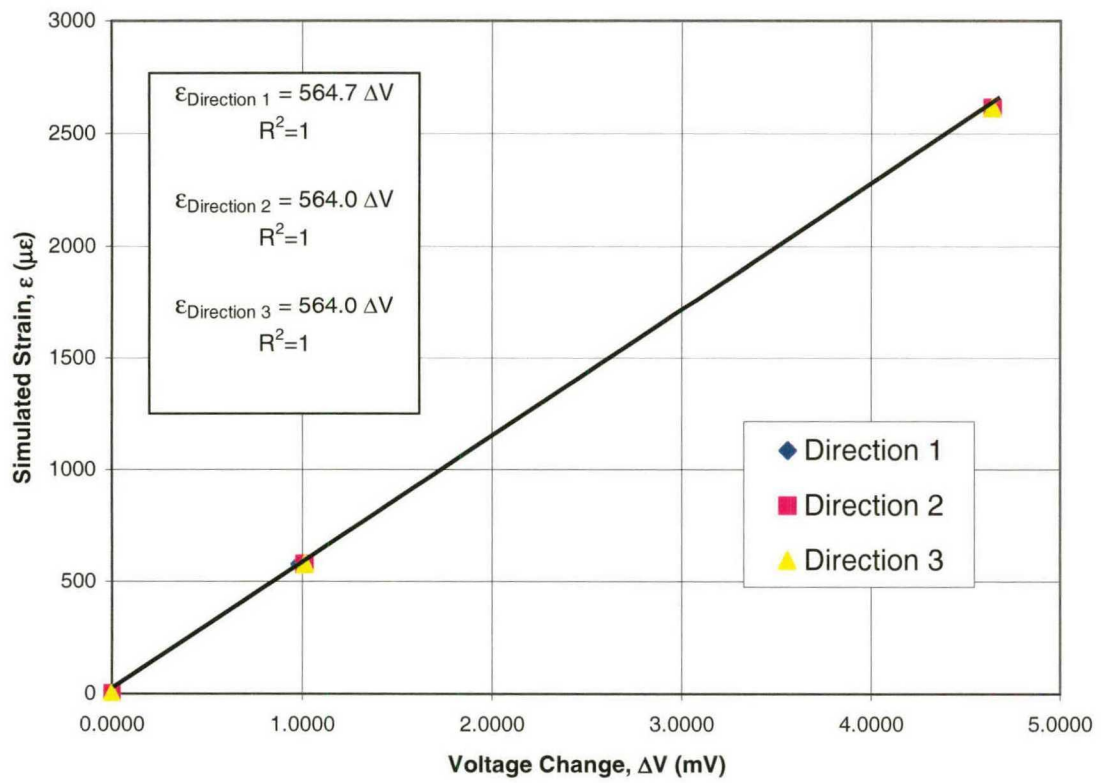


Figure 3.17: Calibration curves for strain gage rosette three.

CHAPTER 4

SIMULATIONS

4.1 Simulations

As experimentation can be costly, oftentimes industry turns to a computer simulation in order to model a process or problem. Finite Element Analysis, or FEA, is a common computational tool used to simulate structural analyses. While models can be complex with large meshes and unique boundary conditions, it is important that a model be a good representation of the physical model itself. Oftentimes this requires experimentation to validate a model.

In parallel to the research performed in this paper, work has been completed on modeling the eight-cavity mold in ABAQUSTM with the in-process loading resulted from the aforementioned experimental Sumitomo settings. In order to create an ABAQUSTM model, much care must be taken in the modeling of the machine parts, as well as loading and boundary conditions. Graduate researcher Claudia Gonzalez has performed the following simulations in ABAQUSTM. The model used in the simulations is a simplified version of the existing mold.

The experimental mold is composed of many parts, while the model of the simulated mold is simplified and contains less parts and features than the experimental mold. This is important because a solid mold is a much more rigid model and may not completely represent the true mold deformation that occurs under loading. More parts modeled in the finite element model (FEM) requires more computational time, finer meshes, additional contact analyses, as well as the use of an explicit solver. Since the parts are cylindrical in nature and the rigidity of the mold in the radial direction from the center of the cavities is more likely to resist deformation than normal to the mold plates, an increase in overall part length or axial features, normal to the mold parting plane, is of importance. Therefore, prediction capabilities are limited.

4.2 MoldFlow™ Simulations

In order to obtain the pressure in the cavity and runner system, MoldFlow was used to analyze the injection process. Using the peak fill pressure at the largest injection velocity from Table 3.3, the MoldFlow model was set to achieve this pressure at the injection location during packing. This would simulate the worst case loading at one point in time and generate the needed correlated pressure data. It also represents the best condition to achieve maximum mold deflection and maximum parting plane separation. The remainder of the experimental conditions were set to match that of the experiments performed. Ideally, a mold cavity and or runner would be equipped with a pressure transducer. An experimental measurement would help validate MoldFlow's results and give a better sense of the true loading over the fill and pack regime. Due to the complex mold geometry and space limitations it was nearly impossible to fit the mold with such a

sensor. In the interest of time it was decided to use MoldFlow solely to estimate the internal cavity-runner pressure distribution.

An IGES model of the part seen in Figure 1.3 was imported into MoldFlow and a midplane mesh was generated. This type of mesh places elements in the middle of a part thickness. The elements in the mesh are three noded, 2-D elements and have the proper thickness properties assigned to them. The gate and runner system are of the 1-D element type. Each element is assigned a cross sectional area, which is representative of the true mold geometry. The mesh was refined using tools available within the software package so that no element had a distortion ratio worse than three. The mesh was also checked for other systematic errors that could cause a potential erroneous solution.

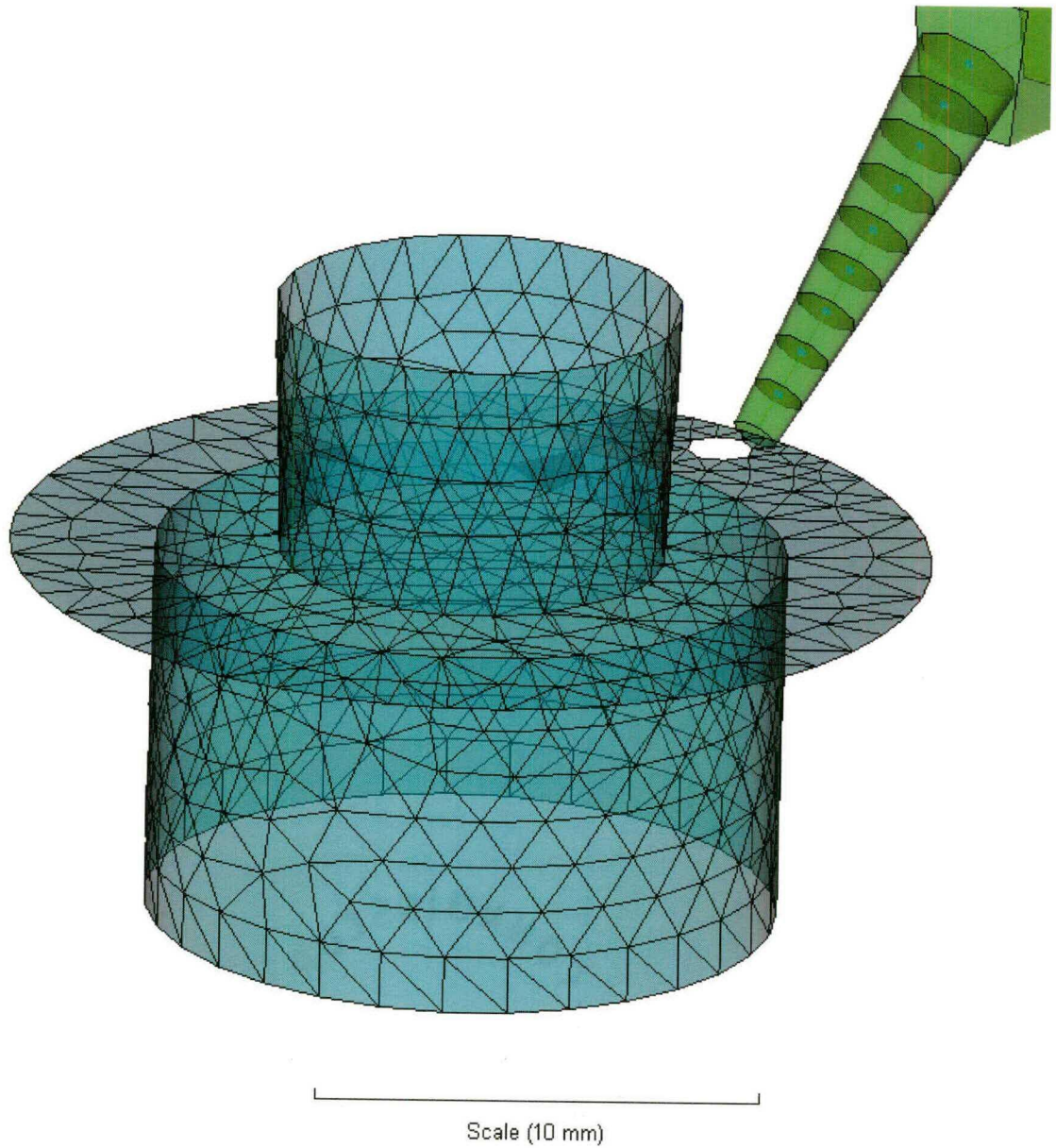


Figure 4.1: Midplane cavity mesh and 1-D tunnel gate mesh in MoldFlow™.

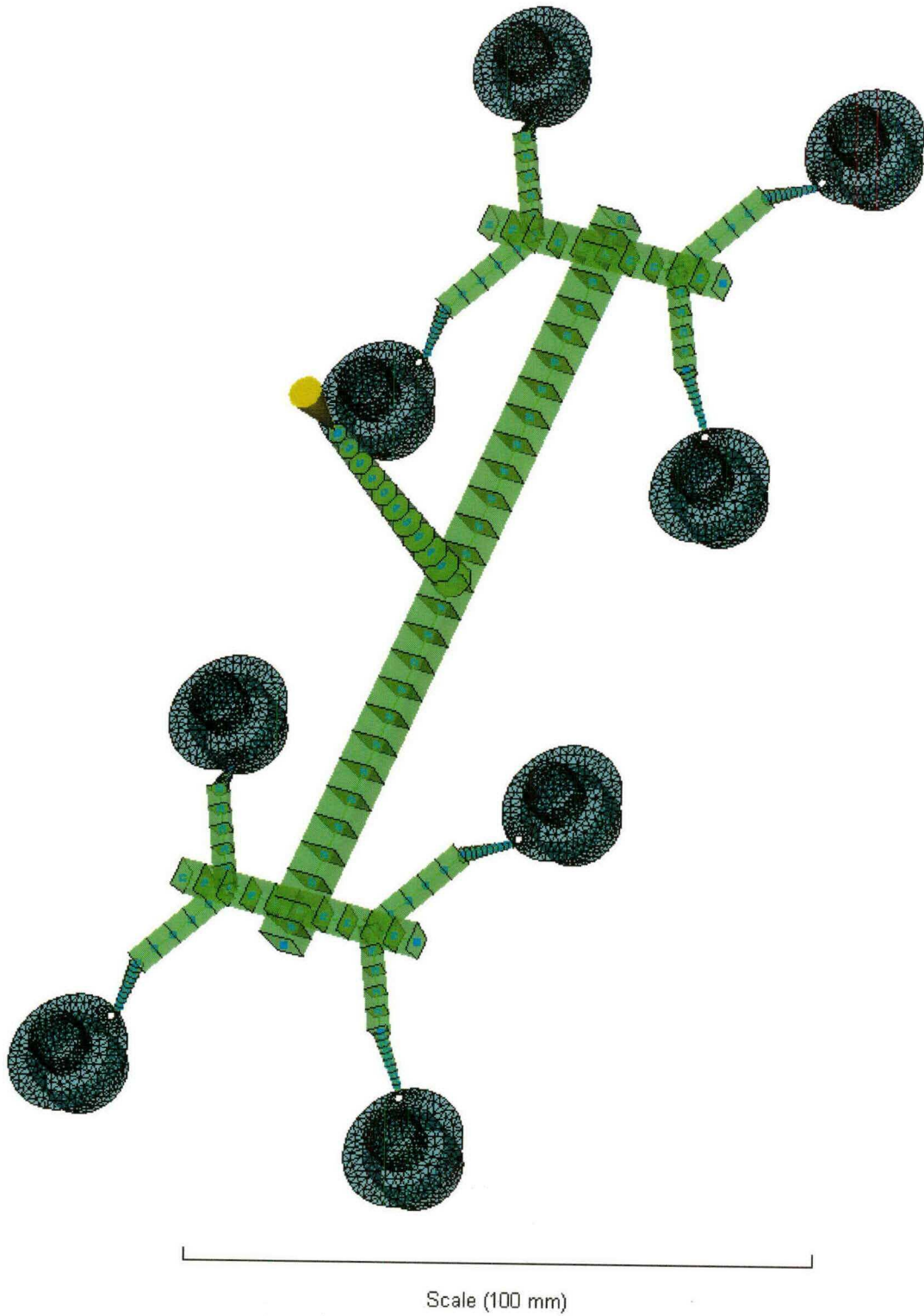


Figure 4.2: Meshed cavity and runner system generated in MoldFlow™.

Figure 4.2, illustrates the full model of the mold cavity and runner geometry. The model was built to be as close to the true mold as MoldFlow's capabilities permit. In order to more accurately represent the gate geometry, actual gate dimensions, as molded on the runners were measured and averaged from ten shots. Then the average gate diameters were entered into MoldFlow in exact location as the performed experiments. Although not shown in the figure, cooling lines and cooling channels were added to the model. The coolant inlet properties were set to match that of the experimental test conditions as well. The MoldFlow injection molding solver gives many options for providing a unique solution to each problem. Because gate freeze-off was calculated in the model as well as pressure distribution, it was important to run a cooling analysis as well. Therefore the solution was obtained using the Fill + Cool + Flow solver.

From Figure 4.3, which shows the injection location pressure versus time graph predicted by MoldFlow, it was determined at what time in the cycle the peak fill pressure occurred. Then the pressure data, shown in Figure 4.4, was analyzed at that instance in time. In order to be completely thorough, it would be best to map the loads from the MoldFlow™ FEA model to the ABAQUS™ model, but the pressure gradient across the cavities and runner system was not extremely large. It appears that the pressures at each node in each cavity, show less than a 2% range from the minimum to the maximum versus the maximum value. For the runner system it was a bit larger, approximately 4%, which is expected because of the greater changes in cross sectional area from the sprue to the gate of each cavity. It is understood that the simulation is only an estimation of what occurs in the cavities and runners during the injection cycle.

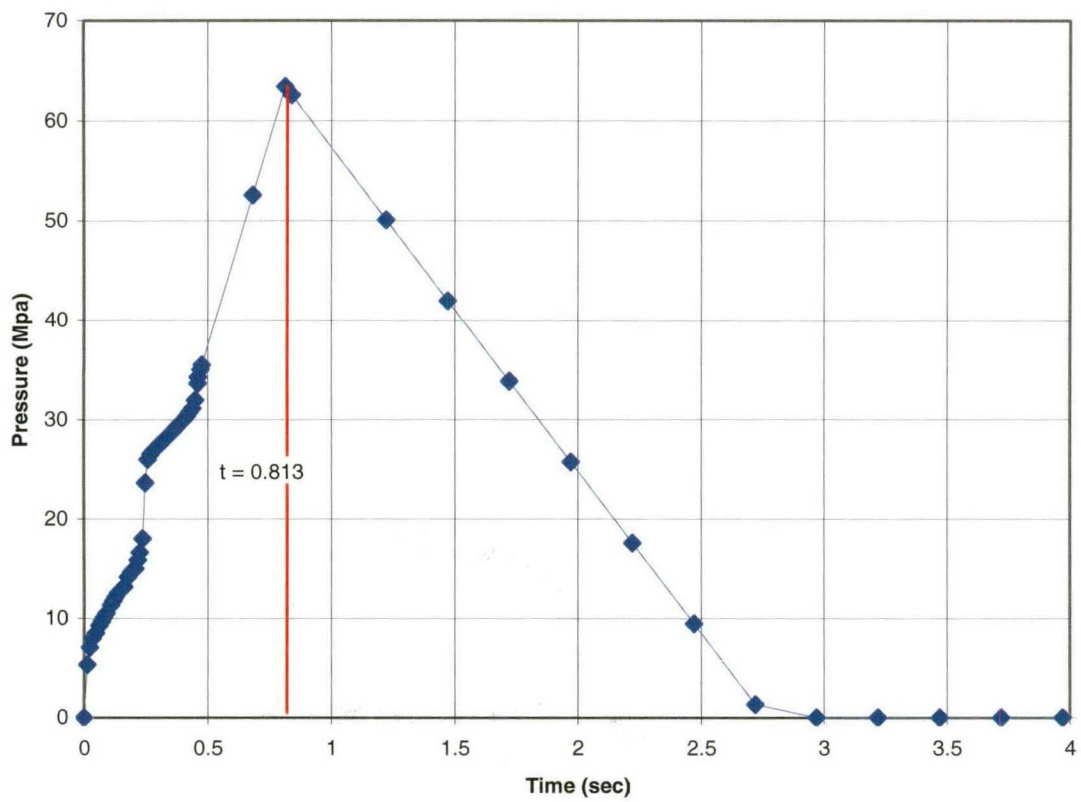


Figure 4.3: Pressure at injection location over an injection cycle.

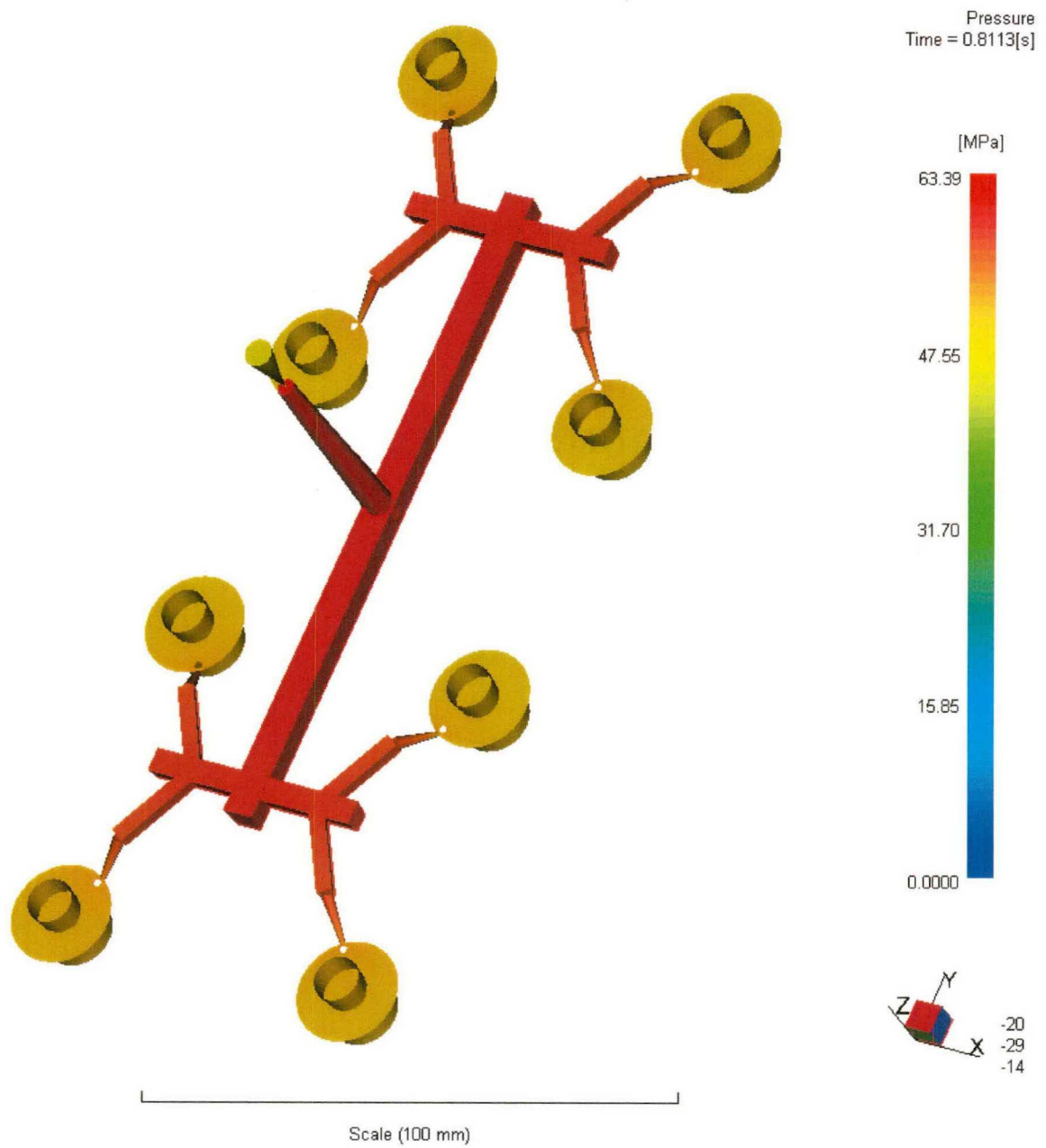


Figure 4.4: Cavity-runner pressure distribution in mold at $t = 0.813$ seconds.
(corresponding to peak fill pressure)

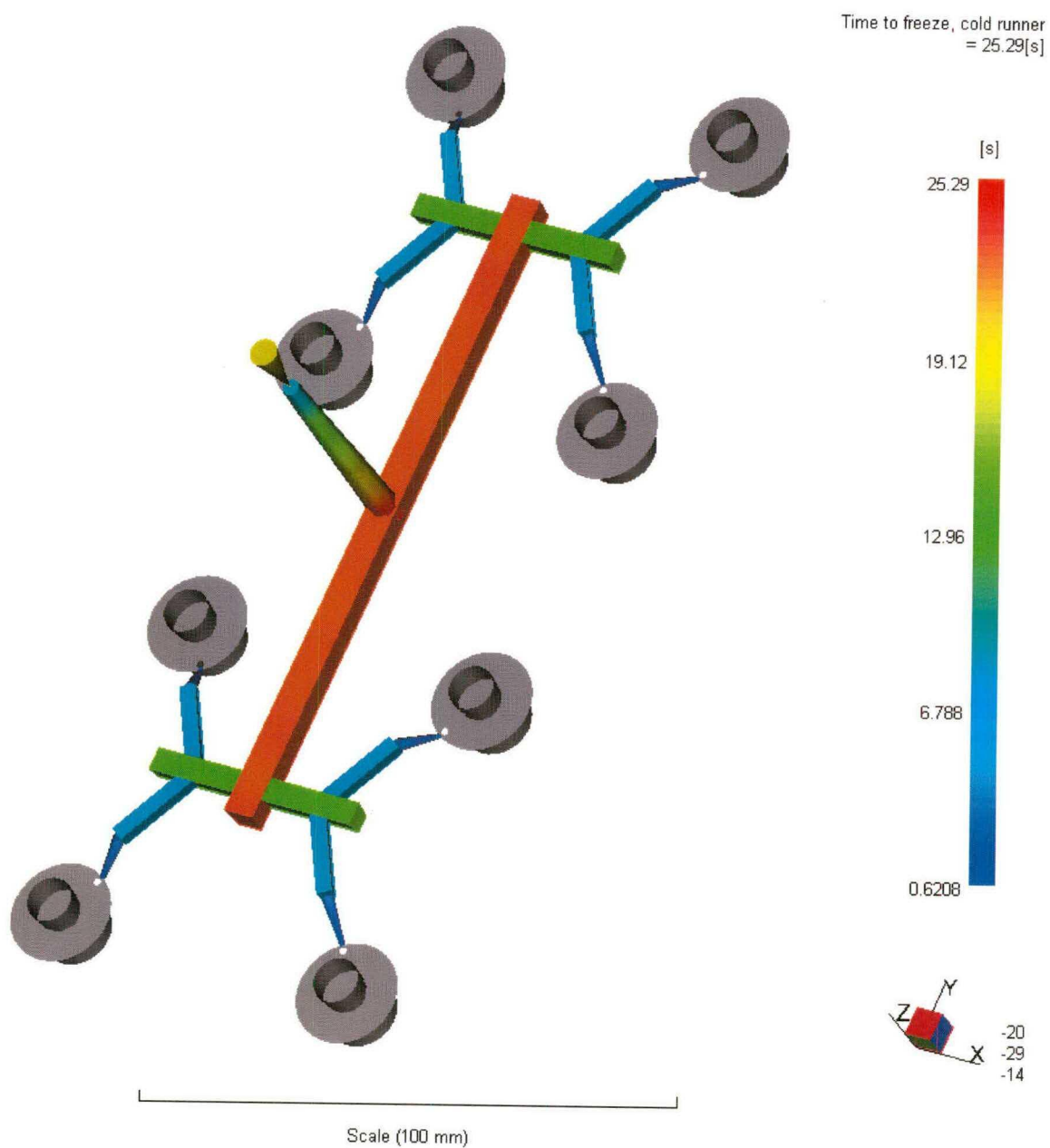


Figure 4.5: Contour plot of melt freeze time for the sprue and runner system.

4.3 ABAQUS™ Simulations

The ABAQUS™ model is composed of the simplified mold halves, the MUD base, and the moving platen. Originally it was thought that the model could be run with just the mold halves, but the true boundary conditions could not be fully represented with this model. Initial simulations showed the contour strain plots to be symmetric, while data from the strain gages indicated otherwise. Therefore, it was decided to improve the modeling by incorporating the MUD base and moving platen into the model. The platen is simplified to a solid block and is used solely for the application of the mold clamping load. Since the MUD base is less rigid on the top than bottom, it plays an important role in the mold deformation, as will be discussed later in the results section. The elements modeled are displayed below in Figure 4.6.

Due to the complex geometry of the runners and cavities a reduction in geometry complexity allowed for simpler meshing and a corresponding reduction in mesh elements. The entire model was meshed using a free mesh with 4 noded block elements. The models were partitioned in order to achieve a mesh of elements with little distortion. The total number of elements in Figure 4.7 is 108546 and requires a computational time of approximately five days to solve on a Dell Precision WorkStation 360 with a Pentium 4 HT Chip, 3.0 GHz processor with 2 Gb of RAM.

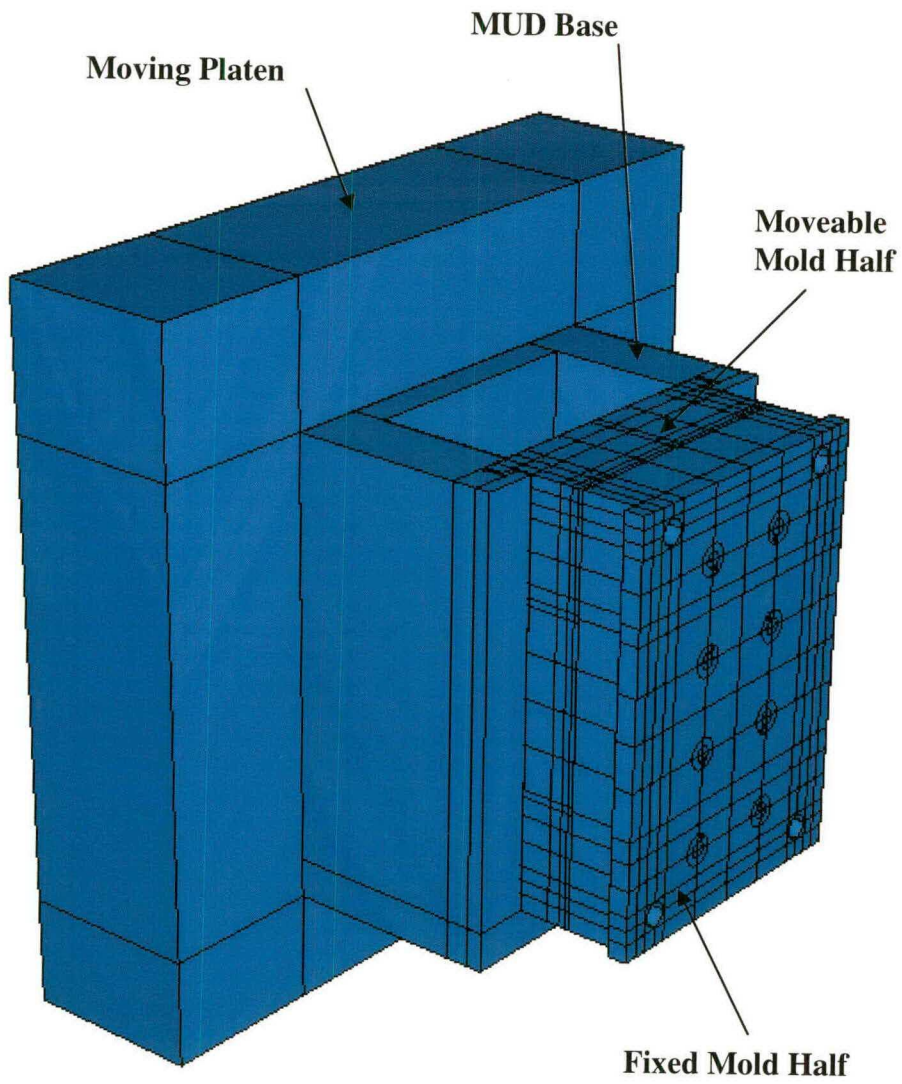


Figure 4.6: Solid, partitioned model generated in ABAQUS™.

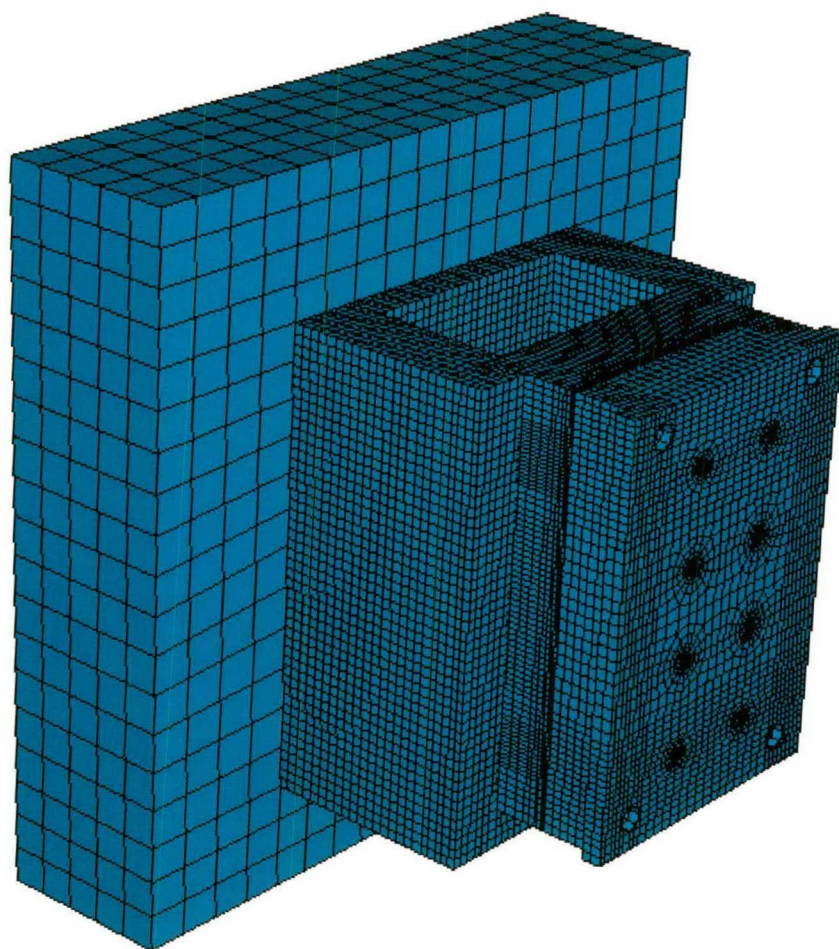


Figure 4.7: FEM free mesh generated in ABAQUS™.

With respect to the boundary conditions, the fixed mold half back surface was fixed in all directions. While this is not representative of what actually occurs, the main concern of this analysis was the deformation of the movable mold half, so the fixturing of the fixed mold half was acceptable. A full contact analysis was performed on the mold faces as well as at the intersection between the movable mold half and the MUD base.

As for the loading, a clamping force was applied to the back face of the moving platen to simulate the clamping tonnage applied in the experiments. The mold was run with a clamping load of 15 metric tonnes. Because there exists a constant nozzle load on the sprue bushing, the actual clamping tonnage applied was less it's value. The clamping load was applied over an 8 inch circle, located on the back of the moving platen, representative of the hydraulic cylinder affixed to the rear of the moving platen.

The internal pressures obtained from MoldflowTM were applied to the elements of a simplified cavity-runner system. Loading parameters to the ABAQUSTM model cavities were set to the maximum cavity pressure, 48 MPa, while the runner system was set to the maximum runner pressure, 58 MPa, as predicted from the MoldFlowTM model above. This was done so that the analysis was somewhat on the conservative side, as well as for ease of load application in the software package.

A visual examination of the runners after molding showed a great deal of sink marks at the intersections of the runner legs, which indicated that shrinkage had occurred. Typically packing reduces this phenomenon, but it is theorized that the tapered sprue froze early in the packing phase, thus allowing the runner to shrink as it cooled. Therefore, during the packing phase, much of the applied pressure compresses the runner

and the applied pressure load is not fully transferred through the mold. Because of this, it is believed that the load is small on the main leg of the runner. Two studies were performed on the FEM, one loading the entire runner system and one loading only the secondary and tertiary legs of the runner system, of which will be further discussed in section 5.3.

CHAPTER 5

RESULTS

5.1 Results

Upon completion of the data acquisition, the collected data as well as the molded parts were analyzed. The electronic data was manipulated and sorted using the spreadsheet program Microsoft Excel. The data was analyzed in three parts: the strain data, LVDT data, and part geometry. As for the parts themselves, it was decided to use two tools to analyze their characteristics. The first method of analysis was to weigh each part individually with the use of a precision balance. Second, two features of size molded from the movable mold half, were measured using a coordinate measuring machine. Prior to discussing the results it is important to define the experimental conditions used in order to understand what data was collected.

5.2 Experimental Conditions

Injection molding is a complex process that has many controllable process parameters. Each parameter setting affects the quality of the final product. It is nearly impossible to achieve optimization of every process parameter, as the process is very “give and take”. As previously noted, the eight-cavity mold has excellent thermal

characteristics. Therefore, holding the mold at a constant temperature will aid in minimizing any thermal effects that may affect the part variance. Three main parameters of interest: injection velocity, packing pressure, and mold cavity configuration, were investigated. While cycle time is typically important, running the mold at a slightly elevated temperature will reduce the chance that the gates will freeze prior to the completion of packing.

Prior to discussing the details of the experimental plan, the material used in the study needs to be mentioned. The material, a BASF Polystyrol 466F, is a high impact polystyrene (HIPS). The material properties were not readily available to the public or published on the Internet. BASF was contacted, but no response was given. While this is not vital for the experimentation itself, any simulations run in MoldFlow require the rheologic material properties. The main property of interest was the melt temperature. Since the mold had been previously run at the Eastman Kodak Company with the same material, and information on those runs was available, the same melt temperature of 450° F was used.

Initial investigations in the mold's capability showed that if all eight cavities were injected above 50% of the full scale (% FS) injection velocity of the machine and 20% FS packing pressure, parts would adhere to the fixed mold half and cause problems during the ejection phase. It was nearly impossible to remove the parts from the fixed half of the mold without dimensionally altering their geometry. Many attempts were made to try to reduce the occurrence of the phenomenon, but to no avail. In order to reduce the risk of this occurring, the maximum packing pressure and peak fill pressure was recorded for

injection velocities from 20 to 50% FS, in 10% increments. Each run was repeated five times to ensure repeatability. The pressures were recorded from a pressure transducer mounted on the rear of the injector screw, not the pressure at the nozzle on the injector screw. In order to achieve the pressure at the nozzle of the screw, the intensification ratio of the machine must be taken into account. The following table summarizes the findings.

Injection Velocity (% FS)	Maximum Pack Pressure (% FS)	Fill Peak Pressure (% FS)
20	25	21
30	22	25
40	20	28
50	18	32

Table 5.1: Summary of maximum pack pressures relative to injection velocity. (All values are %FS of machine capability)

Based upon the information in Table 5.1 it was decided to investigate the effects on part variance by varying three levels of the injection velocity over three levels of packing pressures. Therefore, from Table 5.1, it was decided to use a maximum packing pressure of 20% FS. This constraint limits the maximum injection velocity to be 40% FS without issues of parts adhering to the mold. Table 5.2 contains the levels for the injection velocity and packing pressure used in the investigation of mold deformation and mold separation at the parting plane.

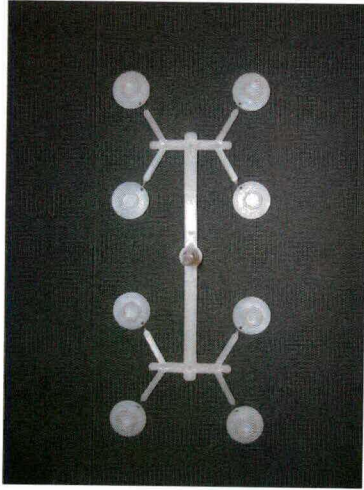
Level	Injection Velocity (% FS)	Packing Pressure (% FS)
1	20	10
2	30	15
3	40	20

Table 5.2: Process parameters varied during the experiments.

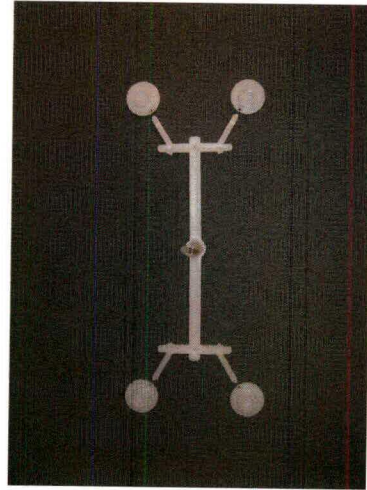
It was also decided to investigate five cavity configurations and how they would affect the results. The first configuration involved the molding of all eight cavities. The next three involved a variation of four cavities. Finally, the last configuration had no cavities molded, but rather the runner system only. This configuration was of interest in order to determine if the runner system plays a dominant role in the mold deformation and/or parting plane separation. The images below show each mold configuration used in the experiments.

A full factorial design of experiments (DOE) matrix was designed for the control variables of interest. A full factorial matrix was used for ease of analysis [8]. While a partial factorial matrix could reduce the number of experiments performed, a full factorial would ensure a complete data set.

While the option of cavity interchangeability was available it was not used during the experiments. It is important to note the location of each cavity for future reference. The cavities were positioned from left to right in decreasing rows starting from the top of the movable mold half as follows: three, five, eight, six, seven, four, one, and two. While this configuration is a bit unorthodox, the cavities were placed at random rather than in chronologic order.



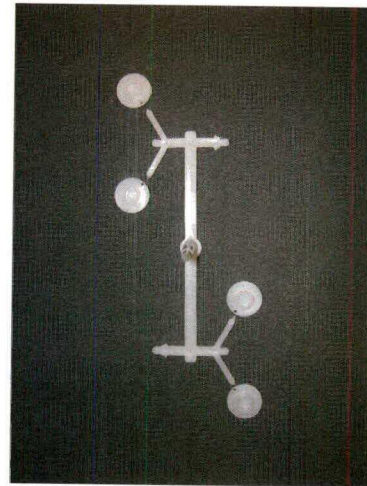
Configuration #1



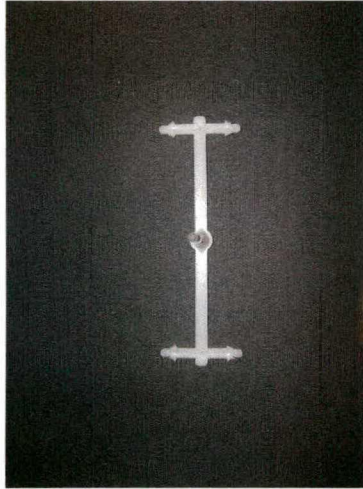
Configuration #2



Configuration #3



Configuration #4



Configuration #5

For each set of process parameters, fifteen shots or runs were made on the injection molding machine. At each run, the strain gage and LVDT data was recorded and stored on the hard disk of the laptop computer. Of the fifteen runs, three sets of five were replicate runs for each strain gage rosette. This was done so that the strain at each point could be analyzed for statistical consistencies. Consequently, the LVDTs had fifteen data points for each group of process parameters. In the end, for each configuration there were a total of one hundred thirty-five shots made. The approximate cycle time for each shot was thirty seconds. Prior to each experimental batch of runs, the mold was run continuously at thirty second cycles to guarantee the mold was in thermal equilibrium before taking data. This would help ensure more consistency in the data as well.

It was important that the packing phase began when the cavities were roughly 98% full. This was accomplished by determining when to switch the machine from the fill to pack stage. To do this, each cavity configuration was run while the injector screw switchover position was incrementally changed, in 0.05 inch increments, until there were no more visible short shots. Regardless of the four-cavity configuration this screw

position occurred at 0.20 inches, while moving from 1.15 inches. While for the eight-cavity configuration it occurred at 0.25 inches, while moving from 1.55 inches. These process settings again ensure there were no inconsistencies in the process from experiment to experiment.

Another important parameter to determine was the length of the packing phase. It was important to make sure the parts were fully packed, reducing any potential part defects. In order to make sure the packing phase is long enough, the gate freeze off time had to be determined. This is the time it takes for the gates to freeze, and is also the point at which packing is no longer effective on a part itself. Additional packing beyond this time only packs the runner system, which is of little or no value. Three methods were used to determine the gate freeze off time: a physical experiment, a heat transfer calculation, and a computer simulation.

During the filling stage, the mold fill time corresponds to the injection velocity. Therefore, only the slowest fill time is of importance to set the packing time. The slowest injection velocity, 20% FS, and all three packing pressures were used in a gate freeze off experiment. During the experiment the length of the packing time was gradually increased and parts were molded. Five replicates were run at each condition and then the parts were weighed on a balance. As the packing time increases and the gates freeze, the parts will no longer increase in weight, at which the resulting gate freeze off time is found.

A heat transfer calculation was also used to determine the gate freeze off time. [9] The calculation was sufficient for the solidification of a diametrical part. Aside from the

unknown material properties, the temperatures used in the calculation were measured with an infrared thermometer. Experimental mold temperatures were recorded multiple times and averaged into the calculations. A small sensitivity study was performed on the material property, thermal diffusivity, and the injection temperature in order to understand the effect on the gate freeze off time. This was done because of the uncertainty in the material properties and injection temperature. In fact, the mean values used to calculate the gate freeze off time have a very good correlation to the weight experiment previously discussed. The range of gate freeze off for the sensitivity study was calculated between 1.8 and 3.8 seconds.

$$t_{cool} = \frac{D^2}{23.14\alpha} \ln\left(0.692 \frac{(T_M - T_W)}{(T_D - T_W)}\right)$$

where

- D = diameter of part, in
- α = thermal diffusivity, sec/in²
- T_M = melt temperature, °F
- T_W = wall temperature, °F
- T_D = average part temperature at ejection, °F

Finally, the analytical injection molding software package, MoldFlow™ was used to determine the gate freeze off time. MoldFlow™ is a finite element based program that simulates the injection molding process. The software can be helpful in the modeling of the injection molding process without actually running a machine. Identical process parameters were set in the software as in the experiment above and a simulation was run. It is important to note as previously mentioned, the exact rheological properties are unknown, so another material was used in the simulations, Polystyrol 495F, a common

HIPS material. The table below contains a summary of results for all three methods of attaining gate freeze off time.

Weight Experiment	Heat Transfer Calculation	MoldFlow Simulation
2.6	2.6	2.0

Table 5.3: Summary of gate freeze off times (sec).

As previously mentioned the process is not being optimized for cycle time, so it was decided that the fill and pack total time would be set to 3.50 seconds. This would ensure a buffer in the packing phase of 0.90 seconds at the slowest injection velocity, and an even larger interval for the larger injection velocities. As for the cooling time, the parts were kept in the mold long enough so that they could be properly ejected. Because of the runner design, if not allowed to cool enough, the runner would adhere to the movable mold half and have to be manually removed. Decreasing the mold coolant temperature could reduce cycle time, yet it was not of importance in the study.

5.3 Strain Gage Results

Electronic strain gage data that was collected during the experimentation was collected as a voltage signal. Visual Basic, embedded within Microsoft Excel, was used to create a macro to analyze the strain data using the calibration sensitivities to convert the Wheatstone bridge voltage change into mechanical strain. Each strain gage was nulled at the beginning of the cycle, when no strain existed. This data shift was also done in order that all three strain gages on a rosette could be plotted correctly.

Once the strain gage data was in the correct units, it was analyzed in more detail. Over an entire injection cycle the strain gage data was analyzed to determine the strain in the mold during the clamping phase, strain at the end of the filling phase, strain at the end of the packing phase, and finally any local extremes existing between the fill and pack phase, such as a minimum or maximum strain value.

In order to locate the points of interest in an injection cycle an analysis of the LVDT data on the injector screw was required. Just as the strain gage data was converted, so was the LVDT injector screw voltage signal. The injector screw signal was used to determine the time in which three of the four data conditions occurred. Clamping strain was analyzed just before the initial displacement of the injector screw. The strain at the end of packing was analyzed when the screw was at its closest position to the nozzle. Strain values at the end of filling were determined by locating the injector screw position during the switchover stage. Finally, the strain curve was analyzed in-between the end of filling and the end of packing phase for a maximum or minimum. In order to determine which extreme was required for analysis, the trends of the strain gage curves were initially studied. This ensured that the data was analyzed for the proper condition.

Once the data was analyzed for one shot it was repeated four more times for each experimental replicate. In turn, it was repeated for each strain gage rosette until an entire cavity configuration was analyzed. When all of the data for each strain gage was analyzed for each shot it was then statistically analyzed for mean and standard deviation values. In reviewing the variance found in the strain gage data, the standard deviation for all of the configurations was found to be within the 1 to 3 microstrain range. This value shows that the strain in the mold is very repeatable. Such a repeatable magnitude

indicates the machine is very consistent in its mechanical loading. While other variables, such as material variability can affect the part quality, the strain gage data seems reasonably stable.

Strain Gage Rosette	Direction	End of Fill	Local Extreme	End of Pack
1	1	-56	-69	-53
	2	73	92	73
	3	198	249	194
2	1	48	59	53
	2	118	145	120
	3	171	218	173
3	1	-14	-13	-14
	2	-16	-16	-8
	3	5	5	18

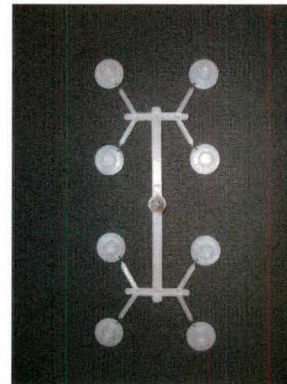


Table 5.4: Summary of average strain at worst case loading condition for the injection of cavity configuration one. (40% FS injection velocity, 20% FS packing pressure)

While it is important to look at the strain data for all of the conditions, only the worst case loading conditions for each cavity configuration will be reported in this chapter. For each cavity configuration there exists nine tables similar to Table 5.4 that summarize the average strain for the five replicates recorded during the experiments. The following tables, 5.5 through 5.8, summarize the strain gage data for the remaining cavity configurations, which include the strain due to clamping.

Strain Gage Rosette	Direction	End of Fill	Local Extreme	End of Pack
1	1	-39	-48	-39
	2	54	80	57
	3	146	199	147
2	1	26	14	37
	2	79	87	85
	3	122	158	129
3	1	-26	-26	-22
	2	-22	-17	-21
	3	14	16	10

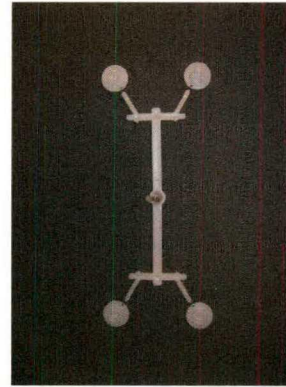


Table 5.5: Summary of average strain at worst case loading condition for the injection of cavity configuration two. (40% FS injection velocity, 20% FS packing pressure)

Strain Gage Rosette	Direction	End of Fill	Local Extreme	End of Pack
1	1	-43	-59	-45
	2	43	54	52
	3	129	160	142
2	1	55	91	59
	2	94	137	99
	3	121	171	133
3	1	-17	-2	-19
	2	-21	-17	-14
	3	4	-7	16



Table 5.6: Summary of average strain at worst case loading condition for the injection of cavity configuration three. (40% FS injection velocity, 20% FS packing pressure)

Strain Gage Rosette	Direction	End of Fill	Local Extreme	End of Pack
1	1	-41	-53	-41
	2	53	80	57
	3	139	187	145
2	1	39	47	47
	2	70	70	79
	3	118	162	128
3	1	-21	-16	-20
	2	-16	2	-15
	3	8	2	10

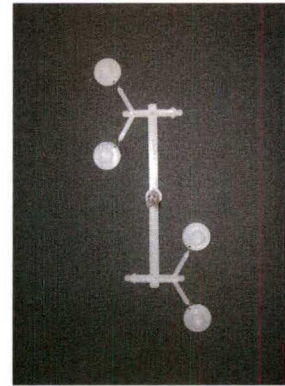


Table 5.7: Summary of average strain at worst case loading condition for the injection of cavity configuration four. (40% FS injection velocity, 20% FS packing pressure)

Strain Gage Rosette	Direction	End of Fill	Local Extreme	End of Pack
1	1	-36	-38	-36
	2	39	41	41
	3	117	120	119
2	1	42	44	43
	2	84	88	84
	3	109	116	111
3	1	-24	-23	-24
	2	-23	-22	-22
	3	11	11	14

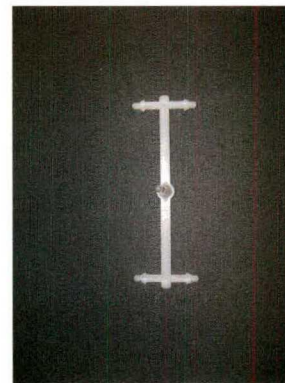


Table 5.8: Summary of average strain at worst case loading condition for the injection of cavity configuration five. (40% FS injection velocity, 20% FS packing pressure)

An interesting trend that occurs in the majority of the cavity configurations is the size of the strain in direction 3 (horizontal) for strain gage rosette 1 and strain gage rosette 2. The trend exhibits a larger strain value in the 3 direction atop the mold rather than near the center of the mold.

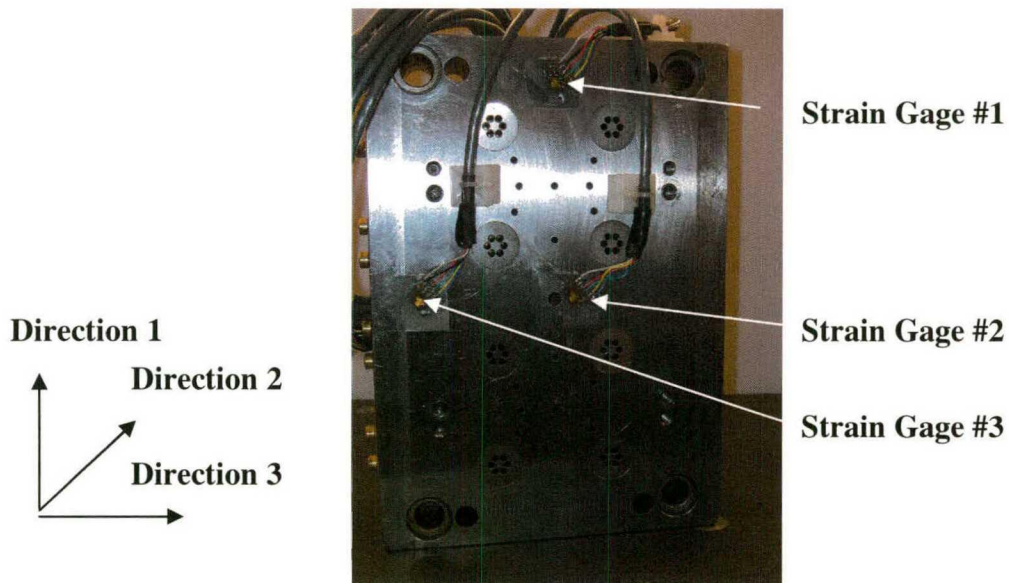


Figure 5.1: Strain Gage Locations and Orientations

While this may seem odd it can be explained simply. The mold itself is constrained in the MUD base by the mold guide slots and the wings on the mold that mate into those slots. Therefore, it would lead one to believe the mold would deform symmetrically about the vertical axis. This would be true except for the fact that the MUD base stiffness is not symmetrical about the vertical axis. The MUD base itself is a box with two open sides, the top and front. Therefore, the boundary constraint imposed by the stiffness of the MUD base at the top of the mold, is less of that than near the bottom of the MUD base. Hence, a larger strain near the top of the mold is seen during the injection cycle. Consequently, this would predict the top of the mold is bending more than the bottom.

Mold deformation would then tend to be more apparent in cavities molded in the upper half of the mold. Furthermore, it is believed that the majority of the load is applied in and around the cavities, as the main runner leg takes a significant time to solidify which minimizes the transfer of any loading effects.

In the cavity configuration where the four inner most cavities are injected, configuration number three, the strain pattern is opposite. This is mostly due to the fact that there is less applied load near the top of the mold, so the strain is larger near the center of the mold. In this case, deformation would exist, but may have less of an effect on part variance because the stiffness differential across the molded cavities is less than that of cavity configuration one. In fact, to minimize the mold deformation imposed by the MUD base boundary constraint, molding parts on the lower half of the mold would likely reduce the effect. This will be further discussed in relation to the mold separation at parting plane in a later section.

Furthermore, strain gage rosette 3 shows a small strain change from equilibrium. This would indicate that the mold may be bulging more in the center, and there is less bending between the four corners of the mold. In fact, the magnitude of strain seen at this location is mostly due to clamping. Therefore in order to get the true strain values due to the injection cycle the clamping strain was removed from the previous data. The strain due to clamping was consistent as well and is summarized in the following table.

Strain Gage	Direction 1	Direction 2	Direction 3
1	-36	48	133
2	40	87	112
3	-25	-22	10

Table 5.9: Average strain on the mold during clamping (microstrain).

Strain due to clamping is approximately half of the overall strain in the mold during an injection cycle. At first it would seem unexpected to see such high strain values prior to the injection of the polymer, yet it can easily be explained. The fixed mold half, which has the tapered inserts, mates to the movable inserts fixed in the moveable mold half. The inserts are designed to have a slight interference fit in order to prevent flashing and ensure the cavities are sealed correctly prior to injection of the polymer. Due to this interference, the inserts will actually deform the mold during clamping. Therefore, the induced strain is inherent to the mold design and not due to an excessive clamping load. While reducing the clamping load can minimize this local strain effect, the inserts will always cause the mold to deform some finite amount prior to the injection of the thermoplastic.

In order to gain an idea of what occurs over the entire cycle the strain gage data was plotted over time against the injector screw position. The following three plots show each strain gage rosette curve for cavity configuration one, all eight cavities. Similar to Figure 1.2 in Chapter 1, the strain gage data tends to follow a typical pressure history plot. This shows a good correlation of strain to what might be expected. Furthermore, this gives confidence in the acquired data.

Positive strain, as showed in the plots, can be interpreted as a tension or local increase in length, where as a negative strain can be interpreted as a compression or local decrease in length. In each plot the clamping, filling, packing and cooling regimes are identified. All three strain gages for each rosette start in null and change accordingly as the mold is clamped shut. As the injection cycle nears the switchover position, the curves become a minimum or maximum depending on the strain direction. The curves then tend to decrease as the gates and sprue begin to freeze, indicative of a decrease in the cavity-runner pressure in the mold. As the injection unit plasticizes its next shot, the injector screw clamping load on the sprue bushing is released. Meanwhile, the clamping unit load is still applied on the movable side, and holds the strain higher than prior to the injection of the thermoplastic. Furthermore, residual stresses exist in the mold from the packing phase, which also contribute to an increase in strain relative to the initial clamping of the system. This is a clear indication that the mold would have some finite elastic deformation and the parts have been over packed. Finally, the mold is opened for part ejection and the strain returned to its null position.

As one might expect, the only negative strain in rosette one is in direction 3. This can be explained as follows: as the mold bulges there exist concavities on the mold back face at the top and bottom of the mold (one on each end of the bulge). The concavity is near the inflection point of the bulge. This is caused by the constraint of the large guide pins locating the four corners of the mold. The concavity produced represents a compression point, so the strain is observed as a negative value. One a side note, these values are also relatively small compared to the strain in directions 1 and 2. The other

two strain directions show a positive strain, which would be indicative of a bulge or convex shape over the strain gage length.

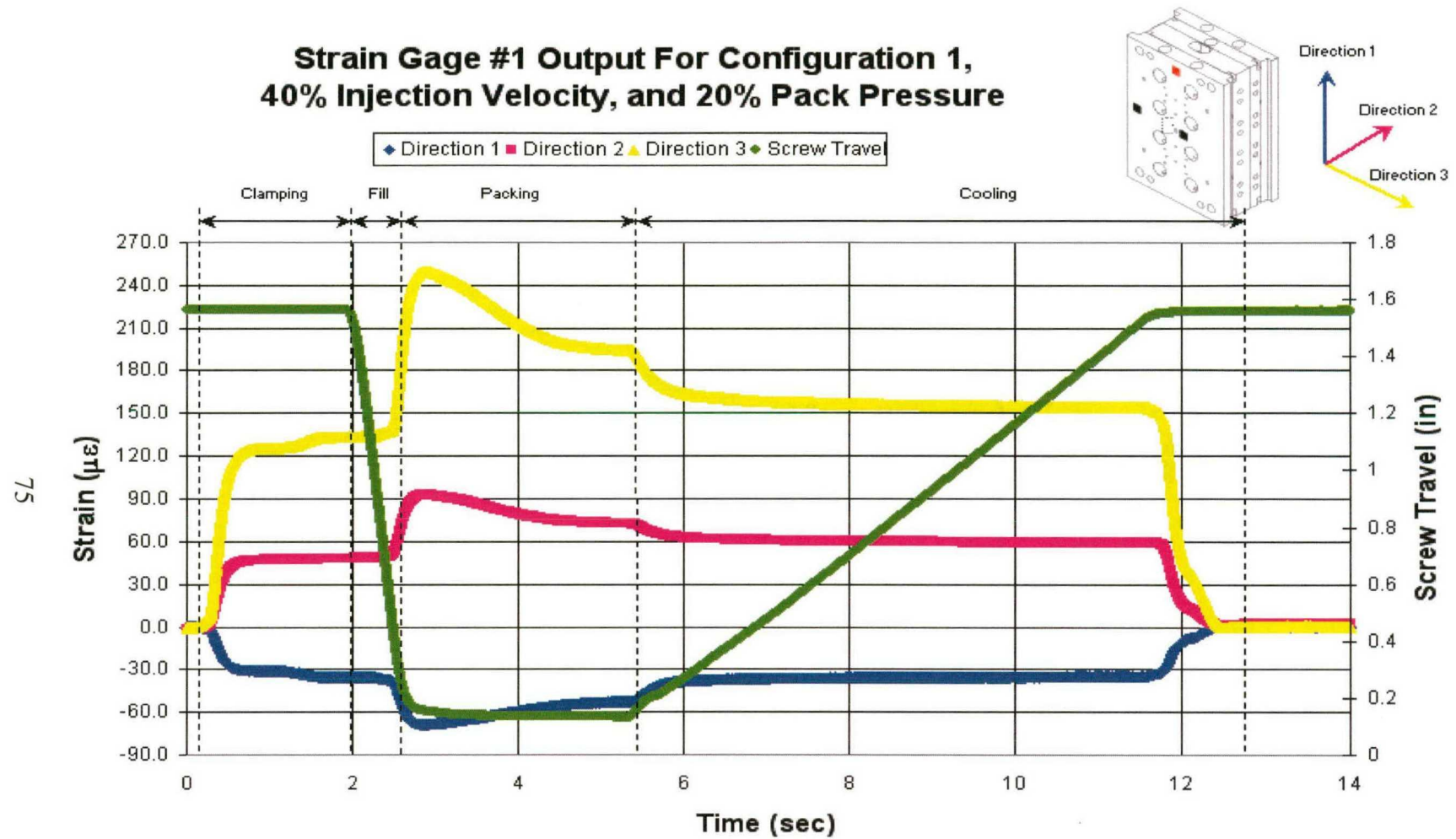


Figure 5.2: Strain gage rosette 1 curves for configuration 1, 40% injection velocity and 20% packing pressure.

Strain Gage #2 Output For Configuration 1, 40% Injection Velocity, and 20% Pack Pressure

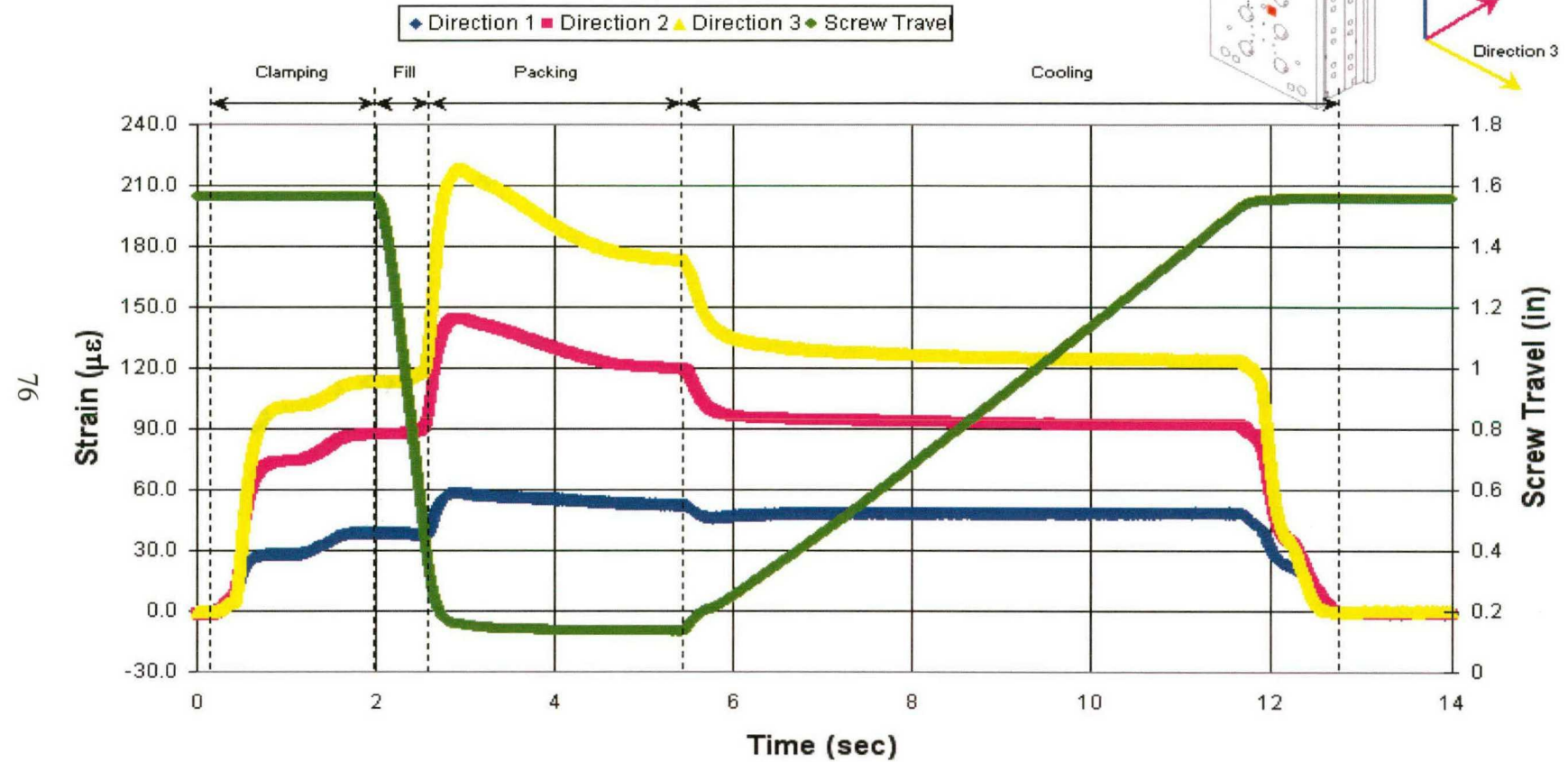


Figure 5.3: Strain gage rosette 2 curves for configuration 1, 40% injection velocity and 20% packing pressure.

Strain Gage #3 Output For Configuration 1, 40% Injection Velocity, and 20% Pack Pressure

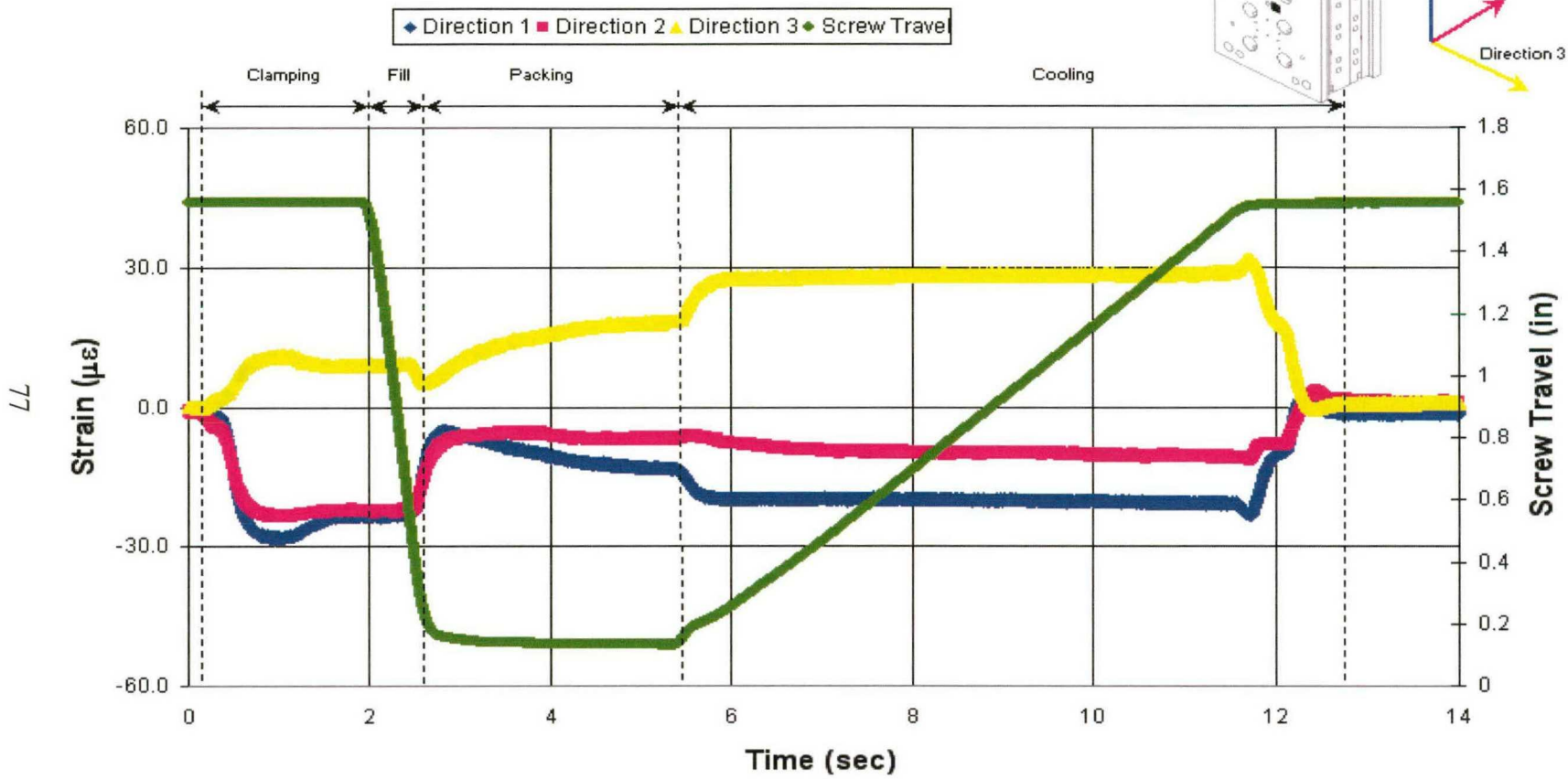
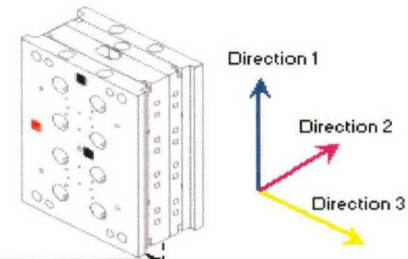


Figure 5.4: Strain gage rosette 3 curves for configuration 1, 40% injection velocity and 20% packing pressure.

Strain gage rosette 2 is located near the center of injection, or atop the expected bulge generated in the mold during the injection cycle. This would be a point of tension in all directions, as indicated in Figure 5.3. The strain gage values are all shown as positive values and closely mimic each other in form. As indicated by the plots, direction 3 tends to be the direction with the largest strain in the mold. This would predict the dominant mold deformation is largely occurring about the vertical axis. Again, based upon the constraint of the mold in the MUD base this makes sense. As discussed in previous tables, the maximum strain in Figure 5.3 is less than that of Figure 5.2 in direction 3.

As previously mentioned the strain gage curves for rosette 3 are mostly comprised of clamping strain. While small strain changes exist, they are even less apparent at lower loading conditions. Even though the wings on the movable mold half most likely deform the strain gage is far removed from the bending point. An analogy to this would be a simply supported beam loaded at its center. The beam would have one pinned end connection and one end with a roller support as seen in Figure 5.5 below. The load would obviously cause the beam to deform the most at its center. While the slope at both ends of the beam would not be equated to zero, the change in slope over a small length near the ends of the beam will be negligible. This is equivalent to what is occurring in the mold during loading. Consequently, the strain curves show little activity during the injection cycle.

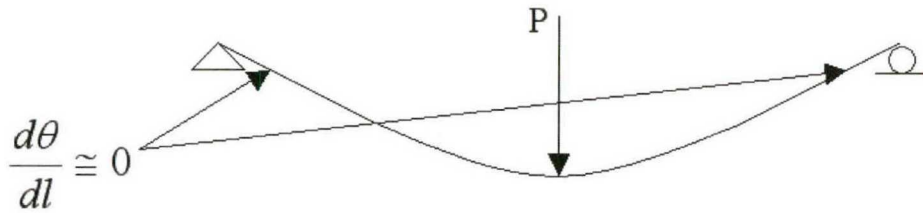


Figure 5.5: Beam analogy for strain apparent in rosette 3.

5.4 ABAQUS™ Strain Results

A total of four simulations were run for the strain analysis comparison in ABAQUS™. Cavity configuration one and cavity configuration four at their worst case loading conditions were analyzed twice; the respective loading was predicted by MoldFlow™. For each case, the cavity pressure loading was applied directly to the cavities, while the applied runner loading was applied as two unique configurations. The first being the runner pressure applied to all legs of the runner system, and the second being applied only to the secondary and tertiary legs of the runner system as previously described in Chapter 4.

The following contour plots show the strain distribution for cavity configuration one with only the secondary and tertiary runner loads. Each contour plot represents the strain in a direction corresponding to the experimental strain directions. While the contour plots display the strain distribution, ABAQUS™ probing tools were used to closely identify the strain values at the true location of the strain gages affixed to the moveable mold half. Results for all of the analyses performed in ABAQUS™ are summarized in Figures 5.9 through 5.14.

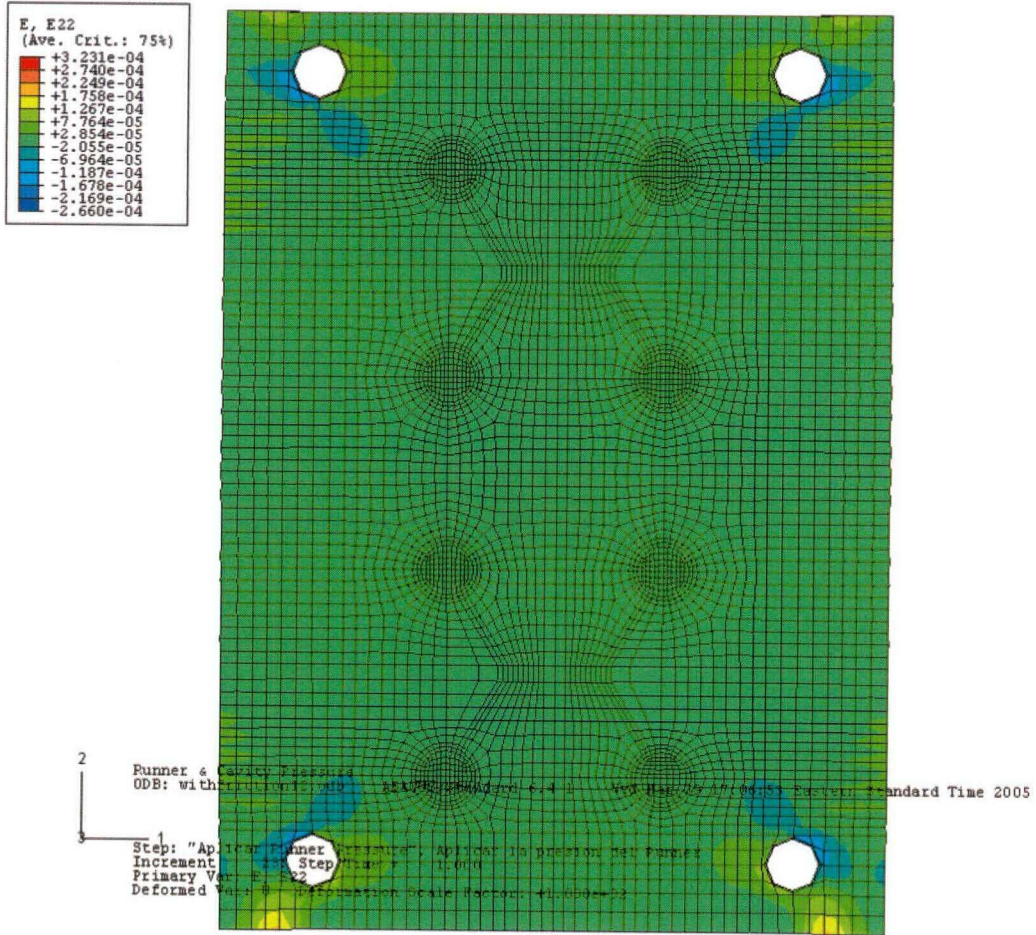


Figure 5.6: Strain results generated in ABAQUS™ for direction 1. (Configuration 1, 40% FS injection velocity, 20% FS pack pressure)

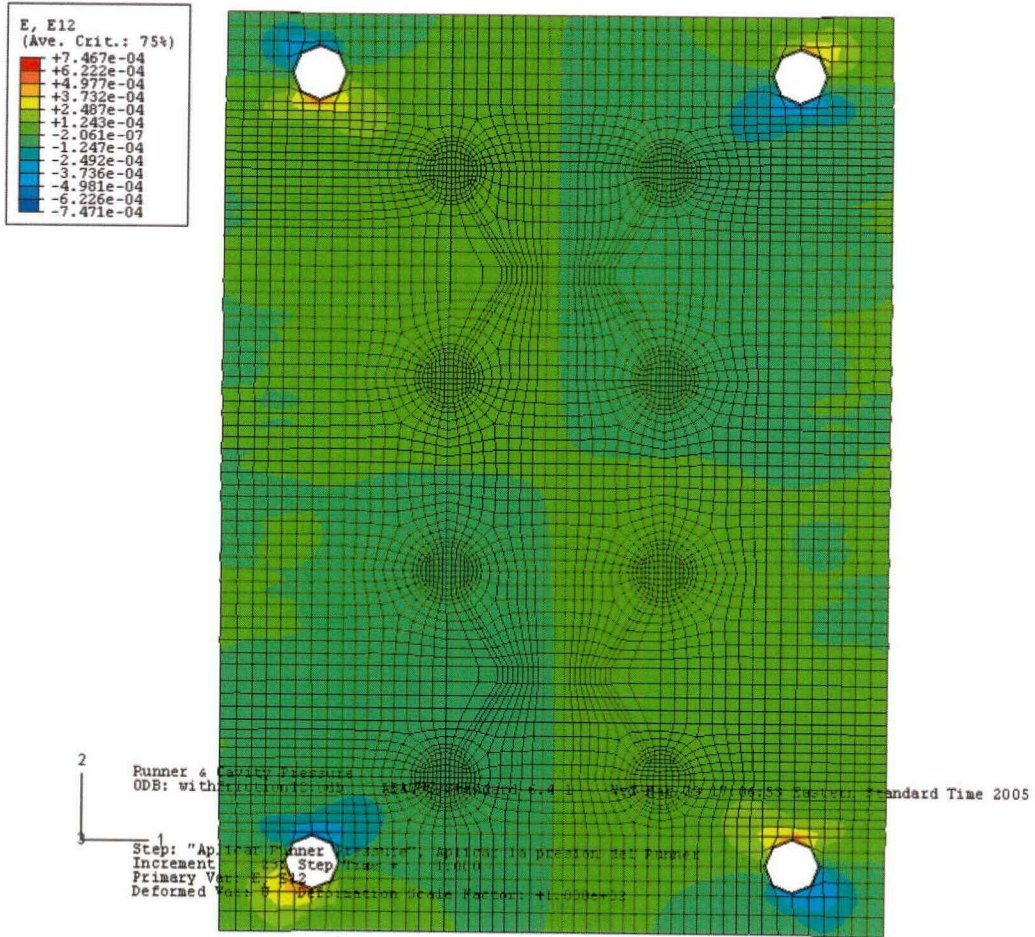


Figure 5.7: Strain results generated in ABAQUS™ for direction 2. (Configuration 1, 40% FS injection velocity, 20% FS pack pressure)

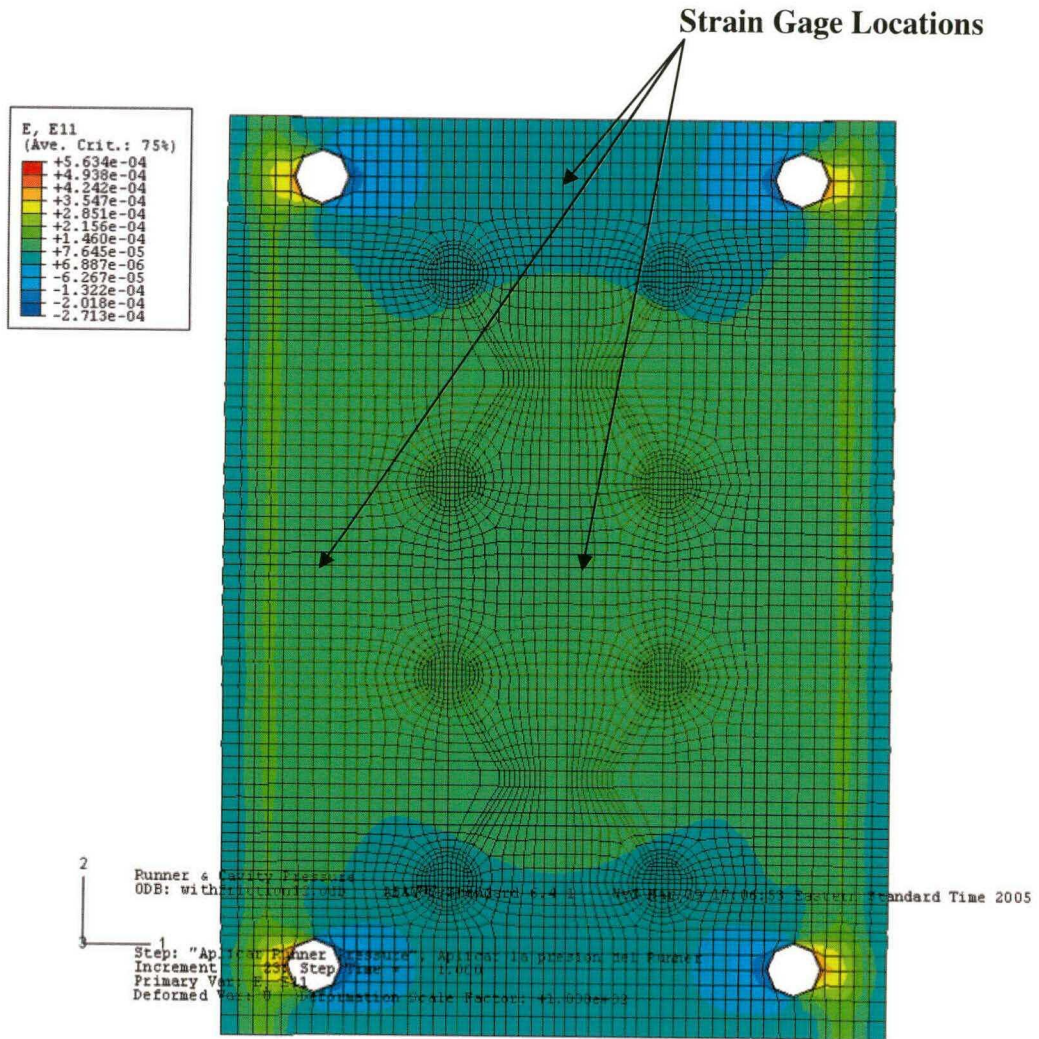


Figure 5.8: Strain results generated in ABAQUS™ for direction 3.
(Configuration 1, 40% FS injection velocity, 20% FS pack pressure)

When reviewing the strain gage data for the validation of the simulations performed in ABAQUS™, it is evident that there is little correlation in direction 2 for all cases. On the other hand, strain gage rosette 2 has the best overall correlation to the simulation results. The results in Figures 5.9 and 5.14 beg the question of the integrity of the FEM and its assumptions. In the experiments the top the mold exhibits the largest strain values, which inherently makes sense per the previous discussion of the rigidity of the MUD base. This would be even more expected of the condition when the main runner leg of mold is not loaded. In fact, the differences in strain are only upwards of 14%, although it is important to note that the strain directional prediction is accurate for strain gage rosette one and two.



Figure 5.9: Strain gage rosette one results comparison for configuration one (µε) for 40% FS injection velocity and 20% FS pack pressure.

**Summary of Strain Results for Rosette 2, Configuration 1,
for 40% FS injection velocity and 20% FS pack pressure**

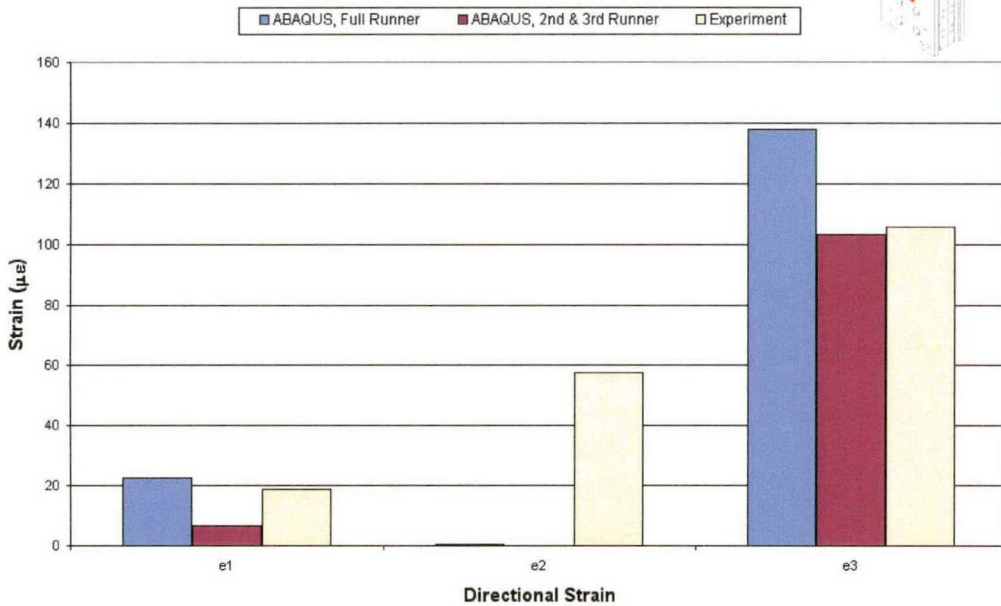
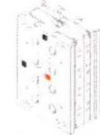


Figure 5.10: Strain gage rosette two results comparison for configuration one ($\mu\epsilon$) for 40% FS injection velocity and 20% FS pack pressure.

**Summary of Strain Results for Rosette 3, Configuration 1,
for 40% FS injection velocity and 20% FS pack pressure**

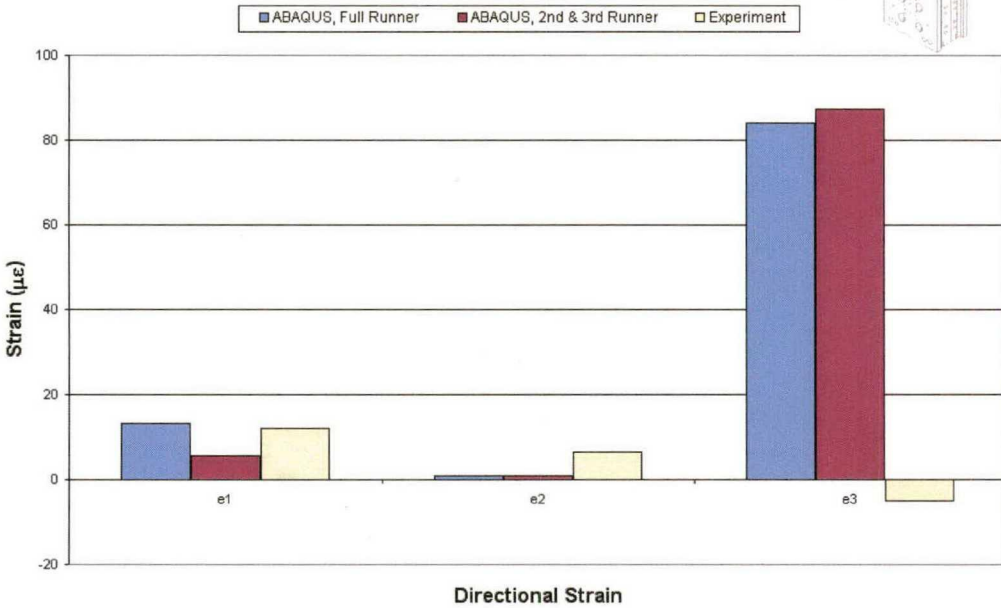


Figure 5.11: Strain gage rosette three results comparison for configuration one ($\mu\epsilon$) for 40% FS injection velocity and 20% FS pack pressure.

While the experimental values at strain rosette one compared to the simulations differ by a factor of 2, the strain prediction of the simulation at rosette location number three is of more concern. It is believed that the element interface used in the computation may have been incorrectly used for prediction. There is also some question as to the predictive capabilities of the contact analysis used. The mold, as it is constrained, will bend at its center, causing the ends to lift from contact. Figure 5.15 below shows the Von Mises stress distribution in the mold, which illustrates this behavior. The support of the mold is easily seen in this figure. The wings on the moveable mold half are not solely supporting the mold, as there is a small width of the entire mold thickness supported by the MUD base slot. The rigidity of the mold at this point is extremely large compared to the thinner wing section. The elements themselves seem to show signs of “hour glassing,” a FEM phenomenon that can cause erroneous results. This is undesired and typically requires the use of a different element type to resolve the issue. Additionally, the FE model would be more rigid than the true mold. Therefore, it would be expected that the strain values are less than that of the experiment. In some of the cases above this statement holds true, but fails the majority of the time.

While the strain gage correlation is important to this research, it is important to note that additional research is currently ongoing in the area of FEM iterations. Through iteration, it was learned that further modeling of additional machine components has greatly increased the precision of the FEM prediction capabilities. Additionally, the additional interfaces required between machine components may in fact complicate the model, while at the same time the predictive capabilities may have been reduced. It should be noted the subject of this paper is to focus on the molding process and data

obtained. It is hoped that the experimental data obtained will help in the ongoing research to develop a numerical solution for elastic mold deformation in the injection molding process.

As previously indicated, an additional configuration was run for the FEM prediction validation. Similar to the results in Figures 5.9 through 5.11, the following tables summarize the comparison of results for cavity configuration four at the worst case loading condition. For the most part, the same discrepancies seen above in the data from configuration one are still applicable. However, the most notable difference is the better correlation for strain gage rosette one versus strain gage rosette two. These discrepancies provide further that support that the FE model needs some further work.

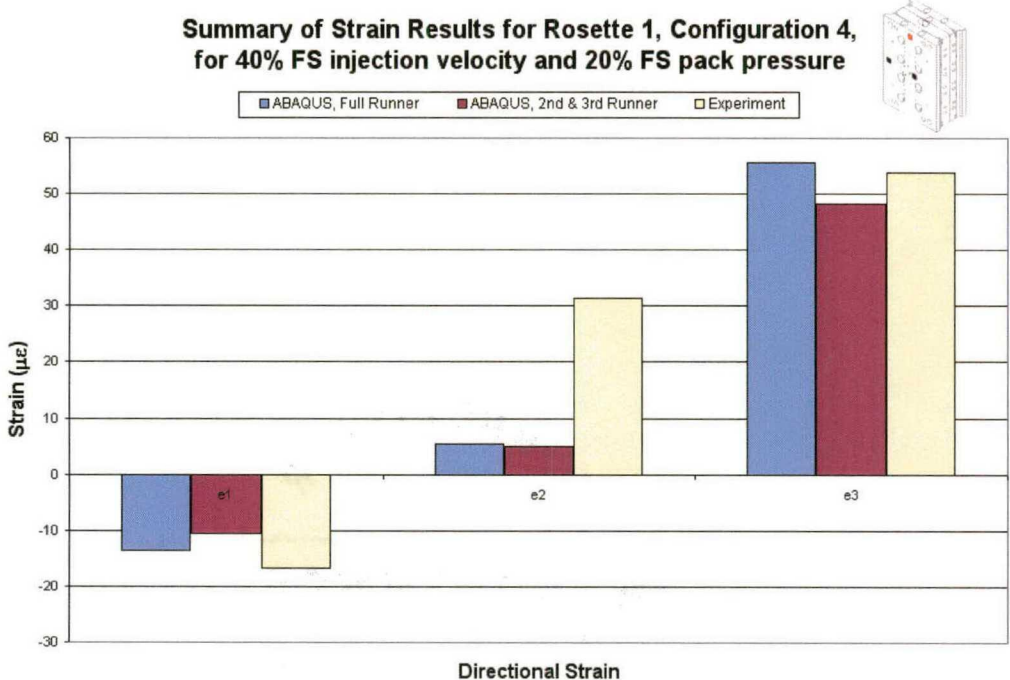


Figure 5.12: Strain gage rosette one results comparison for configuration four ($\mu\epsilon$) for 40% FS injection velocity and 20% FS pack pressure.

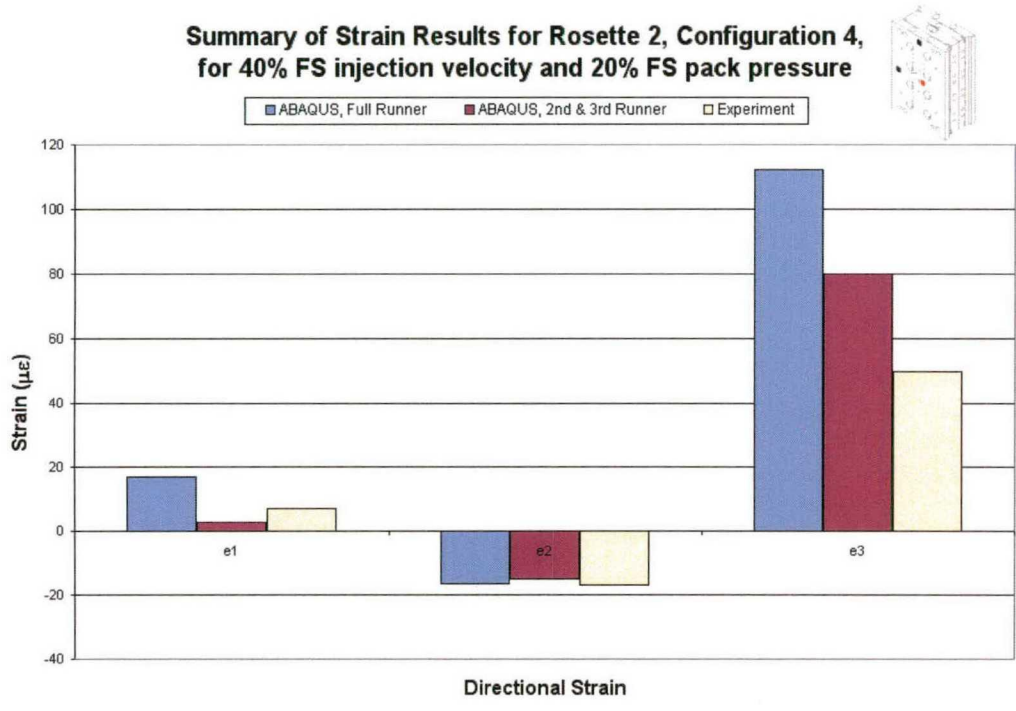


Figure 5.13: Strain gage rosette two results comparison for configuration four ($\mu\epsilon$) for 40% FS injection velocity and 20% FS pack pressure.

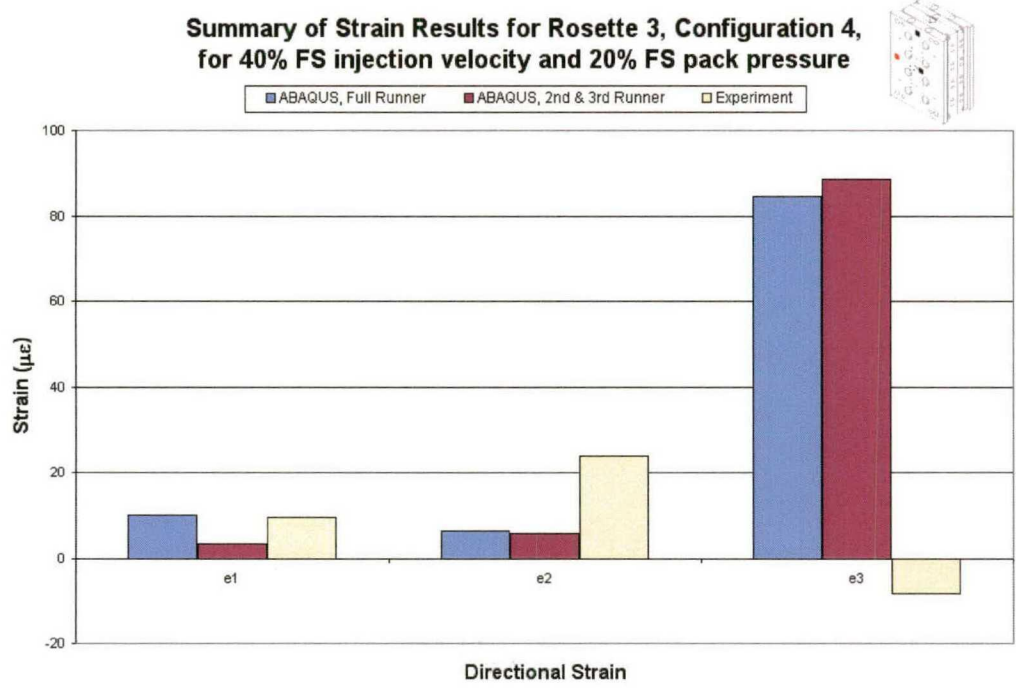


Figure 5.14: Strain gage rosette three results comparison for configuration four ($\mu\epsilon$) for 40% FS injection velocity and 20% FS pack pressure.

Figure 5.15 below illustrates the predicted mold deformation for cavity configuration one at the worst case loading condition. While the expected shape of the deformed mold is visible, the interesting deformation in the contour plot is that of the MUD base itself. While loading and process control is critical to the minimization of excess mold loading, other machine components play a vital role in the response of the mold to the applied loads. It is simulations like the one seen below that could help machine designers optimize machine components to minimize unwanted machine response.

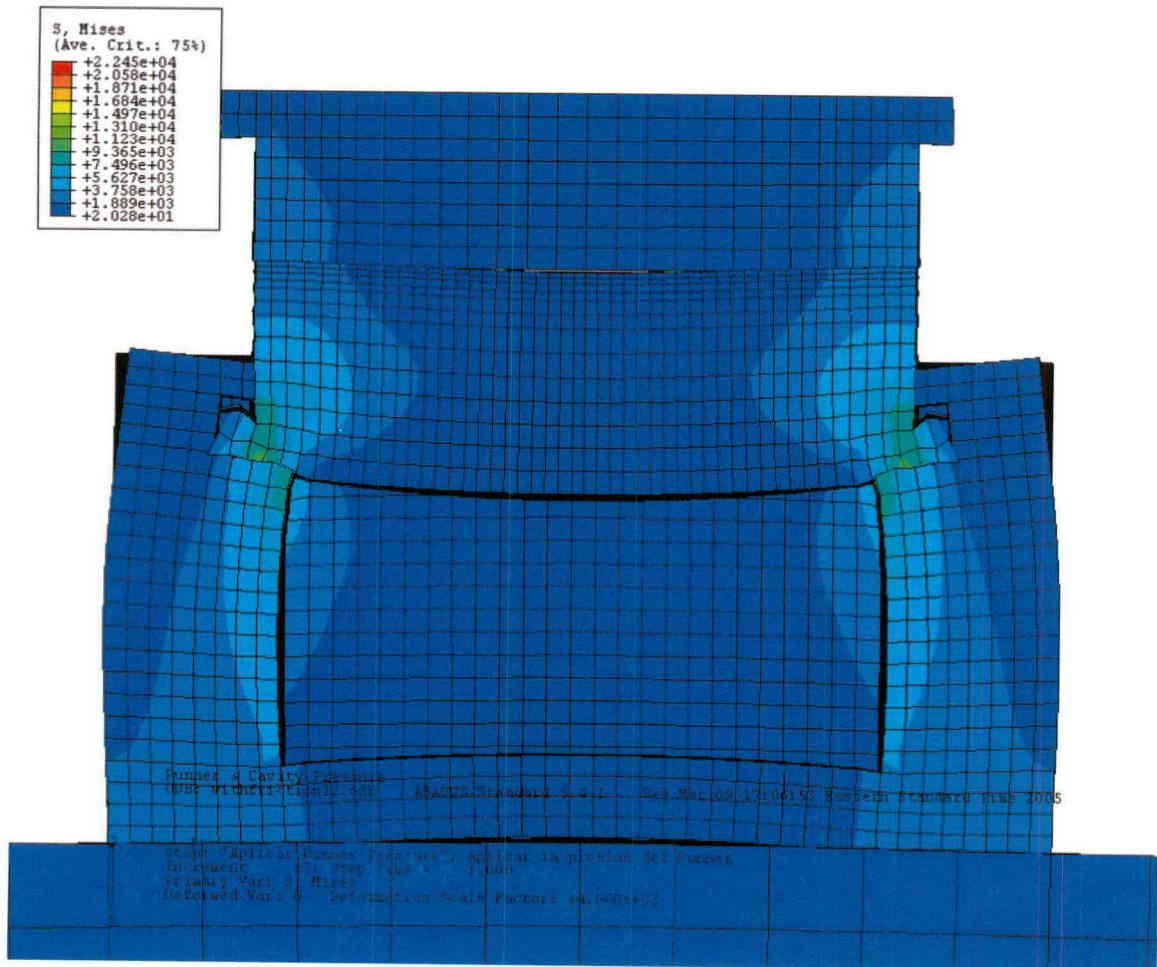


Figure 5.15: Mold deformation prediction by ABAQUS™ for secondary and tertiary runner loading. (Configuration 1, 40% FS injection velocity, 20% FS pack pressure)

5.5 LVDT Results

Similar to the strain gage data, the LVDT data was analyzed using macros within Microsoft Excel. Calibration sensitivities were used to convert voltage values into the corresponding displacements. Since each LVDT has a different zero reference, each LVDT was analyzed separately and transformed later for graphical purposes. The LVDT data was analyzed around the switchover position and at gate freeze off. As seen in the strain data, the switchover position is approximately the time when the mold sees the largest load, which may or may not contribute to a measurable separation of the mold parting plane. Furthermore, if mold separation at the parting plane exists, the LVDT position observed at gate freeze off will determine if the mold returns to its original position. Any residual opening of the mold would result in an overall increase in part length.

The analytical macro used was designed to detect changes in the LVDT position as small as 0.0001 inches. Because of noise inherent in the signal during the small displacement measurements, averaging was performed in 0.010-second intervals. While the device itself has errors due to hysteresis, repeatability, etc., the analysis was designed to be thorough. Errors inherent to the transducer were taken into account when analyzing the overall results attained.

While the strain gage data has five replicates for each strain gage, the LVDT data has fifteen data points. This increase in points gives more confidence in the data for a predictive analysis. Similar to the strain data discussed above, the LVDT results displayed will be for the same conditions of the previously discussed strain data for

parallel comparison and discussion. The LVDT data was averaged and analyzed for variance as well. Standard deviation values range from 0.0000 to 0.0002 inches, while variance in the LVDT was more apparent at larger displacements. Table 5.10 below summarizes the results for configuration one, taken in parallel with the data in Table 5.4. The LVDTs were ordered 0 through 3 with the 0 transducer being located in the top left corner of the mold face relative to the movable mold half. The transducers were positioned clockwise from the LVDT 0.

LVDT	Separation of Parting Plane	Separation at Gate Freeze Off
0	0.0005	0.0000
1	0.0008	0.0000
2	0.0014	0.0001
3	0.0012	0.0001

Table 5.10: Summary of the average mold separation at the parting plane at worst case loading condition for the injection of cavity configuration one. (40% FS injection velocity, 20% FS packing pressure)

Initially, the first thing that stands out in Table 5.10 is the non-uniformity in mold separation at the parting plane. This would suggest the mold is opening like a book, hinged at the top. This is somewhat alarming; since the difference in separation is a factor of 2. Therefore, it is possible the cavities on the lower halves of the mold would produce parts with an increased axial length relative to the upper half. However, reviewing the separation of the mold at gate freeze off compared to the initial clamping there is little evidence to support the fact that the mold remains separated after the gates freeze. Calculated values are within the range of error estimated in the LVDT calibration and repeatability study. Therefore, no concrete conclusions can be made of any residual

separation apparent at the gate freeze off time. This is consistent for all of the configurations run. The following tables summarize the analysis of mold separation at the parting plane for configurations two through four.

LVDT	Separation of Parting Plane	Separation at Gate Freeze Off
0	0.0002	0.0000
1	0.0002	0.0000
2	0.0003	0.0000
3	0.0003	0.0000

Table 5.11: Summary of the average mold separation at the parting plane at worst case loading condition for the injection of cavity configuration two. (40% FS injection velocity, 20% FS packing pressure)

LVDT	Separation of Parting Plane	Separation at Gate Freeze Off
0	0.0002	0.0000
1	0.0003	0.0000
2	0.0003	0.0000
3	0.0003	0.0000

Table 5.12: Summary of the average mold separation at the parting plane at worst case loading condition for the injection of cavity configuration three. (40% FS injection velocity, 20% FS packing pressure)

LVDT	Separation of Parting Plane	Separation at Gate Freeze Off
0	0.0002	0.0000
1	0.0002	0.0000
2	0.0003	0.0000
3	0.0002	0.0000

Table 5.13: Summary of the average mold separation at the parting plane at worst case loading condition for the injection of cavity configuration four. (40% FS injection velocity, 20% FS packing pressure)

Reviewing the data shown in Tables 5.10 through 5.13, the four cavity configurations, it is evident that the mold separation at the parting plane is much more uniform in nature. While mold separation is unwanted, a uniform separation could be easily compensated for. Also the order of magnitude of separation for configurations two through four is much less than seen in configuration one. Furthermore, the separation at gate freeze off is negligible. For all of the data reviewed, the bottom of the mold still showed a slight tendency to open more than the top of the mold. On a side note, the LVDT for configuration five showed no mold separation and therefore was not shown in tabular form.

In order to visualize the deformation recorded, the following plots illustrate the LVDT position curve during the filling and packing phase. The curves have been transformed for a zero displacement prior to the injection of the thermoplastic. The injector screw position curve was also plotted. As seen in each plot, noise is apparent, and increases as the LVDT displacement decreases. Furthermore, the frequency of the noise remains consistent throughout the length of the signals.

Absolute Deflection of Moving Platen Relative to Fixed Platen For Configuration 1, 40% Injection Velocity, and 20% Pack Pressure

(Positive displacement correlates to platen movement towards parting plane)

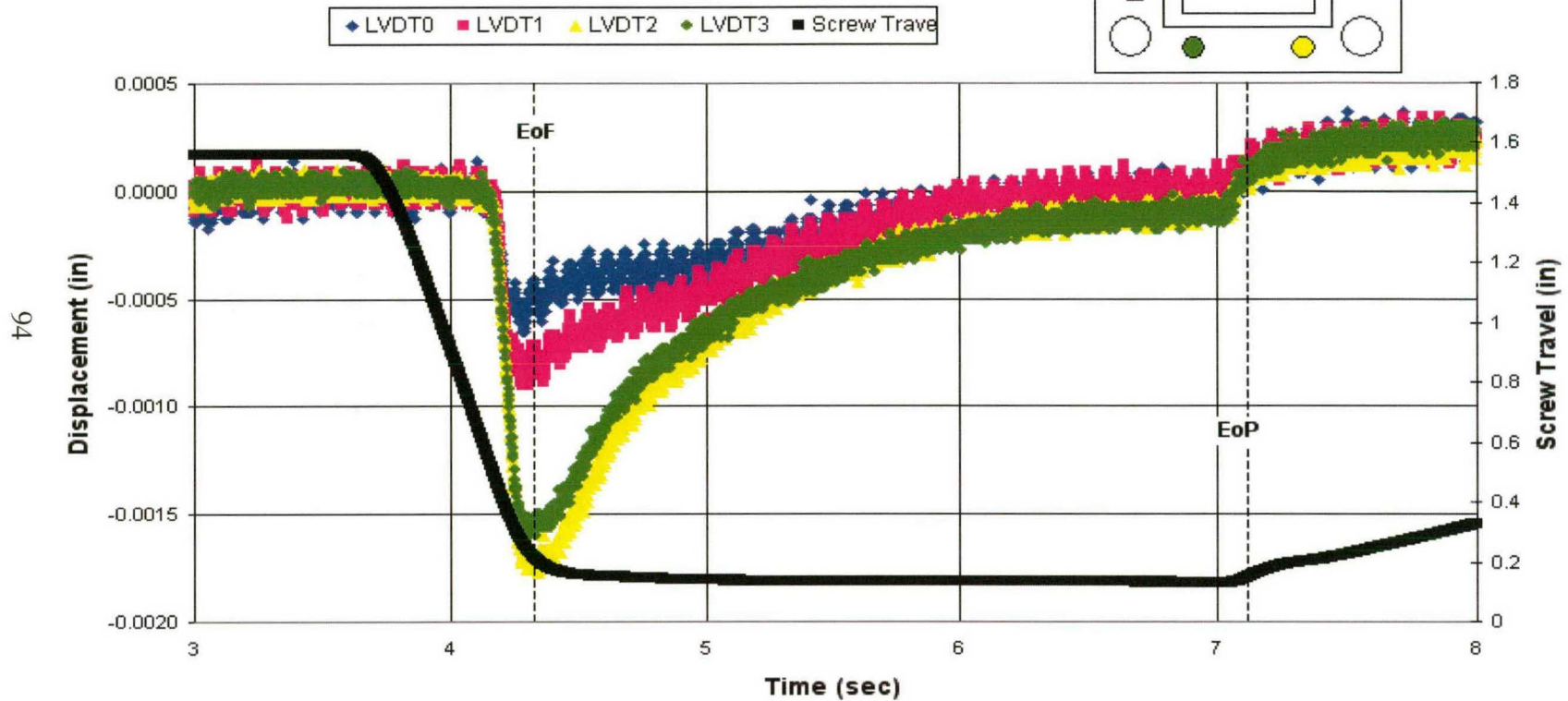
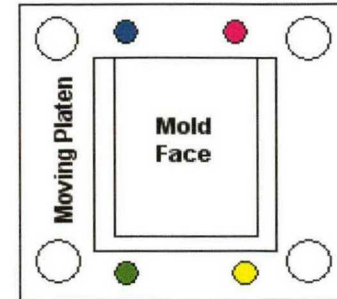


Figure 5.16: LVDT curves for configuration 1, 40% injection velocity and 20% packing pressure.

Absolute Deflection of Moving Platen Relative to Fixed Platen For Configuration 2, 40% Injection Velocity, and 20% Pack Pressure

(Positive displacement correlates to platen movement towards parting plane)

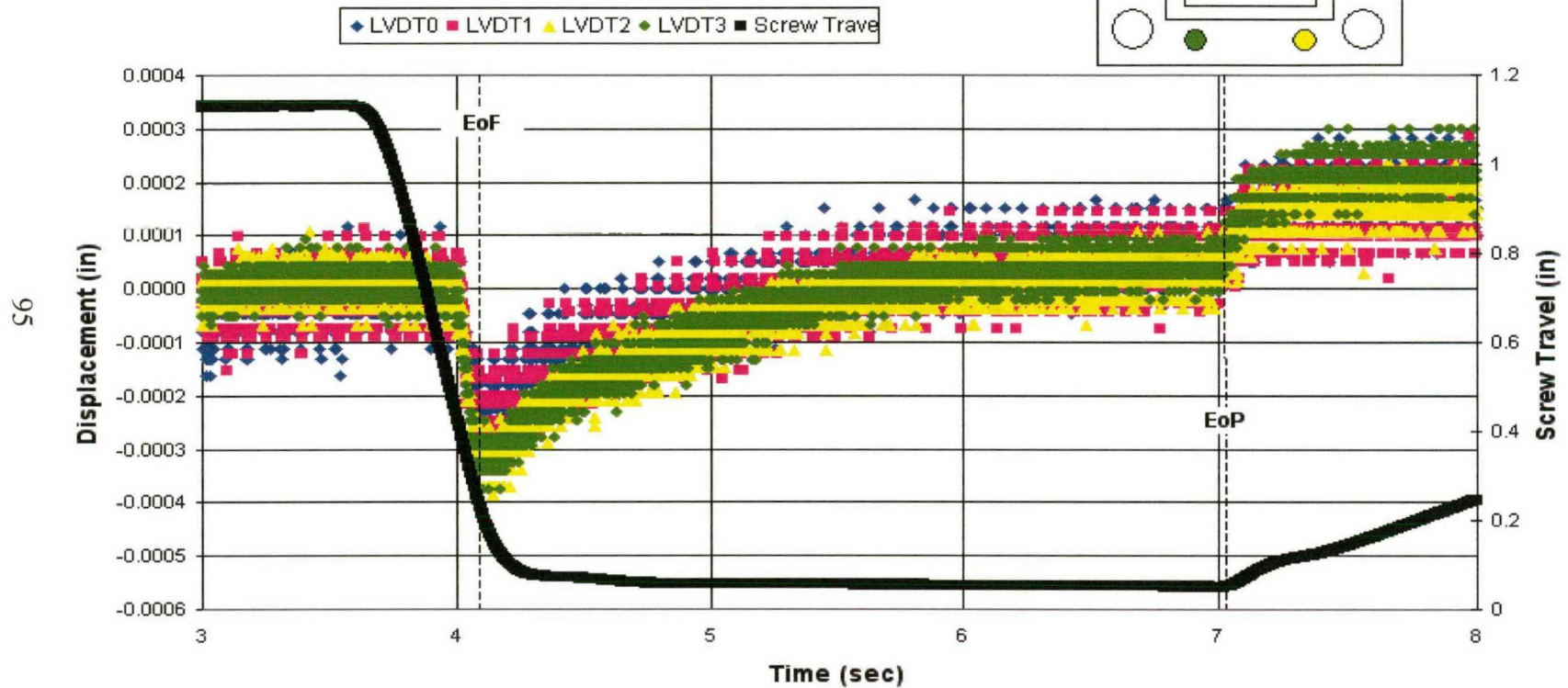
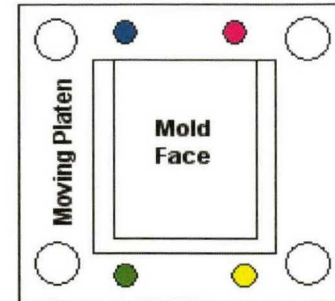


Figure 5.17: LVDT curves for configuration 2, 40% injection velocity and 20% packing pressure.

Absolute Deflection of Moving Platen Relative to Fixed Platen For Configuration 3, 40% Injection Velocity, and 20% Pack Pressure

(Positive displacement correlates to platen movement towards parting plane)

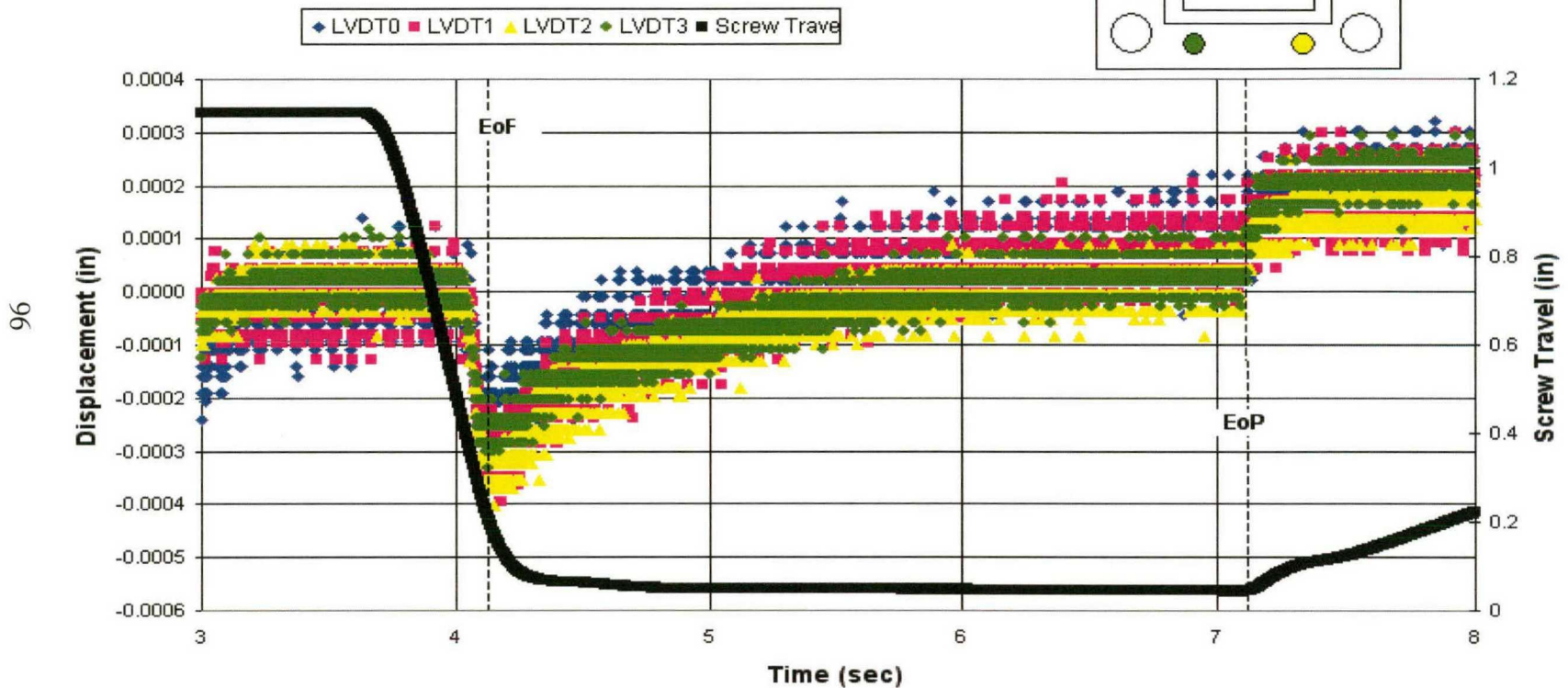
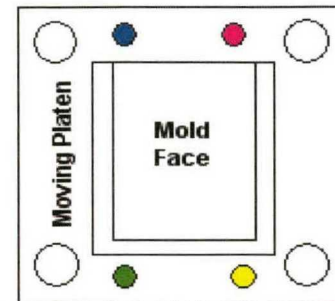


Figure 5.18: LVDT curves for configuration 3, 40% injection velocity and 20% packing pressure.

Absolute Deflection of Moving Platen Relative to Fixed Platen For Configuration 4, 40% Injection Velocity, and 20% Pack Pressure

(Positive displacement correlates to platen movement towards parting plane)

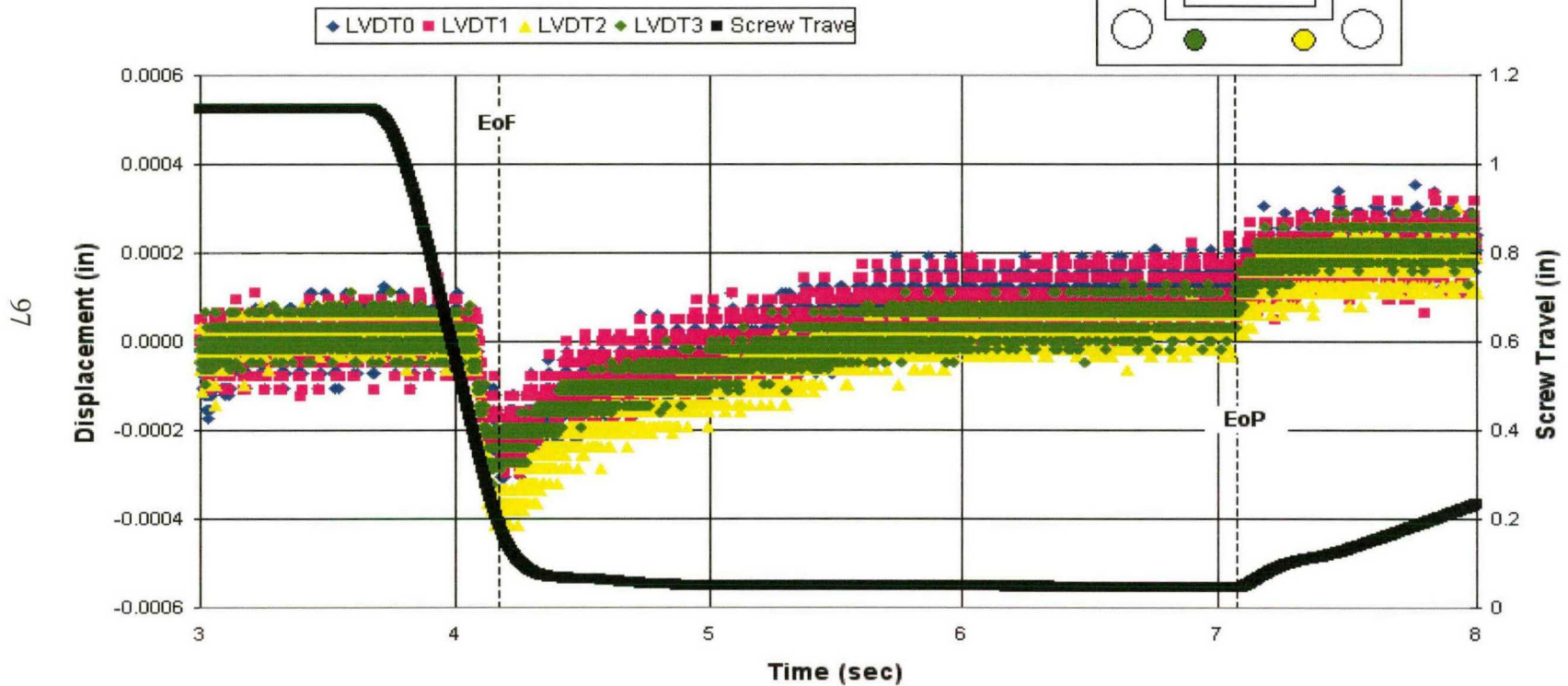
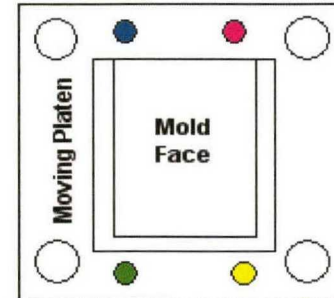


Figure 5.19: LVDT curves for configuration 4, 40% injection velocity and 20% packing pressure.

For each graph investigated a spike in the LVDT curves can be seen around the end of fill stage. In a close examination of the spike occurrence, all instances of the mold separation occurs when the first cavity is filled and the pressure has transferred loading through the mold. Due to the imbalances present in the gate and runner system, the injector screw position for each configuration was recorded when the first cavity filled and when all cavities were full. When comparing the LVDT data and the injector screw position it is obvious the separation began when the first cavity was filled and peaked when all the cavities were full.

In general, at gate freeze off for all the configurations, the mold has returned to its original position, within 0.0001 inches. It is important to note that the mold still separates during the packing phase prior to the gates freezing. This means that the parts were still under the holding pressure and would fill a void created by the mold separation at the parting plane. It is clear that the parts were over packed more than if the mold faces had remained intact.

As the gates and sprue began to freeze, the clamping load would dominate and compress the mold, as explained by the absence of a residual mold separation at the gate freeze off. The parts were then compressed to conform to the cavity dimensions, but once the mold was opened the residual stress in the part(s) and mold would be released. At this point the parts may expand some small amount. A close examination of the part geometry would help in the verification of this theory.

It is important to note that under less severe operating conditions the mold separation at the parting plane tended to be more uniform. This would be important to

know in an optimization plan. It would seem the mold could respond better to slower injection velocities. Furthermore, any unbalances in the mold may have an effect on this phenomenon.

In order to understand the loading of the mold, MoldFlowTM was used to determine the pressure distribution within the cavities. For the eight-cavity configuration, it was hoped that the model would help in the explanation of the non-uniform mold separation at the parting plane. Since the model was built with the actual measured gate diameters it was representative of the actual mold. It is believed that the imbalances in the mold may play a large role in the asymmetric mold separation at the parting plane. A contour plot of the pressure was generated in MoldFlowTM at the time in which the mold separation was recorded. The results are quite interesting.

Figure 5.20 below, predicts the cavity pressure in the bottom cavities of the mold during the injection cycle to peak prior to the upper row. This prediction would parallel with the LVDT results discussed above. Ultimately, this would mean that the unbalance in the gates and runners may play a larger role in the asymmetric mold separation at the parting plane. A previous study on the eight-cavity configuration was performed to determine the percent imbalance in the mold. This value was estimated to be upwards of 28%. While theories exist that predict flow unbalances in cavities tend to dissipate as a cavity is packed [10], it may be that these same imbalances seen during the fill and at the end of fill stage are of great importance as a factor affecting uniform mold separation at the parting plane. This could be extremely important in mold optimization and minimization of part variance.

In order to fully validate this theory the mold could be equipped with pressure transducers in the four outer most cavities. The pressure history of a cycle could then be recorded and compared to the FEM. While this study could prove invaluable, due to the essence of time and funding, it was not pursued at this time. Furthermore, this discovery will open the door for future investigations.

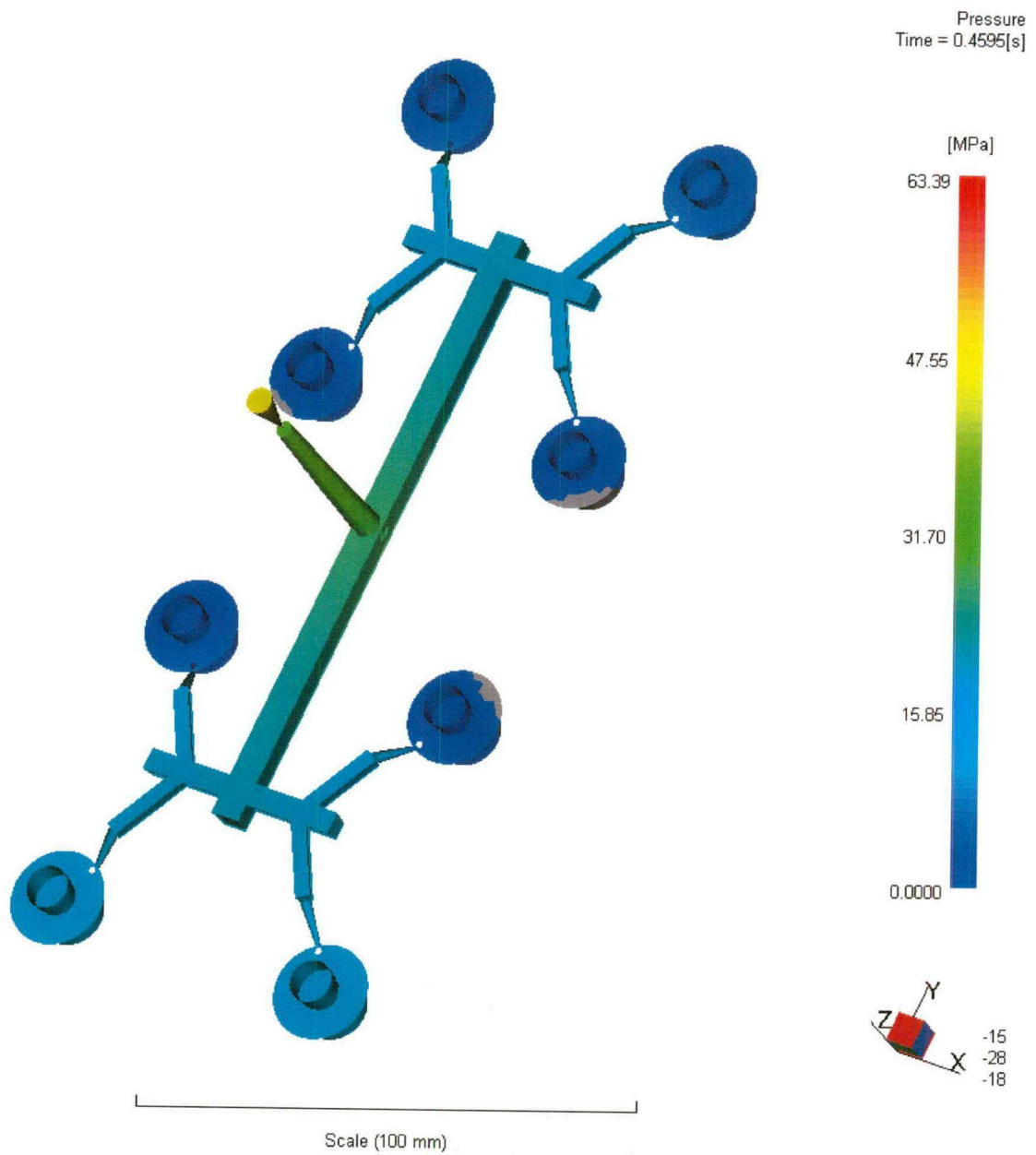


Figure 5.20: MoldFlow™ prediction of cavity pressure distribution at the end of fill.

5.6 Part Results

The information available to study about the injection molding process has become increasingly large. Therefore, it was important to collect some physical data on the parts molded during the process. Two investigations of the parts were performed, the first being, to obtain the mass of each individual part. This was done using an Ohaus Galaxy 110 precision balance. The balance had a decimal place accuracy of four digits and was repeatable to 0.0001 grams. Ten replicates for each cavity were weighed and the mean and standard deviation were generated using Microsoft Excel. An analysis of variance was also performed on the acquired data.

After being weighed, two axial features of size dimensions were measured using a Sheffield Coordinate Measuring Machine or CMM for short. The width of the thin flange of the part and the width of the largest outside diameter were the dimensions of interest. A specific jig was designed and built to hold ten replicates of a cavity at once. This allowed for a quicker measurement of the parts and easier data management. Figures 5.21 and 5.22 shows images of the CMM and the parts mounted in the jig respectively. A 0.5 mm ruby tip sphere on a 20 mm extension was used to measure the parts on the CMM. The tip was calibrated on the calibration sphere affixed to the CMM table. The calibration of the tip was performed using the provided software package, MaxLite™.

The software package, MeasureMax™, was then used to write the program for the CMM to measure the parts located in the jig. The software generated a tab delimited text file after the measurements were complete. This data was then imported into Microsoft

Excel. A macro was developed in Visual Basic to compile and analyze the data statistically.

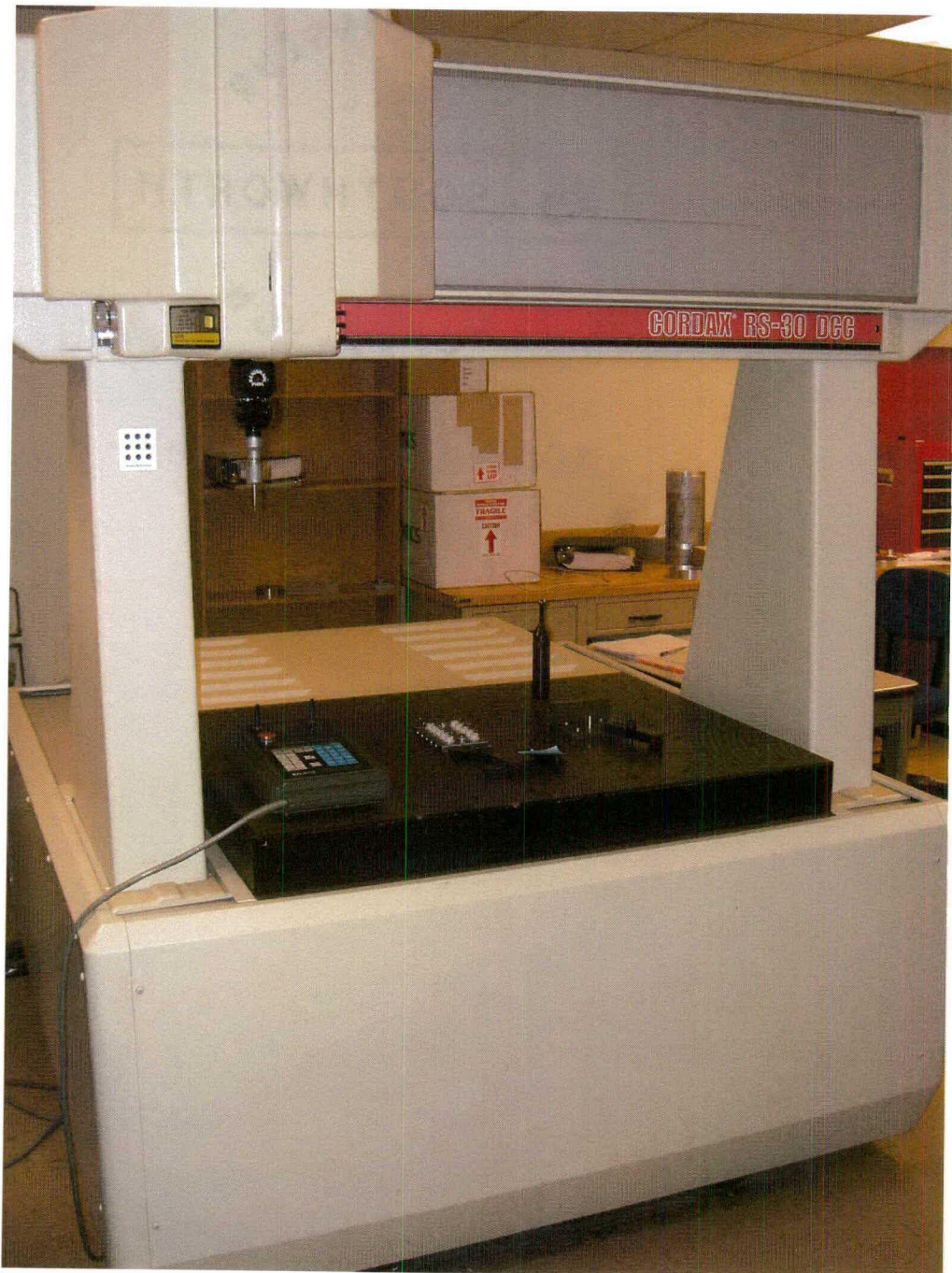


Figure 5.21: Sheffield Coordinate Measuring Machine.



Figure 5.22: CMM jig used to fixture parts during measurement.

When separation at the mold-parting plane occurs, an increase in only one dimension occurs. This is the width of the thin flange of the part as shown a dimension D1 in Figure 5.23 below. The image shows the relevance of separation and its effect on this part feature of size.

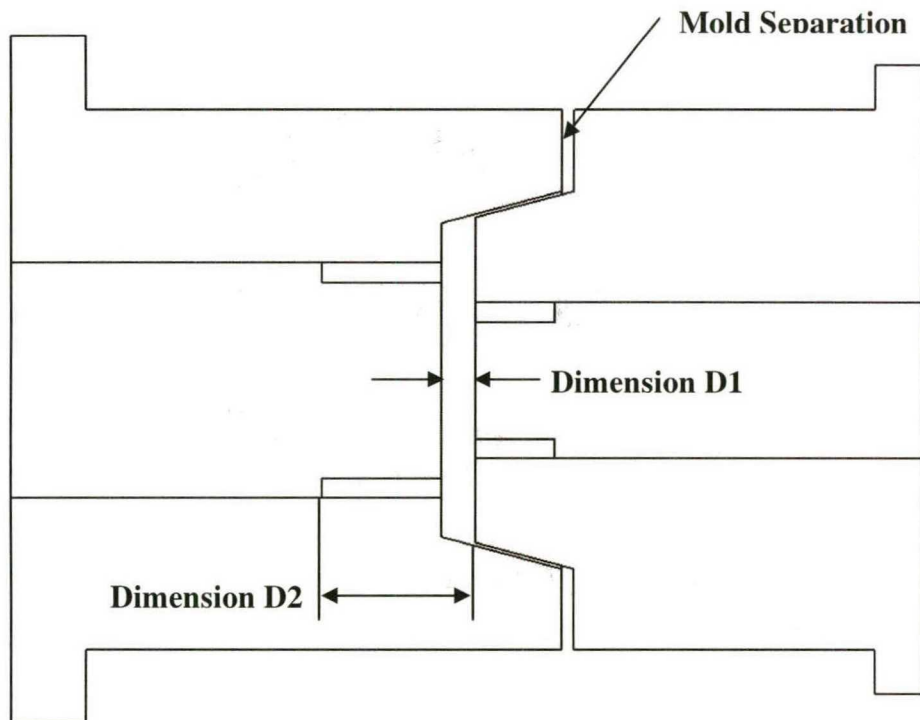


Figure 5.23: Schematic illustrating mold separation at the parting plane.

Upon completion of the analysis of the parts, the data for both the weight and feature of size measurements were combined. The corresponding mold cavity features of size dimensions were also measured on the CMM for comparison. It is important to note that the CMM machine used had a linear accuracy of 0.0002 inches and a repeatability of 0.0001 inches.

Precision injection molding, as classified by Wenskus, [11] occurs when the normalized level of variability in parts is less than 0.1%. Wenskus writes, that weight is “about an order of magnitude better in resolution than dimensional measurement devices and is less susceptible to many forms of operator-induced measurement errors.” Furthermore, his study on the relationship between dimensional and weight characteristics using regression analysis showed no interactions effects when the level of variability was less than 0.1%. This is of relevance because the normalized level of variability for the parts produced in this study are less than or equal to 0.1%.

Using the software program MINITAB, an analysis of variance (ANOVA) was performed on the full factorial data set produced. Data for dimensions and part mass were entered into MINITAB for the corresponding control variables of injection velocity (V) and packing pressure (P). Each control variable was normalized for the three levels as -1, 0, 1. Initially a full quadratic linear regression was run for the each response for each cavity. In order to analyze the results, the minimal probability, p , for an effect was set at 0.05 or a 95% confidence. The mass response showed the best regression prediction upwards of the 95th percentile, while the dimensional models were on average in the 63th percentile.

In regards to the mass response, there is no obvious trend in the full quadratic model, but generally the squared terms showed little to no effect on the response. The injection velocity terms were also seen as negligible, as visible in the main effect plot in Figures 5.24. Additionally, the interaction plot, as seen in Figure 5.25, shows that the interaction effect is relatively constant regardless of the magnitude of the injection velocity. The only cavities having an effect from the injection velocity were cavities 1

and 2, the first cavities predicted to fill by MoldFlow™. Therefore the regression models were regenerated with MINITAB as linear models with interactions. In both models the weights of the pressure term is by far the largest contributor to part mass, exactly what is to be expected.

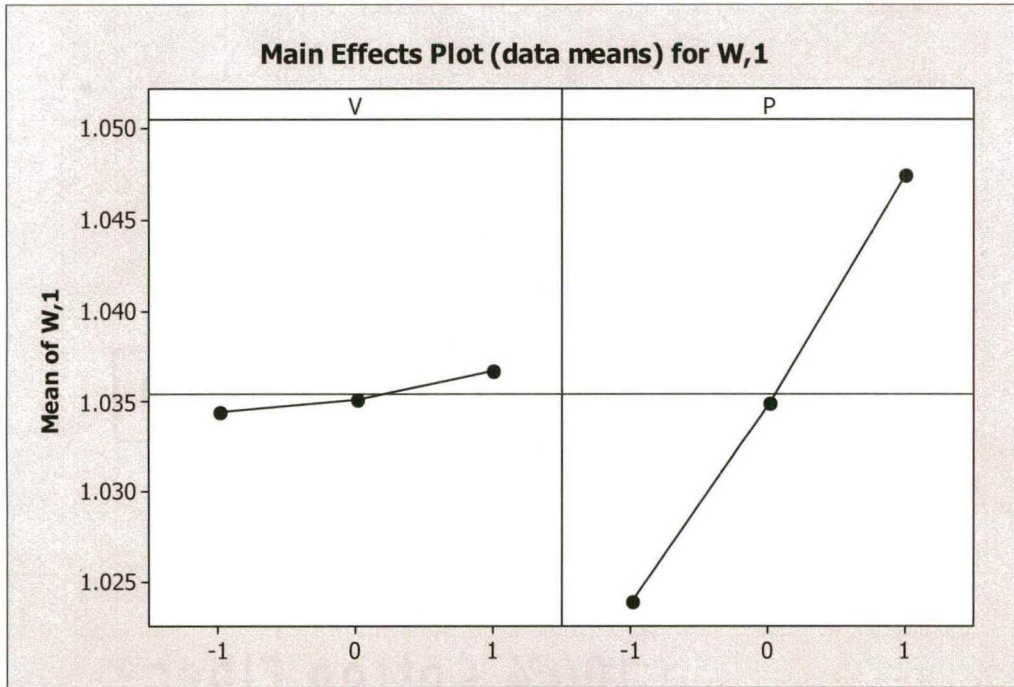


Figure 5.24: Main effects plot for mass (g) of cavity one, configuration one. (V =Injection Velocity, P = Packing Pressure)

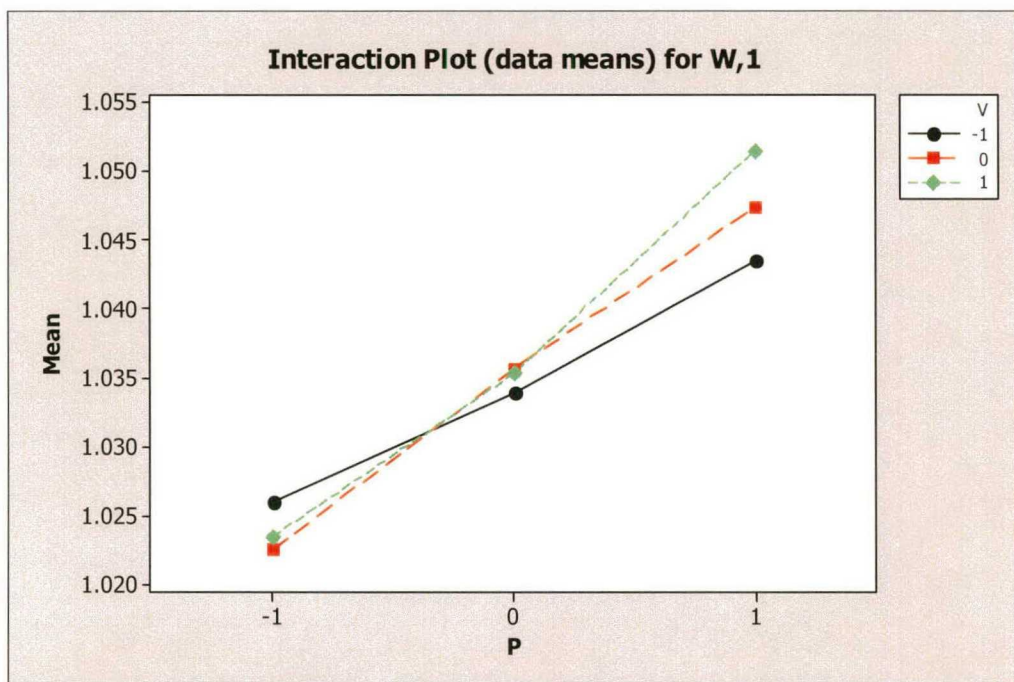


Figure 5.25: Interaction effects plot for mass (g) of cavity one, configuration one. (V =Injection Velocity, P = Packing Pressure)

Furthermore, the integrity of the models were minimally compromised with the loss of the squared terms. Comparing the results, there is no advantage to using the full quadratic model over the linear model with interactions. Additionally, a regression analysis was performed on the average mass of the ten replicates to determine the upper limit to the regression model fit, which increased the prediction confidence to a minimum of the 97th percentile. The comparison of confidence can be seen below in Table 5.14.

Cavity	R ² - Lower	R ² - Upper
1	97.5%	99.3%
2	96.6%	98.9%
3	96.0%	98.9%
4	96.4%	97.5%
5	96.3%	97.5%
6	96.0%	97.4%
7	95.6%	97.5%
8	96.8%	97.2%

Table 5.14: Regression model fits for the mass response (configuration one).

Reviewing the dimensional ANOVA results for the analysis of the CMM measured features of size, as shown in Figure 5.23, no unanimous trend for the weights of the regression models was found. In general the weights of the packing pressure terms were larger than the injection velocity weights. It was also noted that not all cavities had interaction effects between the injection velocity and packing pressure. Furthermore, the dimensional responses showed very poor results for cavity 7. The regression model for cavity 7 in both the feature of size dimensions showed a constant regression model with fits of less than 15% confidence. This phenomenon would be of importance in some instances when the optimization of the molding of multi-cavity parts is critical, as in case

of lens molding. The following tables characterize the regression model fits for each cavity, followed by the main effects and interaction plots for cavity one generated in MINITAB. While these plots show interaction and main effects are present for the dimensions of cavity one, these plots are not relevant for all cavities, especially cavity number 7, as evident in the following tables.

Cavity	R ² - Lower	R ² - Upper
1	79.2%	98.2%
2	53.3%	99.2%
3	76.9%	98.6%
4	60.9%	98.1%
5	77.4%	99.6%
6	70.1%	99.0%
7	4.6%	44.8%
8	60.3%	97.9%

Table 5.15: Regression model fits for the D1 dimension (configuration one).

Cavity	R ² - Lower	R ² - Upper
1	86.7%	98.6%
2	73.2%	98.9%
3	83.8%	98.5%
4	78.0%	98.4%
5	79.8%	98.8%
6	84.2%	97.7%
7	14.1%	79.4%
8	80.0%	99.2%

Table 5.16: Regression model fits for the D2 dimension (configuration one).

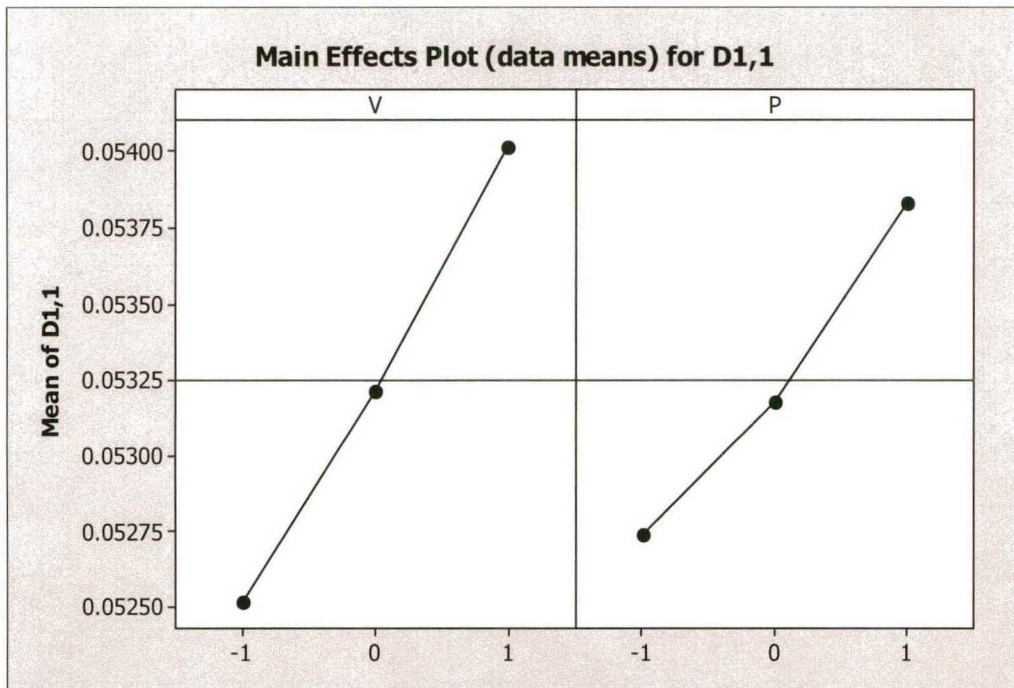


Figure 5.26: Main effects plot for dimension D1 (in) of cavity one, configuration one. (V =Injection Velocity, P = Packing Pressure)

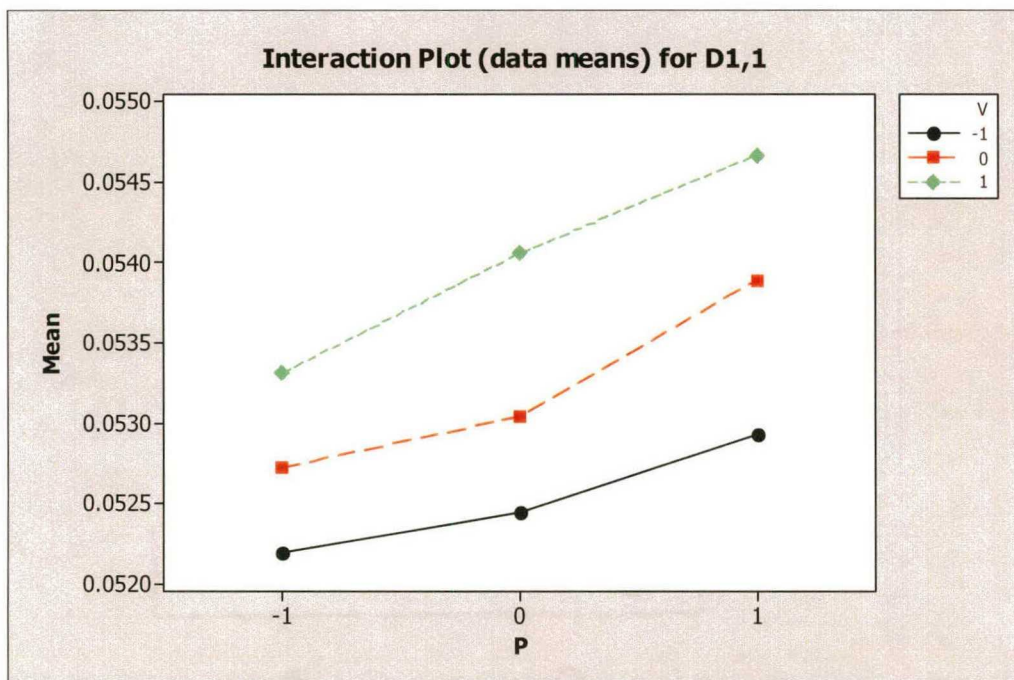


Figure 5.27: Interaction plot for dimension D1 (in) of cavity one, configuration one. (V =Injection Velocity, P = Packing Pressure)

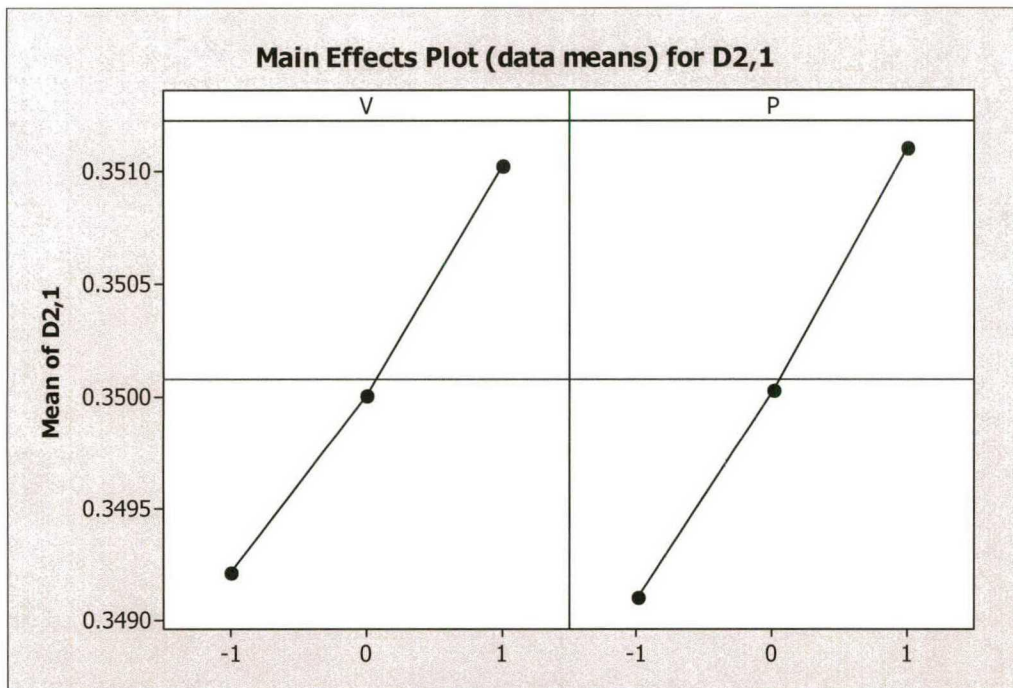


Figure 5.28: Main effects plot for dimension D2 (in) of cavity one, configuration one. (V =Injection Velocity, P = Packing Pressure)

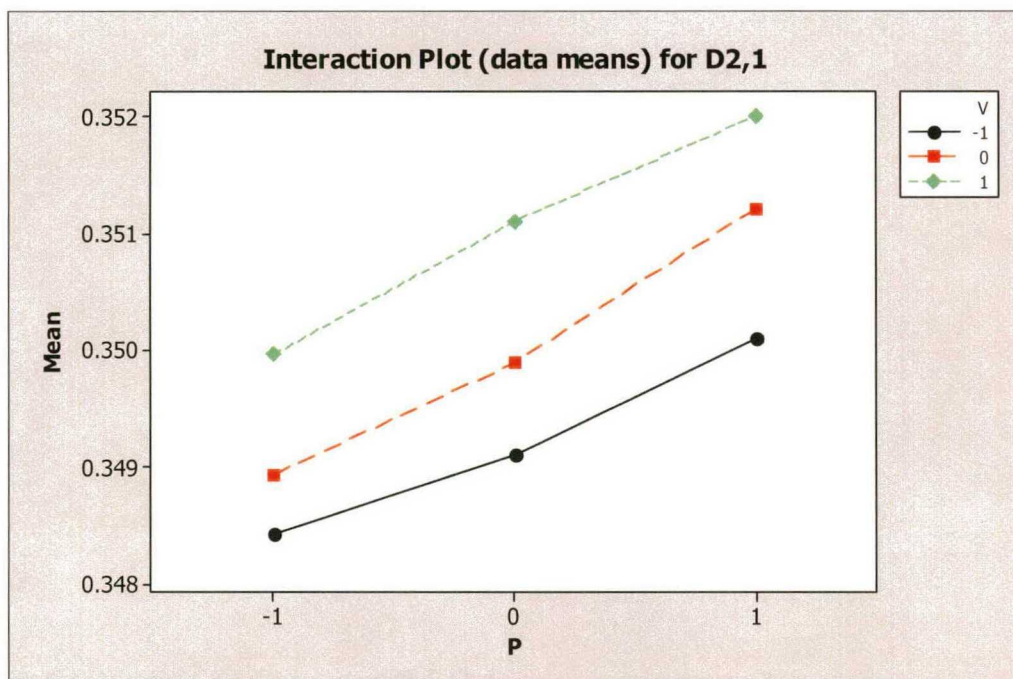


Figure 5.29: Interaction plot for dimension D2 (in) of cavity one, configuration one. (V =Injection Velocity, P = Packing Pressure)

Based upon the results obtained it is very possible that there are other underlying effects that were not investigated that may contribute to the dimensional variance from cavity to cavity. This is especially true in the case of cavity number 7. The gate diameter of cavity 7 is average sized compared to the remaining cavities, so it is unlikely that the imbalances in the mold restrict any injection velocity or packing pressure effects on the cavity. Furthermore, because the parts are precision molded, there would be little interaction between the mass and the dimensional effects, based on Wenskus' study.

Besides the ANOVA, an analysis was performed to compare the part dimensional changes to the mold separation at the parting plane. The only dimension affected by the mold separation at the parting plane is dimension D1. Once again this is evident from Figure 5.23 above. At each experimental condition, dimension D1 is consistently measured larger than the measured value for each cavity size. On average this value ranges from 0.002 to 0.004 inches larger. These values occurred during all magnitudes of the separation of the mold parting plane, even at the null condition. There seems to be some uncertainty about this data due to the fact that parts typically shrink in the mold. While over-packing and a separation at the mold parting plane may cause a slight increase in size and weight, it is not realistic that all the conditions explored would result in an oversized part.

The same measurement strategy was used in measuring the cavities and parts so the procedure should effect the measurements minimally. There is some question if the jig used to grasp the parts may in fact deform the parts slightly. The spring loaded arms were designed to add little force to the parts to minimize deformation. Because the parts are plastic, they deform easily and much care needs to be taken in retention of the parts.

On top of the fixture itself, the parts themselves will undergo some finite amount of warpage when they are released from the mold and cool to their final shape. This may inhibit them from sitting flush in the jig and result in an inaccurate measurement.

Because of the size discrepancies a different approach was used to try to compare the part dimension D1 to the mold separation values. Therefore, the relative increase in dimension D1 was compared to the relative mold separation for each set of injection velocities. So for example, at 40% FS injection velocity, the relative increase in dimension D1 and the relative separation measured at the LVDTs were compared for the 10% to 15% FS packing pressure. The comparison was also done for the 10% to 20% FS and the 15% to 20% FS regimes. The term relative is used because the comparisons are made from the relative difference from one processing condition to the next.

The analysis showed that at the combination of lower injection velocities and lower packing pressures, the relative increase in dimension D1 was small and little to no mold separation was observed. This would indicate that the parts are not being affected by the mold separation. Only an infinitesimal amount of growth was observed as the injection velocity was increased and the mold faces remained intact, presumably this was based on the increase in filling pressure. In the comparison for the cases of 15% to 20% FS packing pressure, the shrinkage effects would be less dominant. It is believed that the over packing effects and or mold separation effects would become dominant.

Reviewing the comparison of data for configurations 1 through 4, regrettably there is no real notable relation in the part dimension D1 and the measured mold separation at the parting plane. The relative comparison generally shows the relative

dimension change of D1 to be consistently larger than the relative mold separation. It would be expected that the part behavior would tend to show the change in D1 to be smaller than the separation magnitude itself. While parts will contain residual stresses in them, it is unlikely an increase would be seen across the board. From this evidence it is believed that the measurements of the parts themselves contain a measurement error in them. As previously mentioned, the jig used to hold the parts in combination with part warpage may contribute to inaccurate measurements. While the CMM can be a versatile machine, it may not be well suited for the parts of interest. Future work may involve a manual measurement of dimension D1 with a tool such as a micrometer. While this process would be tedious because of the large population size, it may minimize error due to the part fixturing and part warpage, although human error will be introduced. Additional error in the measurements may also be a result of measuring the mold separation from platen to platen versus the mold halves themselves. The platen measurements may include unwanted platen deformation.

CHAPTER 6

CONCLUSIONS

6.1 Conclusions

The strain results obtained experimentally and through computer simulation can be summarized as follows: the FE results can generally be used to predict the experimental strain in the multi-cavity mold. While it is evident the results are on the same order of magnitude in the strain gages and simulation, additional work is required in the area of the FEM. The element type used in the FEA is a possible source of error. “Hour glassing” effects have caused some concern in the integrity of the FEM as well as the results obtained. Aside from the meshing characteristics, the interaction constraints and contact analyses have begged further questions. This is especially the case when more of the injection molding machine components are modeled in the FEM. While additional components would complicate the model, it is evident from the FE iterations performed so far, the rigidity of the model is important to the results. At minimum, the MUD base should be included in all analyses performed in order to replicate the true boundary conditions imposed on the movable mold half. While it was not the goal of this study to concentrate on the FEM, it has become critical that these areas be resolved in order to generate a working computational tool to predict and analyze elastic mold deformation accurately.

The effect of elastic mold deformation is apparent from the strain gage data obtained experimentally. Controlling and or minimizing this effect could be crucial in the molding of high precision, multi-cavity parts. Furthermore, it is evident that elastic mold deformation is not the only contributor to an increase in part size. Variance of experimental control variables showed magnitudes of mold separation upwards of 0.002 inches, as well as some non-uniform separation conditions.

While larger values of separation were observed, the separation was no longer evident around the time of gate freeze off. As the thermoplastic parts cool and the load transfer is reduced the mold will close. Furthermore, accurately proving a relationship between the mold separation and an increase in part size has been difficult. Part measurements taken with a CMM have shown excellent repeatability but raise some question with respect to accuracy. The measurements of the features of size consistently show an increase in part size over the actual cavity size. While this may be true at some of the loading conditions to the mold, it should not be prevalent at the lower injection velocities and packing pressures, especially where no mold separation was observed.

An ANOVA has shown a variance of effects of control variables from cavity to cavity. Interestingly enough, some cavities show little to no effect from a change in control variables. This would allow minimal room for optimization of individual cavities relative to the entire set for the studied control variables. The regression analyses used for each response for each cavity were also different. Some cavities' regression models showed more weight related to interaction effects than others, which may or may not be related to the unbalances present in the mold.

6.2 Future Work

While much has been learned throughout this study, many more areas of study have been unearthed. In the interest of time and funding many of these areas of the mold have not been researched, but are worth noting for future endeavors. In the area of strain correlation, more work needs to be done in the area of FEM refinement. This includes the modeling of the machine components as well as improving meshing characteristics. Additional strain gages could be affixed to the mold in other areas of interest in order to try to better correlate the overall simulation. This would be helpful in determining if the top of the mold experiences more strain than the bottom due to the boundary constraint imposed by the MUD base. Strain gages affixed on the MUD base were not utilized during experimentation, but could be used in future experimentation.

Along with the strain study, a pressure transducer could be integrated in the mold to verify the mold cavity pressure. This would give more rigidity to the FEM and MoldFlow™ results. Finally, more information on the material used, Polystyrol 466F, also is required in order to better use MoldFlow™ for its prediction capabilities. This is especially true in the prediction of the loading of the lower two cavities that would correlate to the non-uniform mold separation observed at the worst case loading conditions.

In the area of the mold separation, fixtures can be made for the mold halves so that measurements can be taken relative to the mold faces and not the platen faces. This would reduce the chance of measuring any potential platen deformation and inducing error in the measurements. With proper modifications, an LVDT or other displacement

transducer could be mounted in a cavity and the separation at the cavity itself could be measured as well.

Most of the future work involved with the mold itself would be in the area of the machine control variables as well as in the mold setup. While the mold offers extreme versatility, only one arrangement of the insert-core system was studied. In the mold separation at the parting plane study the mold was noted to open like a book from the bottom of the mold. It would be interesting to invert the insert-core arrangement to try to produce the negative of what was observed experimentally. Furthermore, the arrangement could be studied in order to optimize for minimal non-uniformity in the mold separation. This relationship along with the gate diameters may prove critical in the optimization problem pertaining to imbalances in the mold. As for as the machine control variables, there are may be other variables that could have contributed to the study above, but the sensitivity of their effect have not been reviewed. Control variables such as switchover position and clamping force could be potential irritants.

While heat transfer effects were assumed negligible, there is reason to perform a heat transfer study to rule out any underlying effects. This may be especially helpful in cavities that seem to be unaffected by certain control variables, as seen in the case of cavity number seven. Additionally, the coolant lines offer a great experimental platform. While the experiments performed in this study were held near room temperature, further experimentation with a reduction in the coolant temperature may result in different effects. Mold surface temperature will play into the gate freeze off effect, which will have an effect on the loading over time.

Finally, there may be a need to study the effect of the MUD base constraint on the mold. The MUD base itself has two threaded holes on the top to which a fourth side could be designed to close the loop of the MUD base during loading. This would change the rigidity of the MUD base and potentially reduce unnecessary mold deformation.

APPENDIX A

SPECIFICATION FOR SUMITOMO SH50M

Clamping unit	Clamping system		Fully hydraulic
	Clamp force	t _f	50
	Opening force	t _f	3.2
	Distance between tie-bars (H×V)	mm	325×325
	Overall size of platen (H×V)	mm	470×467
	Mold space	mm	Min. 160
	Opening stroke	mm	440
	Daylight	mm	600
	Ejector type		Hydraulic and cross multipoint ejection (5 points)
	Ejector stroke	mm	70
Ejector force	t _f	2.2	
Injection unit	Plasticizing unit		C160S
	Screw diameter	mm	28
	Injection pressure	kg _f /cm ²	2,230
	Injection capacity	cm ³	70
	Injection weight (GPPS)	g	67
		oz	2.4
	Plasticizing capacity (GPPS) (Screw rotation speed)	kg/h (r.p.m.)	37 (400)
	Injection rate	cm ³ /s	99
	Screw stroke	mm	114
	Max. injection speed	mm/sec	160
	Screw driving system		Hydraulic motor
	Screw torque	kg _f m	36
	Torque selector		1
	Screw rotation speed	r.p.m.	400
	No. of temperature control zone		4
	Heater capacity (for open nozzle only)	kW	4.6
	Nozzle contact force	kg _f	4,670
	Injection unit displacement stroke	mm	245
Hopper capacity	ℓ	15	
Others	Machine dimensions (L×W×H)	mm	3,703×936×1,635
	Machine weight	ton	2.2

Table A.1: Specifications for the Sumitomo SH50M injection molding machine.

REFERENCES

- [1] Ahuett-Garza, H., Hedge, K., Miller, R.A., *Computer Simulation of Die Casting Die Deflection*, Die Casting Engineer, Vol. 39, No. 2, 1995.
- [2] Ahuett-Garza, H., Hedge, K., Miller, R.A., *Computer Simulation of Die Casting Die Deflection, Part 2*, Die Casting Engineer, Vol. 39, No. 6, 1995.
- [3] Carpenter, B., Masters Thesis, The Ohio State University, Columbus, OH, 2002.
- [4] Chen, S. et al., *Investigation of Mold Plate Separation in Thin-Wall Injection Molding*, Advances in Polymer Technology, Vol. 22, No. 4, 2003.
- [5] Sanschagrín, B., *Process Control of Injection Molding*, Polymer Engineering and Science, Vol. 23, No. 8, June 1983.
- [6] Delaunay, D. et al., *Nature of Contact Between Polymer and Mold in Injection Molding. Part II: Influence of Mold Deflection on Pressure History and Shrinkage*, Polymer Engineering and Science, Vol. 40, No. 7, July 2000.
- [7] Leo, V., Cuveilliez, Ch., *The Effect of the Packing Parameters, Gate Geometry, and Mold Elasticity on the Final Dimensions of a Molded Part*, Polymer Engineering and Science, Vol. 36, No. 15, August 1996.
- [8] Del Vecchio, R.H., *Understanding Design of Experiments*, Hanser Publishers, 1997.
- [9] Osswald, T., *Polymer Processing Fundamentals*, Hanser Publishers, 1998.
- [10] Beaumont, J. et al., *Solving Mold Filling Imbalances in Multi-Cavity Injection Molds*, Journal of Injection Molding Technology, Vol. 2, No. 2, June 1998.
- [11] Wenskus, J., *Part Weight as a Control Metric for Injection Molding*, Journal of Injection Molding Technology, Vol. 1, No. 3, September 1997.
- [12] Dally, J.W., Riley, W.F., *Experimental Stress Analysis*, McGraw Hill, 3rd Edition, 1991.